

THESIS

THE EFFECT OF ALTITUDE ON TURBOCHARGER PERFORMANCE PARAMETERS
FOR HEAVY DUTY DIESEL ENGINES: EXPERIMENTS AND GT-POWER MODELING

Submitted by

Andrew T. Thompson

Department of Mechanical Engineering

In partial fulfillment of the requirements

For the Degree of Master of Science

Colorado State University

Fort Collins, Colorado

Spring 2014

Master's Committee:

Advisor: Anthony J. Marchese

Daniel Olsen

Michael A. De Miranda

Copyright by Andrew T. Thompson 2014

All Rights Reserved

ABSTRACT

THE EFFECT OF ALTITUDE ON TURBOCHARGER PERFORMANCE PARAMETERS FOR HEAVY DUTY DIESEL ENGINES: EXPERIMENTS AND GT-POWER MODELING

Operation at high altitude increases the risk of high cycle fatigue (HCF) failure on turbine blades in internal combustion engine turbochargers. Because engine manufacturers rarely acquire performance data at the high altitude limits of their engines, it is imperative that manufacturers rely on computer simulation to visualize, quantify and understand turbocharger performance when experimental tests are not practical. Typically, CFD and FEA models are used to predict HCF damage for turbine wheels. However, the boundary conditions and other input data required for such simulations are often unknown at high altitudes. The main objective of this thesis was to develop these critical boundary conditions and input data for a Cummins QSK19 CI engine and a Cummins QSK50 CI engine. This objective was accomplished by installing and testing both of these engines at 5000ft elevation and calibrating GT-Power computer simulation models against the experimental data at 5000ft elevation. After the models were calibrated against experimental data, the models were extrapolated to the altitude capability of these engines and the critical boundary conditions were recorded.

In addition to the diesel engine experiments and modeling, a single cylinder HCCI computer simulation model was developed to evaluate the performance of Woschni and Hohenberg heat transfer correlations by comparing GT-Power model predictions with measured in-cylinder pressure data. Analysis was performed by generating a single zone GT-Power model of a modified John Deere DI 2.4L four-cylinder engine, which was previously converted at CSU to operate in HCCI port injection mode. The HCCI engine was operated at an equivalence ratio

of 0.33 and a fuel mixture of 40% iso-octane and 60% n-heptane by volume. The combustion chemistry was modeled using a reduced Primary Reference Fuel (PRF) mechanism from Ra and Reitz with 41 species and 130 reactions.

The Cummins modeling results indicate that GT-Power can predict turbocharger performance within 7.59% variation from measured data at 5000ft. When the model was extrapolated to 8000ft, GT-Power predicted an average expansion ratio increase of 1.81% and an average turbine inlet temperature decrease of 2% for the QSK19 CI engine. The Cummins QSK50 GT-Power model predicted an average expansion ratio increase of 2.73% and an average turbine inlet temperature decrease of 9.12% from 5000ft to 8000ft. The HCCI simulation results showed that GT-Power can accurately predict the start of combustion. In addition, the simulation results showed that the pressure rise rate has a low sensitivity to the in-cylinder heat transfer rate.

ACKNOWLEDGMENTS

There are a number of people I would like to thank that have made this thesis possible. First of all, I would like to thank God. God has given the ability and the passion to pursue my dreams. I could never have done this without faith in you.

To my family, friends and wonderful Mother, Linda, who continue to support me and encourage me throughout my life. My family and friends have supported me through my spiritual, my academic and my professional journey. Thank you for inspiring me and helping me realize my potential. Without the support of my family and friends, this thesis wouldn't have been written.

I would like to express my appreciation to my advisor, Dr. Anthony Marchese, who has given me an opportunity that I am eternally grateful for. Thank you for your great attitude, shared knowledge and opportunity to work at the Engines and Energy Conversion Lab. Without your guidance and willingness to help, this thesis would not have been possible. Kirk Evans is a true genius and an incredible resource. Thank you very much for being patient with me and guiding me through this process. I would still be trying to figure out how to get the QSK50 off the ground if it wasn't for Kirk. A special thanks to Marc Baumgardner for helping me with the HCCI modeling work. I would like to also thank Swapnil Dorle, Rex Ralston, Olushola Afolabi and Dan Turner who helped with the GT-Power modeling work for the two Cummins engines. Lastly I would like to thank the control room staff (Mark, Chris, Phil, Pete, Brandon, Corey, Evan, Cody, Colin and Erik) who dedicated many hours helping me install and run the engines. Thank you for all for your help and support!

TABLE OF CONTENTS

ABSTRACT	ii
ACKNOWLEDGMENTS	iv
LIST OF TABLES.....	viii
LIST OF FIGURES	ix
LIST OF SYMBOLS.....	xii
CHAPTER 1: INTRODUCTION AND BACKGROUND	1
1.1 MOTIVATION AND OVERVIEW	1
1.2 TURBOCHARGING	3
1.3 TURBINE WHEEL HIGH CYCLE FATIGUE	5
1.4 GT-POWER MODELING SOFTWARE.....	6
1.4.1 REQUIREMENTS TO BUILD AN ENGINE MODEL	7
1.4.2 GT-POWER IN-CYLINDER COMBUSTION METHODOLOGY	8
1.4.3 GT-POWER TURBOCHARGER THEORY.....	10
1.4.4 GT-POWER ENGINE CALIBRATION PROCESS	11
CHAPTER 2: QSK19 ENGINE INSTALLATION	14
2.1 ENGINE SPECIFICATION.....	14
2.2 SOLIDWORKS TEST CELL MODEL.....	14
2.3 ENGINE MOUNT BRACKETS.....	15
2.4 FLYWHEEL ADAPTER, DRIVESHAFT AND DYNAMOMETER CONNECTION	17
2.5 PLUMBING SYSTEMS	17
2.5.1 DIESEL FUEL PLUMBING	17
2.5.2 INTAKE AIR PLUMBING	21
2.5.3 EXHAUST AIR PLUMBING	23
2.5.4 CHARGE AIR COOLER PLUMBING.....	24
2.5.5 COOLANT PLUMBING.....	25
2.5.6 OIL DRAIN PLUMBING.....	26

2.6 AIR STARTER	27
2.7 INSTRUMENTATION.....	28
2.7.1 BATTERY INSTALLATION	28
2.7.2 ENGINE INSTRUMENTATION AND CONTROL PANEL.....	28
2.7.3 ENCODER INSTALLATION	30
2.7.4 PRESSURE TRANSDUCER AND COMBUSTION CART	30
CHAPTER 3: QSK50 ENGINE INSTALLATION	32
3.1 ENGINE SPECIFICATION.....	32
3.2 SOLIDWORKS TEST CELL MODEL.....	32
3.3 ENGINE MOUNT BRACKETS.....	33
3.4 FLYWHEEL ADAPTER, DRIVESHAFT AND DYNAMOMETER CONNECTION	35
3.5 PLUMBING SYSTEMS	36
3.5.1 DIESEL FUEL PLUMBING	36
3.5.2 INTAKE AIR PLUMBING	37
3.5.3 EXHAUST AIR PLUMBING	38
3.5.4 AFTER COOLER PLUMBING	39
3.5.5 COOLANT PLUMBING.....	41
3.5.6 OIL DRAIN PLUMBING.....	43
3.6 AIR STARTER	43
3.7 INSTRUMENTATION.....	44
3.7.1 BATTERY INSTALLATION	44
3.7.2 ENGINE INSTRUMENTATION AND CONTROL PANEL.....	44
3.7.3 ENCODER INSTALLATION	45
3.7.4 PRESSURE TRANSDUCER AND COMBUSTION CART	46
CHAPTER 4: GT-POWER MODELING RESULTS	47
4.1 QSK19 RESULTS.....	47
4.1.1 QSK19 IN-CYLINDER COMBUSTION RESULTS.....	47
4.1.2 QSK19 CALIBRATION RESULTS FOR THE FIRST OPERATING POINT	49

4.1.3 QSK19 CALIBRATION RESULTS FOR THE TURBOCHARGER.....	52
4.1.4 QSK19 EXTRAPOLATION CASE STUDY RESULTS	54
4.1.5 QSK19 EXTRAPOLATION RESULTS FOR THE TURBOCHARGER	56
4.2 QSK50 GT-POWER MODELING RESULTS	60
4.2.1 QSK50 IN-CYLINDER COMBUSTION RESULTS.....	60
4.2.2 QSK50 CALIBRATION RESULTS FOR THE FIRST OPERATING POINT	62
4.2.3 QSK50 CALIBRATION RESULTS FOR THE LP TURBOCHARGER	65
4.2.4 QSK50 EXTRAPOLATION CASE STUDY RESULTS	67
4.2.5 QSK50 EXTRAPOLATION RESULTS FOR THE LP TURBOCHARGER.....	68
CHAPTER 5: SINGLE CYLINDER HCCI ENGINE	72
5.1 HCCI MOTIVATION FOR MODELING IN-CYLINDER HEAT TRANSFER.....	72
5.2 HCCI HEAT TRANSFER MODEL.....	73
5.3 HCCI ENGINE SETUP	76
5.4 RESULTS AND DISCUSSION.....	77
CHAPTER 6: CONCLUSION AND FUTURE WORK	84
REFERENCES	86
APPENDIX A – QSK19 AND QSK50 INSTALLATION INFORMATION	90
APPENDIX B – QSK19 GT-POWER EXTRA INFORMATION	99
APPENDIX C – QSK50 GT-POWER EXTRA INFORMATION	108

LIST OF TABLES

Table 1: QSK19 Engine Geometry and Rating.....	14
Table 2: QSK50 Engine Geometry and Rating.....	32
Table 3: Operating Conditions for QSK19 GT-Power Modeling.....	47
Table 4: Experimental vs. GT-Power Results for the First Operating Condition.....	50
Table 5: QSK19- Case Study to Determine Target Rotor Speed at 8000ft	56
Table 6: GT-Power Predictions for Rotor Speed from 5000ft to 8000ft	57
Table 7: GT-Power Predictions for Expansion Ratio from 5000ft to 8000ft	58
Table 8: GT-Power Predictions for Turbine Inlet Temperature from 5000ft to 8000ft.....	59
Table 9: Operating Conditions for QSK50 GT-Power Modeling.....	60
Table 10: QSK50- Measured vs. Simulated Results for the First Operating Point	63
Table 11: QSK50- Case Study to Determine Target Rotor Speed at 8000ft	68
Table 12: QSK50 – GT-Power Rotor Speed Extrapolation from 5000ft to 8000ft	69
Table 13: QSK50 – GT-Power Expansion Ratio Extrapolation from 5000ft to 8000ft	69
Table 14: QSK50 – GT-Power Turbine Inlet Temperature Extrapolation from 5000ft to 8000ft	71
Table 15: HCCI Engine Geometry	77
Table 16: HCCI Engine Operating Conditions.....	77
Table 17: Woschni and Hohenberg Comparison for HTR to AHRR	83

LIST OF FIGURES

Figure 1: Power and Torque Curves for a Turbocharged and a Naturally Aspirated engine [11]..	4
Figure 2: 3D QSK19 Solidworks Render Model.....	15
Figure 3: Model - Front Mounting Bracket (left), Actual- Front Mounting Bracket (right)	16
Figure 4: Model – Rear Mounting Bracket (left), Actual – Rear Mounting Bracket (right)	16
Figure 5: Flywheel Adapter (left), Installed Driveshaft and Flywheel Adapter (right).....	17
Figure 6: Positive Displacement Pump.....	18
Figure 7: Installation of the Micron Filter, Flow Meter and Pressure Gauge.....	19
Figure 8: Installation of the Fuel Pressure Regulator	19
Figure 9: Cummins Integrated Lift Pump/Filter	20
Figure 10: Fuel Heat Exchanger	21
Figure 11: Roots Supercharger (left), Humidity Chest for Intake System (right)	22
Figure 12: Air Intake System.....	22
Figure 13: Exhaust SCR Catalyst and Butterfly Valve.....	23
Figure 14: Charge Air Cooler and Plumbing.....	24
Figure 15: Coolant Supply Line.....	25
Figure 16: Coolant Bypass Valve (left), Coolant Return Line (right)	26
Figure 17: Oil Drain Plumbing	27
Figure 18: Air Starter	28
Figure 19: Rosemount Pressure Transducers.....	29
Figure 20: Encoder Mounting System	30
Figure 21: Colorado State University Combustion Chart and Heat Exchanger	31
Figure 22: 3D QSK50 Solidworks Render Model.....	33
Figure 23: Model – Front Mounting Bracket (left), Actual- Rear Mounting Bracket (right).....	35
Figure 24: Model- Rear Mounting Bracket (left), Actual – Rear Mounting Bracket (right).....	35
Figure 25: Flywheel Adapter (left), Driveshaft Cover and Dynamometer Connection (right)	36
Figure 26: Orifice Installation for Intake Air Plumbing	37

Figure 27: Left Bank Intake System (left), Right Bank Intake System (right).....	38
Figure 28: Plumbing from Engine (left), Plumbing post SCR Catalysts (right).....	39
Figure 29: QSK50 Aftercooler Supply Plumbing.....	40
Figure 30: Aftercooler Return Plumbing	41
Figure 31: Coolant Supply Plumbing	42
Figure 32: Coolant Return Plumbing (left), Victaulic Drain Elbow (right)	43
Figure 33: QSK50 Air Starter.....	44
Figure 34: Portable NI PXIe-1078 Chassis Chart.....	45
Figure 35: QSK50 Encoder Installation.....	46
Figure 36: QSK19 Normalized Cylinder Pressure vs. CA for Operating Conditions 1 & 2	48
Figure 37: QSK19 Normalized Cylinder Pressure vs. CA for Operating Conditions 3 & 4	48
Figure 38: QSK19 Normalized Cylinder Pressure vs. CA for Operating Conditions 5 & 6	49
Figure 39: QSK19 Normalized Cylinder Pressure vs. CA for Operating Conditions 7 & 8	49
Figure 40: Normalized Pressure: Experimental vs. Simulated Results for Operating Point:1	51
Figure 41: Experimental vs. Simulated Temperature Results for Operating Point:1	51
Figure 42: QSK19: Normalized Rotor Speed vs. Engine Speed	52
Figure 43: Expansion Ratio vs. CA Considering Pressure Pulsations.....	53
Figure 44: Normalized Expansion Ratio vs. Engine Speed.....	54
Figure 45: QSK19: Normalized Turbine Inlet Temperature vs. Engine Speed.....	54
Figure 46: Power Predictions from 5000ft to 8000ft for the QSK19 Operating Points	58
Figure 47: QSK19-GT-Power Equivalence Ratio Comparison from 5000ft to 8000ft.....	59
Figure 48: QSK50 Normalized Cylinder Pressure vs. CA for Operating Conditions 1&2	61
Figure 49: QSK50 Normalized Cylinder Pressure vs. CA for Operating Conditions 3&4	61
Figure 50: QSK50 Normalized Cylinder Pressure vs. CA for Operating Point 5& 6	62
Figure 51: Normalized Pressure: Experimental vs. Simulated Results for Operating Point:1	64
Figure 52: Experimental vs. Simulation Temperature Results for Operating Point:1	64
Figure 53: QSK50 - Normalized Rotor Speed vs. Engine Speed Comparison.....	65

Figure 54: QSK50 – LP Simulated vs. Experimental Expansion Ratio Comparison	66
Figure 55: QSK50 – LP Simulated vs. Experimental TIT Comparison	66
Figure 56: Power Predictions from 5000ft to 8000ft for the QSK50 Operating Points	70
Figure 57: QSK50-GT-Power Equivalence Ratio Comparison from 5000ft to 8000ft	70
Figure 58: Single cylinder HCCI GT-Power model	78
Figure 59: Measured and Predicted in-Cylinder Pressure from 0-D CHEMKIN Simulation and GT-Power Simulations using the Woschni and Hohenberg Heat Transfer Correlations.	79
Figure 60: Measured and predicted apparent rate of heat release (J/deg) from 0-D CHEMKIN simulation and GT-Power simulations using the Woschni and Hohenberg heat transfer correlations.....	80
Figure 61: Measured and Predicted Low Temperature Heat Release (J/deg) from 0-D CHEMKIN Simulation and GT-Power Simulations using the Woschni and Hohenberg Heat Transfer Correlations.....	81
Figure 62: HCCI: Heat Flux vs. CA (left), Heat Transfer Coefficient vs. CA (right)	82
Figure 63: Apparent Heat Release Rate and Heat Transfer Rate for Woschni and Hohenberg ...	82

LIST OF SYMBOLS

EPA	Environmental Protection Agency
HCF	High Cycle Fatigue
FEA	Finite Element Analysis
CFD	Computational Fluid Dynamics
SCR	Selective Catalytic Reduction
CAC	Charge Air Cooler
HCF	High Cycle Fatigue
AGA	American Gas Association
PRF	Primary Reference Fuel
HCCI	Homogeneous Charge Compression Ignition
THC's	Total Hydrocarbons
PM	Particulate Matter
FSN	Filter Smoke Number
MCRS	Modular Common Rail System
IVC	Intake Valve Close
TPA	Three Pressure Analysis
PID	Proportional-Integral-Derivative
BSFC	Brake Specific Fuel Consumption
GIMEP	Gross Indicated Mean Effective Pressure
PMEP	Pumping Mean Effective Pressure
IMEP	Indicated Mean Effective Pressure
BMEP	Brake Mean Effective Pressure

CHAPTER 1: INTRODUCTION AND BACKGROUND

1.1 MOTIVATION AND OVERVIEW

The United States of America is composed of a variety of plateaus and mountain ranges that extend beyond 4000ft elevation. The Colorado Plateau is the largest plateau in North America (337,000km²) and ranges across areas of Utah, Colorado, Arizona and New Mexico. Within the Colorado Plateau, the elevation can vary anywhere from 2000ft to 12,700ft [1]. Large mountain ranges such as the Rocky Mountains stretch more than 3000 miles (4830km) and extend with an average elevation of 9670ft [2]. In these regions, large turbocharged diesel engines are commonly used to power fracking pumps, haul trucks and even used for stationary power generation. Due to the large market for large turbocharged diesel engines at high altitude, it is important that engine manufacturers address the performance of their engines at high altitude.

As atmospheric pressure decreases with increased altitude, the inlet air density decreases. This decrease in inlet air density causes the performance of internal combustion engines to deteriorate drastically. For example, research has shown that an altitude increase of 2000 meters above sea level can lead to a reduction of 24% in power and an increase of 5% in brake specific fuel consumption (BSFC) [3,4,5]. Fortunately, engineering advancements such as the exhaust turbocharger can compensate, to some extent, for this reduction in power and fuel economy. However, the performance of turbochargers is also affected by altitude. Specifically, as inlet air density decreases with increased altitude, the inlet air mass flow rate decreases. For the same fueling, the exhaust temperature and pressure increase due to a richer air-fuel ratio. Since the turbine receives more exhaust energy, the rotor speed increases resulting in increased boost pressure [3]. The increase in turbine inlet pressure coupled with the drop in turbine outlet pressure causes the pressure ratio to increase.

Unfortunately, the increase in rotor speed, turbine inlet temperature and expansion ratio increases the risk of high cycle fatigue (HCF) failure due to excessive vibration and centrifugal stresses. Researchers have determined that the rotor speed, the expansion ratio and the turbine inlet temperature directly affect the amount of stress induced on the turbine wheel [6,7]. Therefore, it is imperative that engine manufacturers quantify these risks at the high altitude limits of their engines. Since engine manufactures sell their product for applications at various altitudes, they must rely on computer simulation to quantify these effects over a wide range of altitudes. CFD models are typically used to predict the pressure distribution on the turbine wheel and then an FEA analysis is performed to predict HCF damage [7]. Because engine manufacturers rarely acquire performance data at the high altitude limits of their engines, the boundary conditions (rotor speed, expansion ratio, and turbine inlet temperature) for a CFD model are not typically available from experiments. Instead, manufacturers must rely on data acquired at lower altitudes and then use engine simulations to extrapolate the data to higher altitudes. GT-Power, the engine simulation software described herein, is an example of one such simulation tool that can be used to predict the boundary conditions by extrapolating a calibrated engine model to the engines altitude capability.

The research presented in this thesis was performed by using a GT-Power model to acquire the boundary conditions for a CFD model for a Cummins QSK19 CI engine and a Cummins QSK50 CI engine. This objective was accomplished by calibrating a GT-Power engine model against measured data at the Engines and Energy Conversion Laboratory (EECL) at the CSU Powerhouse Campus located in Fort Collins, Colorado. As part of this thesis research, both engines were installed at the EECL and tested over a range of operating conditions at 5000ft above sea level. Once the steady state GT-Power points were calibrated at 5000ft, GT-Power

predictions were extrapolated to 8000ft and the results were reported back to Cummins for further evaluation.

In addition to the combined experimental and GT-Power modeling study performed on the diesel engines, a second GT-Power modeling study was also performed on a homogeneous charge compression ignition (HCCI) engine. In-cylinder heat transfer processes have a direct effect on autoignition timing, burn rate and in-cylinder pressure in HCCI engines. Because of the complexity of the physical processes (e.g., turbulent flow, heat transfer, molecular diffusion and detailed chemical kinetics) in an HCCI engine, development of HCCI engine models that accurately reproduce in-cylinder pressure measurements (i.e. pressure rise rate and maximum pressure) requires an empirical treatment of the in-cylinder heat transfer. The goal of this second GT-Power modeling study was to evaluate the performance of the Woschni and Hohenberg heat transfer correlations by comparing GT-Power engine model predictions with measured in-cylinder pressure data from a single cylinder HCCI engine. Analysis was performed by generating a single zone GT-Power model of a modified John Deere DI 2.4L four-cylinder engine, which was previously converted at the EECL to operate in HCCI port injection mode. The HCCI engine was operated at an equivalence ratio of 0.33 and a fuel mixture of 40% iso-octane and 60% n-heptane by volume. The combustion chemistry was modeled using a reduced Primary Reference Fuel (PRF) mechanism from Ra and Reitz with 41 species and 130 reactions [8].

1.2 TURBOCHARGING

Turbocharging is a common method used by engine manufacturers to increase power and efficiency [9,10]. The goal of a turbocharger is to increase the inlet air density above atmospheric conditions so that more fuel and air can be delivered to the engine to increase power

[11]. This objective is accomplished by expanding the exhaust gas across a turbine that drives a compressor on a common shaft. Turbochargers for internal combustion engines (ICE) are composed of a radial inflow turbine, a centrifugal compressor and a center rotating assembly that connects the turbine to the compressor. The following figure represents the increase of power and torque over a naturally aspirated (NA) engine for a Chrysler 2.2L engine from Allen and Rinschier [11].

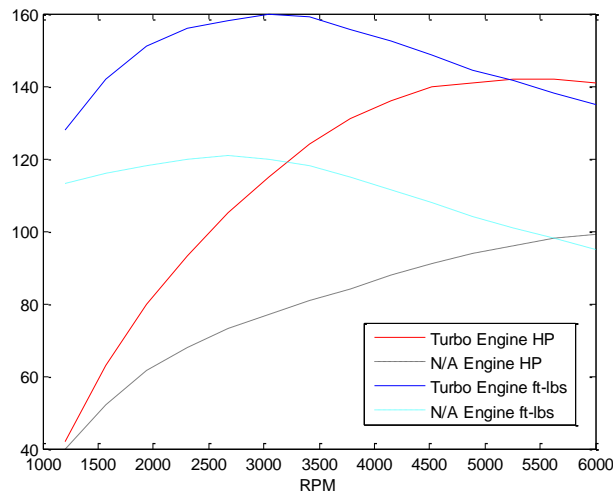


Figure 1: Power and Torque Curves for a Turbocharged and a Naturally Aspirated engine [11]

A wastegate is a common component that is typically integrated with a turbocharger. Its purpose is to control the power of the turbine by opening and closing a valve (inside or next to the turbine housing) that can be either pneumatically actuated or electronically controlled. If the wastegate is pneumatically controlled, a wastegate is used to limit the boost pressure so that it doesn't inflict physical damage to the engine or turbocharger [10]. An electronically controlled wastegate can be used to limit boost pressure, control the air flow rate or limit heat rejection to the engine per customer requirements. Heat rejection can be calculated using the following equation [12]:

$$\dot{Q}_{HR} = \dot{m}_{air} c_p (T_{outlet} - T_{inlet}) \quad (1)$$

where \dot{m}_{air} the air flow rate into the engine, c_p the specific heat of the air, T_{outlet} the temperature leaving the compressor of the turbocharger, T_{inlet} the temperature entering the compressor of the turbocharger.

1.3 TURBINE WHEEL HIGH CYCLE FATIGUE

High cycle fatigue has been defined from Bauccio as fatigue that occurs above 10^3 or 10^4 cycles [6]. This occurs when stress is low and deformation is elastic. In modern engines, high cycle fatigue (HCF) has been identified as one of the primary failure modes for turbine blades [7,13]. The pressure distribution in the turbine housing causes the turbine blade to be exposed to unsteady aerodynamic forces that induce vibration at their natural frequencies. These dynamic pressure fluctuations cause the turbine blade to oscillate at its resonant frequency. Specifically for turbine blades described herein, the natural frequency is determined by the critical rotor speed and can be up to 10,000 Hz [14]. Researchers have shown that the expansion ratio has a direct effect on the amplitude of the unsteady aerodynamic forces [6, 7]. The expansion ratio or the pressure ratio is described on the following equation:

$$ER = \frac{P_{inlet}}{P_{outlet}} \quad (2)$$

where ER the expansion ratio, P_{inlet} the turbine inlet pressure, and P_{outlet} the turbine outlet pressure. The turbine inlet temperature has a direct effect on the material properties which reduces the fatigue life margin. As previously mentioned, this thesis research is focused on providing the effects of expansion ratio and turbine inlet temperature as inputs to a full 3D computational fluid dynamic model that predicts the pressure distribution in the turbine housing. The study was calibrated and extrapolated using a commercial simulation software tool called GT-Power.

1.4 GT-POWER MODELING SOFTWARE

The modeling approach described herein utilizes the commercial engine simulation tool GT-Power™. A GT-Power simulation relies on the one dimensional solution of the fully unsteady, nonlinear Navier-Stokes equations of continuity, energy, and momentum to simulate gas flow dynamics [15]. GT-Power discretizes the system by breaking up the volume into many sections using the staggered grid method. The scalar variables (pressure, temperature, density etc.) in Navier-Stokes are assumed to be uniform, whereas, the vector variables (fluxes, velocity, etc.) are calculated at each boundary. There are three methods of time integration (explicit, implicit, and quasi-steady) that affect the solution variables used in the Navier-Stokes equations. The explicit method is primarily used for engine performance where crank angle resolved solutions are required and wave dynamics are important [15]. The implicit method is primarily used for non-engine simulations where wave dynamics are not important. The implicit method uses longer time steps and is typically used only for thermal management simulations such as Waste Heat Recovery or exhaust warm-up simulations. The quasi-steady method is used for aftertreatment modeling where fast running chemical kinetics is important.

GT-Power uses a graphical user interface known as GT-ISE to construct a virtual engine by building a block diagram of engine components such as: cylinders, fuel injectors, pipes, compressors, gears, flowsplits, etc. After the model has been constructed and executed, GT-Power uses a post processing tool called GT-Post to output and plot performance parameters such as: rotor speed, turbine inlet temperature, turbine inlet pressure, cylinder pressure, cylinder temperature, burn rate, indicated mean effective pressure (IMEP), brake mean effective pressure (BMEP) etc. Once a model has been calibrated, GT-Power has the advantage to easily perform parametric studies of intake pressure, intake temperature, equivalence ratio, RPM etc.

1.4.1 REQUIREMENTS TO BUILD AN ENGINE MODEL

Since internal combustion engines consist of many components, the following list of components and input data are required to develop a GT-Power engine model:

- Engine Characteristics and Cylinder Geometry: These data include bore, stroke, compression ratio, firing order, connecting rod length, inline or V configuration, 2 or 4 stroke, pin offset, piston TDC clearance height, piston bowl geometry (DI only), piston area, and head area (heat transfer model).
- Intake and Exhaust System: These data include the geometry of all components such as runners, manifolds, etc. The geometry includes: lengths, internal diameters, volumes, and layouts. Additional data on head loss coefficients and/or discharge coefficients may also be used.
- Intake and Exhaust Valves: These data include valve diameter, lift profile, discharge coefficients, valve lash, swirl and tumble coefficient, if available.
- Throttles: These data include throttle location and discharge coefficients versus throttle angle in both flow directions.
- Fuel Injectors: These data include location of fuel injectors and number of injectors; number of nozzle holes and nozzle diameter, injection rate, air to fuel ratio and fuel type
- Turbocharger Components (optional): These data include turbine and compressor maps, turbocharger inertia (transient), performance characteristics (pressure ratio, turbocharger speed, temperatures, etc.)
- Wastegate/VGT Component: These data include the wastegate diameter, target boost and airflow rate.

- Ambient Conditions: Ambient conditions such as pressure, temperature, and humidity must be specified.

The accuracy of the engine model is highly dependent on the extent of performance data acquired experimentally to calibrate the model. If less experimental performance data is available, the accuracy of the model decreases.

1.4.2 GT-POWER IN-CYLINDER COMBUSTION METHODOLOGY

Because of the complexity of any engine system, development of a combustion model that accurately reproduces in-cylinder pressure measurements (i.e. pressure rise rate, maximum pressure, GIMEP etc.) is critical to modeling the performance of an engine. For a CI and SI engine, GT-Power divides the air-fuel mixture into two non-spatial zones: an unburned zone and a burned zone. At each time step, GT-Power transfers the air-fuel mixture from the unburned zone to the burned zone. The amount of air-fuel that is transferred from the unburned zone to the burned zone is governed by the burn rate. Therefore, the major goal of all SI and DI combustion models is to accurately determine the burn rate.

To accomplish this task, GT-Power has a variety of predictive, non-predictive and semi-predictive combustion models available. A non-predictive model will impose a burn rate that is prescribed by a Wiebe function or prescribed from measured in-cylinder pressure data. A non-predictive model is recommended if measured cylinder pressure is available. A GT-Power predictive combustion model predicts a burn rate based on in-cylinder inputs such as temperature, pressure or equivalence ratio. A semi-predictive model can be used when the study at hand directly affects the burn rate. A study that varies the injection timing would have a direct effect on the burn rate. In this case, a semi-predictive model should be used.

After constructing the model in GT-ISE, the first step in calibrating an engine model is to decide which combustion model should be used (predictive, non-predictive or semi-predictive). In this study, in-cylinder pressure measurements were taken and a non-predictive combustion model ('EngCylCombProfile') was selected for both the QSK19 and QSK50. The 'EngCylCombProfile' object allows the user to import the pressure trace, apply an encoder error shift and even apply a low pass filter. For the non-predictive combustion model, the burn rate is the integral of the heat release rate which is calculated from the cylinder pressure trace. The heat release rate is calculated using the first law of thermodynamics:

$$\frac{d(m_{cyl}u)}{dt} = \dot{Q}_{cv} - \dot{W}_{cv} \quad (3)$$

where m_{cyl} is the total mass inside the cylinder (fuel and air), u the internal energy, \dot{Q}_{cv} the heat transfer to the gas from cylinder walls and \dot{W}_{cv} the instantaneous PdV power generated by the gas in the cylinder. The power term can be expressed as follows:

$$\dot{W}_{cv} = p_{cyl} \frac{dV_{cyl}}{dt} \quad (4)$$

where p_{cyl} is the instantaneous cylinder pressure, V_{cyl} is the cylinder volume at the given pressure. The heat transfer term includes the heat transfer through the cylinder walls, head and piston. By further assuming the system is closed and the mass, gas constant and specific heat do not change with time, the heat release rate can be calculated using the following equation found in Heywood and Ferguson [16,17]:

$$\frac{dQ_{comb}}{d\theta} = \frac{1}{\gamma-1} V_{cyl} \frac{dp_{cyl}}{d\theta} + \frac{\gamma}{\gamma-1} p_{cyl} \frac{dV_{cyl}}{d\theta} + \frac{dQ_{HT}}{d\theta} \quad (5)$$

where Q_{comb} is the chemical heat release rate, γ is the ratio of specific heats, Q_{HT} the heat transfer to the walls, head and piston. Finally, the burn rate is calculated by the following:

$$x_b = \int \dot{Q}_{comb} d\theta \quad (6)$$

1.4.3 GT-POWER TURBOCHARGER THEORY

GT-Power turbocharger performance is characterized by the compressor and turbine maps supplied by the user. Specifically, the speed and pressure ratio across each compressor and/or turbine must be specified at each time step. The mass flow rate and efficiency are determined from the compressor and turbine maps and imposed on the adjacent boundaries. The user imposes the pressure ratio, intake manifold pressure, exhaust manifold pressure, ambient pressure, and rotor speed for the first cycle. The power of the compressor and turbine is determined by first law principles where the turbocharger is assumed isentropic.

The outlet temperature is calculated by the change in enthalpy across the turbine or compressor. GT-Power uses the following equations for turbocharger performance [15]:

Compressor:
$$h_{outlet} = h_{inlet} + \Delta h_s \frac{1}{\eta_s} \quad (7)$$

$$\Delta h_s = c_p T_{inlet} \left(PR^{\frac{\gamma-1}{\gamma}} - 1 \right) \quad (8)$$

Turbine:
$$h_{outlet} = h_{inlet} - \Delta h_s \eta_s \quad (9)$$

$$\Delta h_s = c_p T_{inlet} \left(1 - PR^{\frac{1-\gamma}{\gamma}} \right) \quad (10)$$

where h_{inlet} is the inlet enthalpy based on upstream conditions, h_{outlet} the predicted outlet enthalpy based on isentropic efficiency and upstream conditions, Δh_s the isentropic change in enthalpy, η_s the isentropic efficiency, PR the pressure ratio, c_p the specific heat of the inlet air or exhaust, γ the ratio of specific heats based on inlet conditions and T_{inlet} the inlet temperature.

Steady state is reached once the power of the compressor and turbine are equal to each other. The assumed power of the compressor and turbine are time averaged values over the 720 degree cycle. The power is evaluated as:

$$P = \dot{m}(h_{inlet} - h_{outlet}) \quad (11)$$

where \dot{m} is the mass flow rate. The speed is determined when the torque associated with the compressor and turbine powers are equal to each other. GT-Power uses the following equation under the ‘ShaftTurbo’ object:

$$\Delta\omega = \frac{\Delta t(T_{turbine} - T_{compressor} - T_{friction})}{I} \quad (12)$$

where $\Delta\omega$ is the change in rotor speed, T the torque, I the moment of inertia for the shaft [15].

1.4.4 GT-POWER ENGINE CALIBRATION PROCESS

As previously mentioned, the first step in calibrating an engine model is deciding which combustion model should be used. Since a non-predictive model was selected for this study, the following will only focus on the mythology that calculates the burn rate based on measured cylinder pressure. GT-Power has two approaches. The first method is termed as a ‘Stand-Alone Burn Rate Calculation’. This method requires a measured cylinder pressure and a separate, but simple, model that includes only the cylinder and crank train. The inputs are the engine geometry, wall, head and piston temperatures, a heat transfer model and initial conditions which include residuals. Since in-cylinder residuals are very difficult to collect, the user often has to approximate the residual fraction. This can lead to uncertainty and is typically used if intake and exhaust pressures are not available.

The second method, which is termed by GT-Power as ‘Three Pressure Analysis’ (TPA), was used for this study and will be described in full detail. The name is derived from the three

measured pressures required as inputs: intake pressure, cylinder pressure and exhaust pressure. This technique is favorable since the in-cylinder residuals can be calculated by GT-Power at intake valve close (IVC). Similar to the ‘Stand-Alone Burn Rate Calculation’ method, a TPA model is a single cylinder representation of the engine that includes the following objects: cylinder crank train, intake valve, exhaust valve, intake runner, exhaust runner, and fuel injector. Since the TPA model does not include a turbocharger object, intake and exhaust manifold conditions (temperature and pressure) were imposed on the ambient environments.

After the single cylinder representation of the engine has been constructed in GT-Power, the cylinder pressure at each operating condition was matched as closely as possible. The model described herein matched the pressure at Bottom Dead Center (BDC), Intake Valve Close (IVC), and Start of Injection (SOI). This was done by pegging the cylinder pressure trace to the intake manifold pressure as described by Poonawala [18]. Frequently the pressure at BDC and IVC match extremely close, however, the SOI was slightly off. In this case, the compression ratio was slightly adjusted, within reason, to match SOI pressure. The last two criteria to match cylinder pressure were Gross Indicated Mean Effective Pressure (GIMEP) and peak cylinder pressure. The gross mean effective pressure is the closed loop work that is calculated using the following equation found in Heywood [16]:

$$\text{GIMEP} = \text{IMEP} - \text{PMEP} \quad (13)$$

where IMEP is the indicated mean effective pressure, PMEP is the pumping mean effective pressure. IMEP and PMEP are calculated using the following equation found in Ferguson [17]:

$$IMEP = \frac{pdV}{V_d} \quad (14)$$

$$PMEP = P_e - P_i \quad (15)$$

where p is the cylinder pressure, V is the cylinder volume for a single cylinder, V_d is the displaced volume for a single cylinder, P_e is the exhaust pressure, P_i is the intake pressure.

If peak cylinder pressure was off, the heat transfer multiplier in the cylinder object was adjusted accordingly. A spatially non-uniform heat transfer model was selected as described by Morel and Keribar [19]. Morel and Keribar convective heat transfer model is directed for Bowl-in-Piston combustion chambers. Other heat transfer correlations from Woschni or Hohenberg are also available [20,21]. Once the cylinder pressure is matched in the TPA model, the ‘EngCylCombProfile’ object was copied from the TPA model to the full engine model. The burn rate profile was imposed on all the cylinders. It is important to note that each cylinder received the same burn rate profile.

Once the burn rate was complete, minimal GT-Power adjustments were needed to match measured data. The most common adjustments were correcting the power and the rotor speed to match measured data. The power was adjusted by varying the fueling (mg/stroke) within two percent of the measured data. The rotor speed was adjusted by varying the friction term outlined in equation 10 on page 11. The heat exchanger effectiveness was adjusted to match intake manifold temperature.

CHAPTER 2: QSK19 ENGINE INSTALLATION

2.1 ENGINE SPECIFICATION

The Cummins QSK19 is a 19L 6-cylinder diesel engine that utilizes a single-stage Holset turbocharger coupled with an electronic wastegate and intercooler. The engine has a two-stage oil filter, steel pistons and operated using a modular common rail fuel system (MCRS). The Cummins QSK19L produces a peak power of 597 kW (800 hp) at 1900 rpm and a maximum torque of 3118 N-m (2300 ft-lbs) at 1500 rpm. The engine geometry and rating can be found on the following table.

Table 1: QSK19 Engine Geometry and Rating

Engine	Cummins QSK19
Configuration	I-6 Turbocharged
Displacement	19 liter
Bore	159 mm
Stroke	159 mm
Compression Ratio	14.7:1
Rated Power	597 kW @1900 rpm
Maximum Torque	3118 N-m @ 1500 rpm

2.2 SOLIDWORKS TEST CELL MODEL

The project began in January 2013 when a 69L natural gas Caterpillar engine occupied the test cell for the QSK19 diesel engine. To help with the transition of removing the Caterpillar engine and installing the Cummins diesel engine, a three dimensional engine model using Solidworks was created. The model includes all the necessary engine mounts, plumbing and connections to the engine. Since the QSK19 diesel engine has the same base engine components (engine block,

oil pan, flywheel housing, flywheel, etc) as a pre-existing QSK19G natural gas engine, the diesel base engine components were taken from the natural gas model provided by Frank H. Sutley. Sutley extracted the critical engine dimensions from a model provided by Cummins [22]. The height of the engine mount brackets were determined by the 2500 HP eddy current dynamometer. The center line of the flywheel was offset from the dynamometer to ensure proper wear on the driveshaft bearings. The 3D Solidworks model is shown in Figure 2.

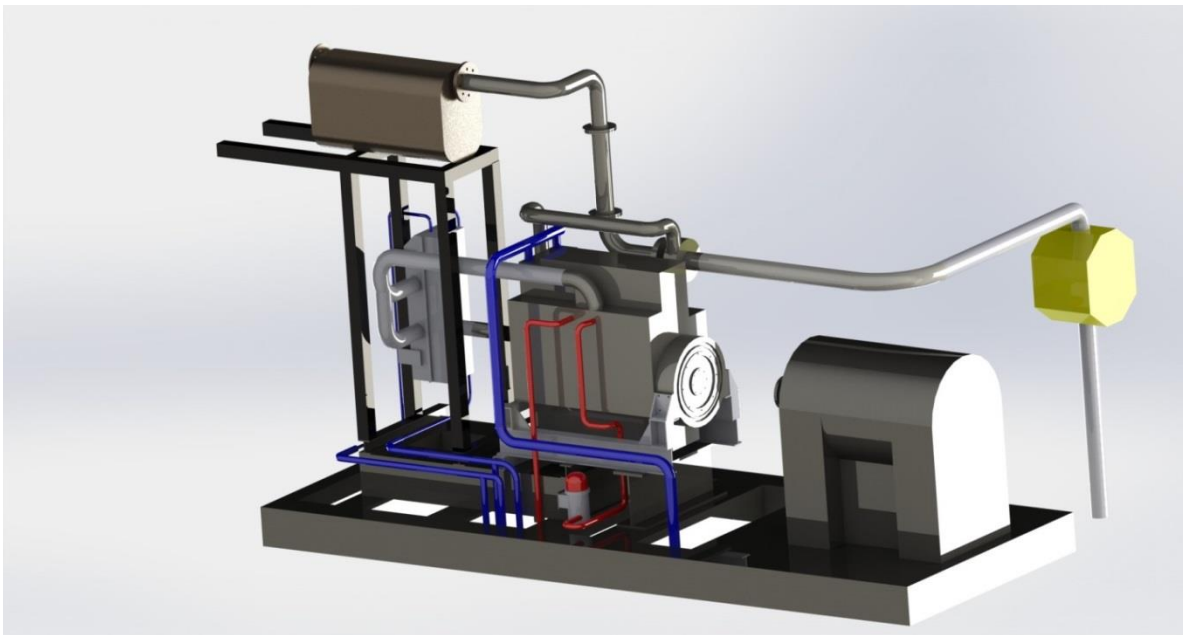


Figure 2: 3D QSK19 Solidworks Render Model

2.3 ENGINE MOUNT BRACKETS

The aforementioned 3D model was used to design the front and rear engine mounting brackets. Since the QSK19 diesel engine would be removed halfway throughout the test and replaced with a Cummins QSK50 engine, both the front and rear engine mounting brackets were welded to an 8in (203.2mm) X 4in (101.6mm) X 62 in (1574.8mm) thick I-beam for easy engine removal with a forklift. The front engine mount bracket was constructed from a 30in (762mm) section of 3in (76.2 mm) square tubing with 3/8in (9.53mm) steel plate open boxes on each side. The 3/8in

(76.2mm) steel plate boxes were cut from a water jet; whereas, the square tubing was cut with the horizontal band saw. After the pieces were cut, they were welded together. To reduce the stress concentration on the corners of the box, 3/8in (76.2mm) steel triangular pieces were welded to the side of the boxes. Figure 3 shows the model and the actual front engine bracket.

The rear engine mounting bracket was constructed similarly to the front mounting bracket. The 3/8in (76.2mm) steel plates were cut with the water jet and formed an open box. The mounting hole locations were taken from the natural gas flywheel adapter dimensions. Figure 4 is the model and actual rear mounting bracket.

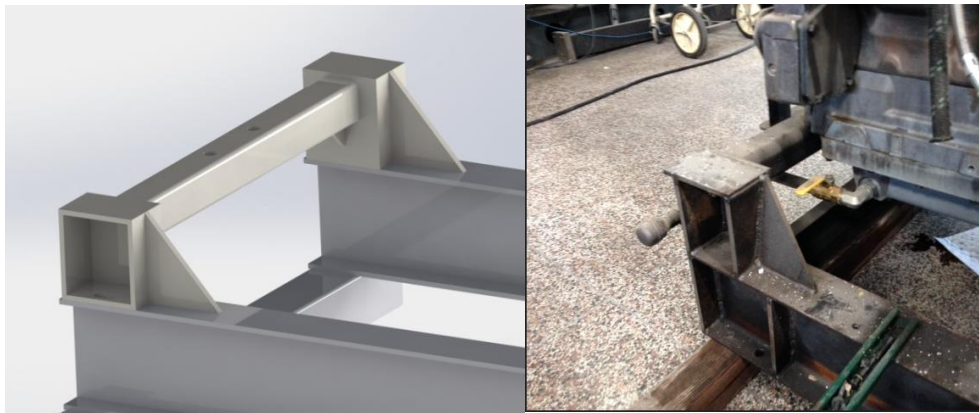


Figure 3: Model - Front Mounting Bracket (left), Actual- Front Mounting Bracket (right)



Figure 4: Model – Rear Mounting Bracket (left), Actual – Rear Mounting Bracket (right)

2.4 FLYWHEEL ADAPTER, DRIVESHAFT AND DYNAMOMETER CONNECTION

Since the dynamometer and driveshaft were pre-existing components within the test cell, the flywheel adapter was modified from the 69L natural gas Caterpillar engine that occupied the test cell prior to the QSK19 engine. The flywheel adapter diameter was reduced to fit with the QSK19 from 26 7/16in (671.513mm) to 19in (482.6mm) with a water jet. After roughly cutting out the diameter, the adapter was shipped to a private machinist who reduced the adapter an additional 5/8in (15.875mm) to its final diameter of 18 3/8in (466.725). The machinist finished the flywheel adapter by drilling holes and applying a chamfer to the edge. Based on the position of the engine mounts, the driveshaft has a driveline angle of 3° where the maximum angle is specified at 7 ° for parallel shafts operating at a maximum of 2500 RPM [22].



Figure 5: Flywheel Adapter (left), Installed Driveshaft and Flywheel Adapter (right)

2.5 PLUMBING SYSTEMS

2.5.1 DIESEL FUEL PLUMBING

The diesel fuel plumbing system required more work than the rest of the plumbing systems. At the start of the project, no fuel lines were installed. For the QSK19 testing, a 500 gallon tank was used that was previously purchased by the Engines and Energy Conversion Laboratory (EECL).

The supply line is 1 in (25.4mm) threaded black steel pipe. The fueling system starts out with a threaded ball valve for easy flow control. A water/fuel separator leads into an Oberdorfer 3/8in (9.525 mm) positive displacement pump (Figure 6) with a pressure relief valve that leads back to the fuel tank.



Figure 6: Positive Displacement Pump

After the fuel pump, an electronic 1.5in (38.1mm) solenoid valve was installed. This is used to block the flow of diesel fuel in case the control room loses power. After the solenoid valve and approximately 80 feet of plumbing, another micron filter was installed before a Coriolis flow meter. A pressure gauge was installed after the flow meter per Cummins request- see Figure 7.

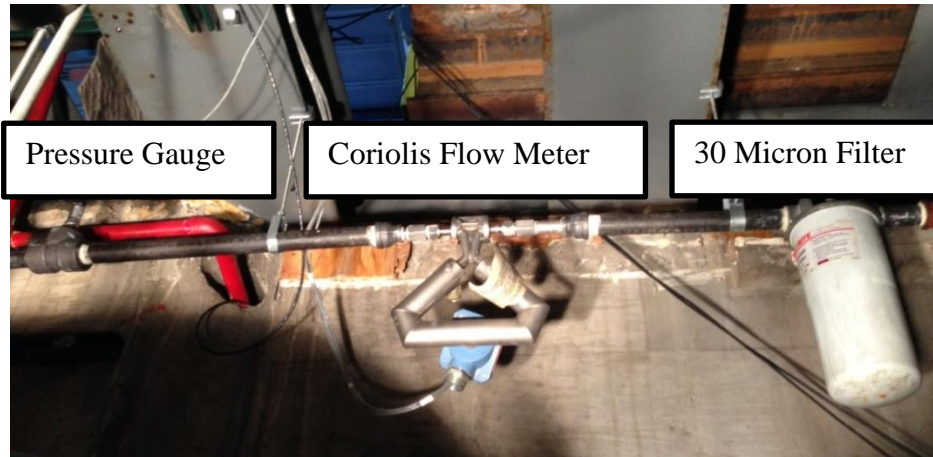


Figure 7: Installation of the Micron Filter, Flow Meter and Pressure Gauge

A pressure regulator (2–15 psi) was installed to ensure the fuel pressure did not exceed requirements outlined by Cummins. After the regulator, a check valve was installed to ensure the fuel return from the heat exchanger did not flow back towards the flow meter. Another pressure gauge was installed to monitor the pressure going into the Cummins integrated lift pump/filter.

Figure 8 show the installation of the pressure regulator, check valve, fuel return from the heat exchanger and the second pressure gauge. Figure 9 shows the lift pump/filter. After the lift pump, a flexible line was installed that connects directly to the engines JIC fitting.

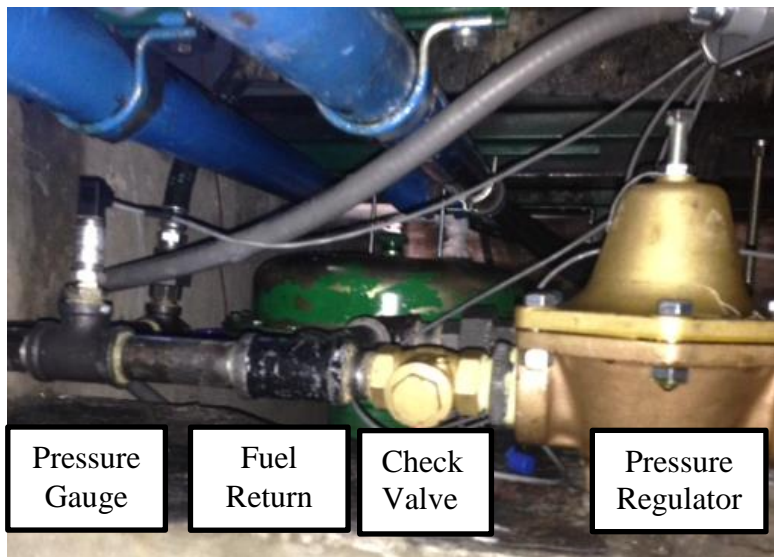


Figure 8: Installation of the Fuel Pressure Regulator



Figure 9: Cummins Integrated Lift Pump/Filter

The excess fuel from the engine is routed to a cross-flow coolant/fuel heat exchanger from Thermal Transfer Products. The heat exchanger is required to lower the fuel temperature below 159°F. The coolant is supplied from the charge air cooler (CAC) loop. Once the fuel leaves the heat exchanger, it is returned back into the fuel supply loop. Figure 10 shows the shell and tube heat exchanger used for the fuel return. A completed fuel diagram can be found in the appendix.

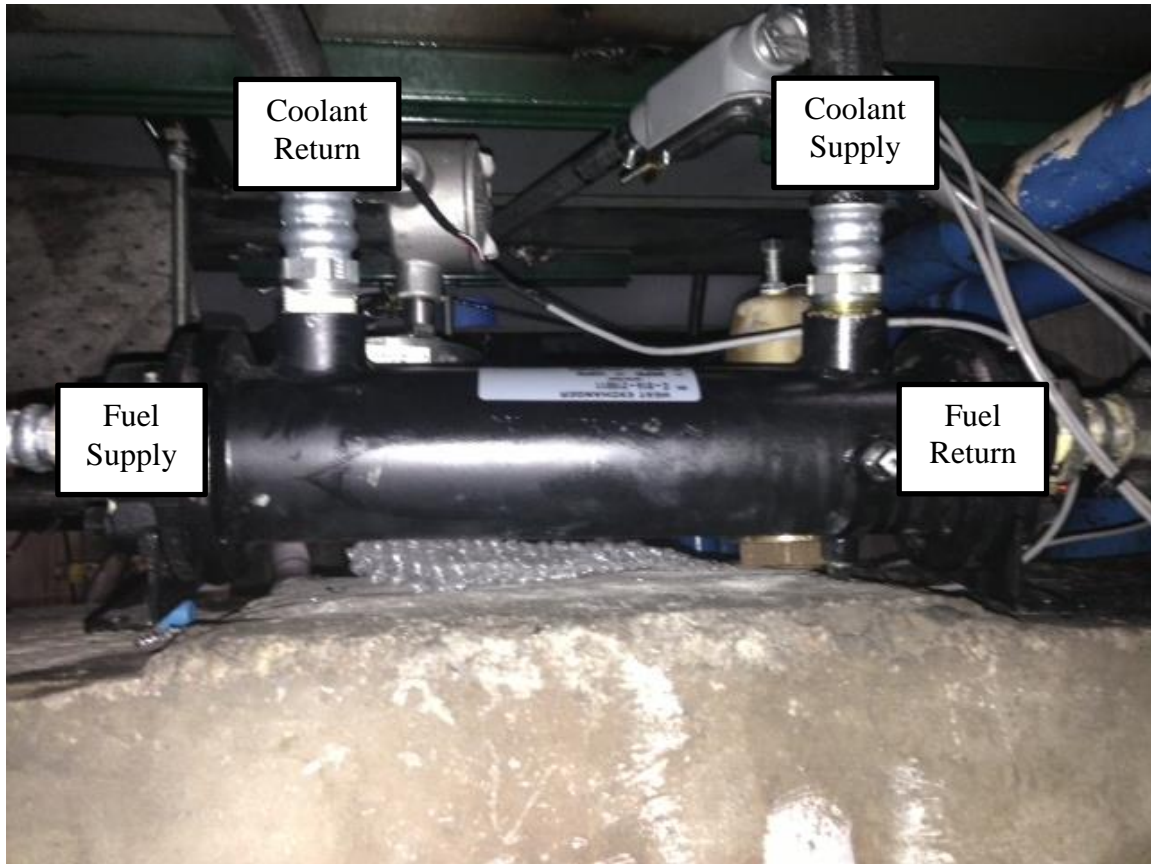


Figure 10: Fuel Heat Exchanger

2.5.2 INTAKE AIR PLUMBING

A new intake air plumbing was added to the test cell for the QSK19 engine testing. 8in (203.2mm) schedule 40 pipe was installed from the roots supercharger to the air filter flange.

The supercharger at the laboratory has the ability to mimic temperature, pressure and humidity – see Figure 11. An orifice was installed below the engine for flowrate measurements. After the air filter, temperature and pressure taps were installed and the pipe diameter was reduced to 5in (127 mm) to match the diameter on the engine connection. Figure 12 shows the intake air connection to the engine.



Figure 11: Roots Supercharger (left), Humidity Chest for Intake System (right)

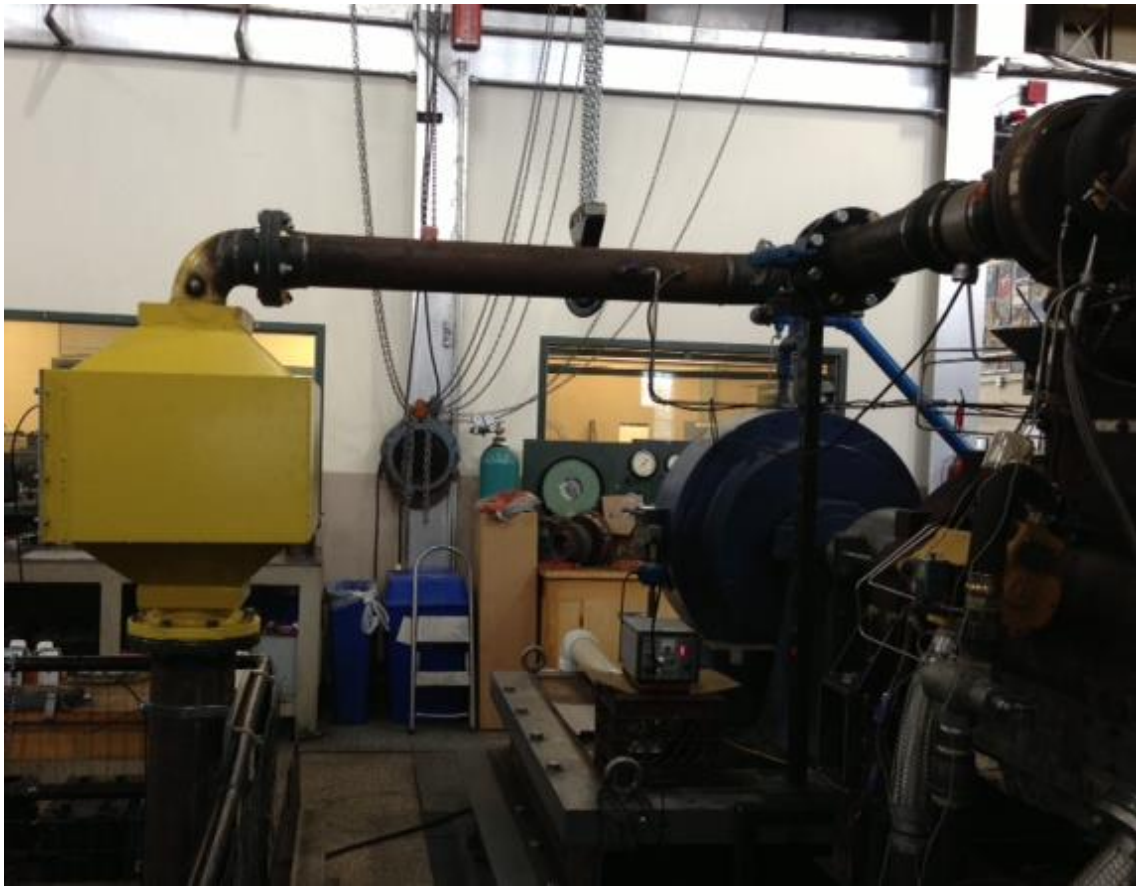


Figure 12: Air Intake System

2.5.3 EXHAUST AIR PLUMBING

The turbine outlet connection from the engine is 5in (127 mm). From the turbine connection, a reducer was installed from 5in (127mm) to 6in (152.4 mm) to mate to a 36in (914.4 mm) long flexible straight section that helps account for tolerance stack-up and engine vibration. From the straight section, the pipe diameter is increased further to 8in (203.2 mm) to mate to the selective catalytic reduction (SCR) flange connection. The SCR catalyst and a Fisher pneumatic butterfly valve are the two main contributors to the exhaust plumbing. Urea is not being used prior in the SCR because the catalyst and butterfly valve are being used to simulate exhaust back pressure for altitudes lower than 5000ft. After the butterfly valve, another short flex-section was added followed by a reducer to 12in (304.8 mm) that mounts to the exhaust stack. Figure 13 shows the SCR catalyst and the butterfly valve.



Figure 13: Exhaust SCR Catalyst and Butterfly Valve

2.5.4 CHARGE AIR COOLER PLUMBING

The charge air cooler (CAC) was provided by Cummins and mounted directly to the catalyst support bracket. A silicone and meta-aramid hose connects the engine compressor outlet housing to the CAC supply pipe constructed of 5in (127 mm) steel pipe. The CAC return pipe is also 5in (127 mm) and mounted to the intake manifold via a silicone hose with two t-bolt clamps.

The intercooler plumbing was modified from the pre-existing test cell plumbing setup. At the CAC, the intercooler plumbing was 1in (25.4mm) threaded black steel pipe. As the plumbing leaves the CAC, the diameter was increased to 2 in (50.8 mm) to match the pre-existing test cell pipe. A threaded ball valve was installed to help control flowrates into the CAC. Two other ball valves were installed to control the flow rate for the fuel/coolant heat exchanger. Figure 14 shows the CAC and associated plumbing. The intercooler plumbing lines are connected to the EECL cooling water system via a centrifugal pump.



Figure 14: Charge Air Cooler and Plumbing

2.5.5 COOLANT PLUMBING

The coolant plumbing lines were modified from the Caterpillar engine to fit with the QSK19 engine. The coolant supply line was re-routed from the flange connection with the blue valve to the water pump inlet on the engine (Figure 15). From the blue valve, a 4in (101.6 mm) Y fitting was installed to drain and pump the engine with coolant. From the Y fitting, a flange connects to Victaulic orange fittings. The pipe diameter was reduced to 3in (76.2 mm) at the flange to match the diameter at the water pump inlet. A 16in (406.4 mm) stainless steel flex-section was added to help with tolerance stack-up and engine vibration.

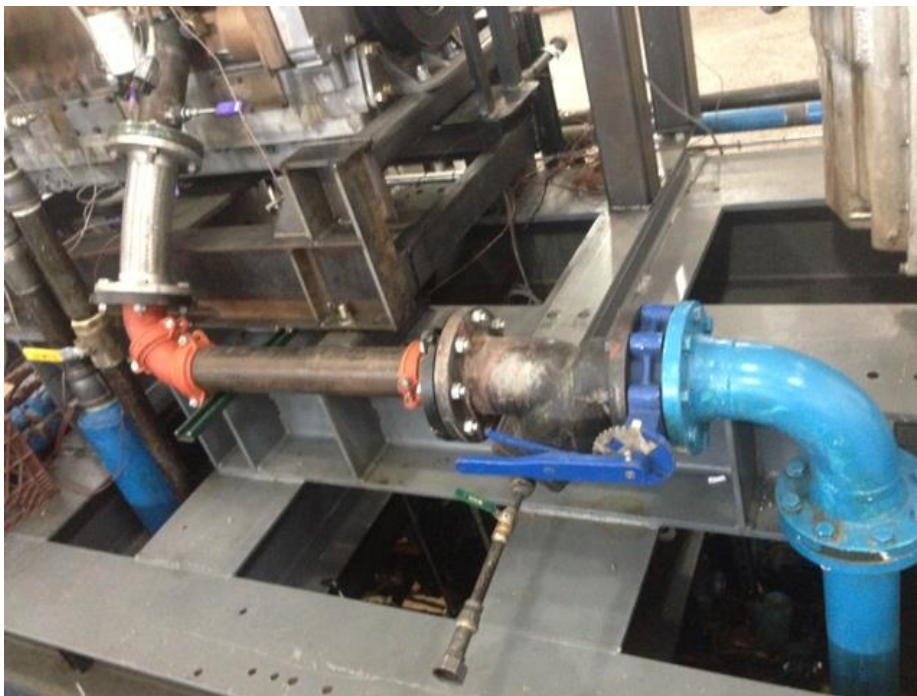


Figure 15: Coolant Supply Line

Prior to the coolant inlet, a pneumatic Fisher coolant bypass valve (Figure 16) was installed below the engine since the onboard coolant thermostat was controlling coolant flow. The bypass valve rejects coolant flow to the coolant return line. The engine returns coolant at the highest point on the engine. The coolant return line utilizes Victaulic fittings with a stainless

steel flexible section. The jacket water return pipe and the engine coolant outlet pipe were both 3in (76.2 mm) in diameter. After leaving the engine, the coolant return plumbing passes through a cooling tower and then was pumped back into the coolant supply loop.

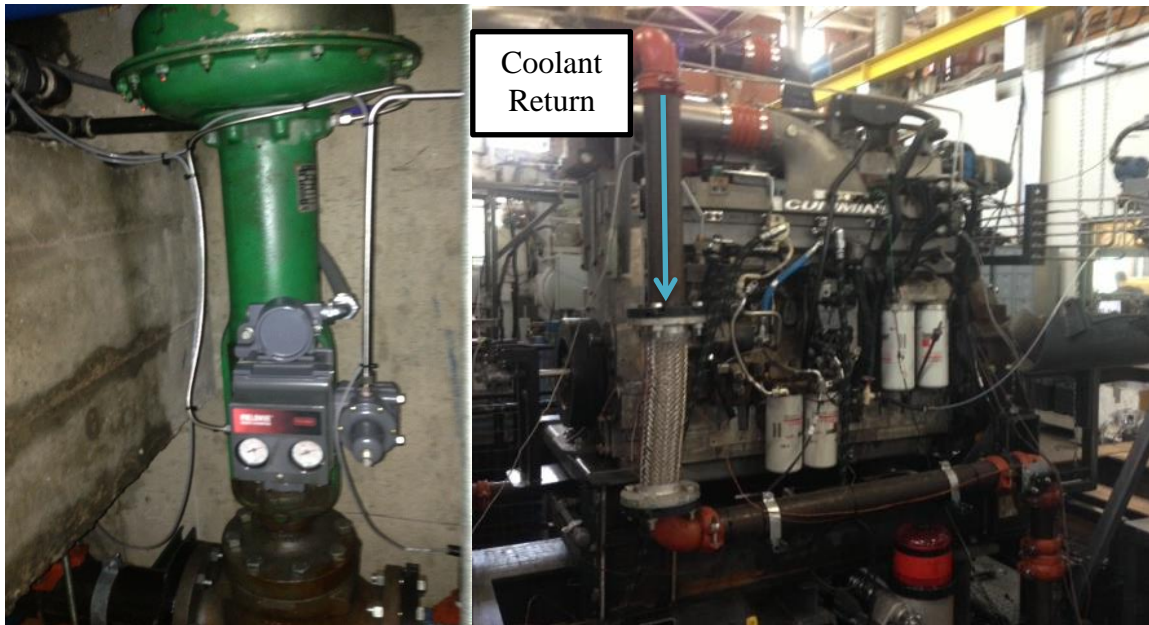


Figure 16: Coolant Bypass Valve (left), Coolant Return Line (right)

2.5.6 OIL DRAIN PLUMBING

An oil drain line was added to an oil pan port in order to perform an oil change. The piping consists of a 90° elbow with a straight thread O-ring seal going into the engine and National Pipe Thread (NPT) going into the 3/4in (19.05mm) threaded ball valve. The plumbing was attached to a section of unistrut that was welded to the front engine mount bracket. The oil drain plumbing is shown in Figure 17.

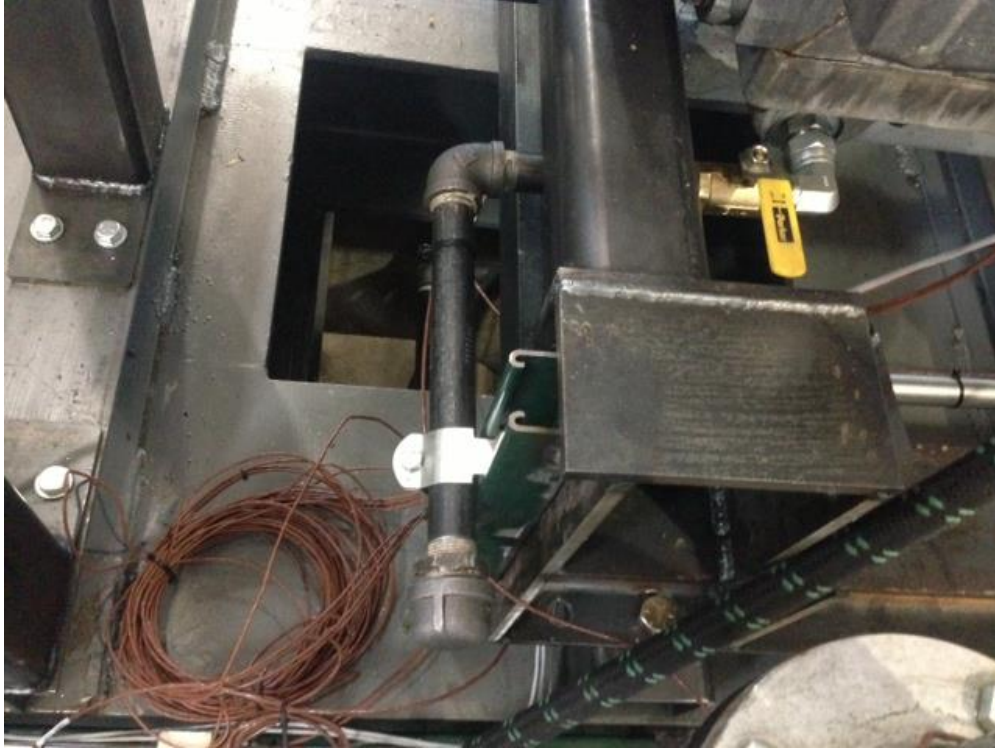


Figure 17: Oil Drain Plumbing

2.6 AIR STARTER

Cummins sent a pneumatically controlled starter. The compressed air comes from the facility which can be pressurized up to 10 bar. The compressed air can be shut-off with a threaded ball valve. By closing the valve, it ensures that the starter cannot be accidentally triggered while working on the engine. The oil reservoir, not being pressurized, can be refilled while being isolated from the compressed air. Figure 18 shows the air starter and the associated plumbing.



Figure 18: Air Starter

2.7 INSTRUMENTATION

2.7.1 BATTERY INSTALLATION

Two 12 volt batteries were wired in series to supply power to the ECM and to the control panel. The batteries were installed next to the engine and sit next to the control panel. Both batteries were maintained with a low current battery charger.

2.7.2 ENGINE INSTRUMENTATION AND CONTROL PANEL

Cummins provided CSU with an instrumentation list for the test cell. A total of twenty-five temperature measurements and twenty-nine pressure measurements were installed on the QSK19 engine. Of these, eight temperature and pressure measurements were required to monitor test cell (test cell ambient temperature, SCR inlet temp, water pump inlet pressure, exhaust restriction

etc). The remaining temperature and pressure measurements were required to monitor engine parameters (fuel filter inlet pressure, crankcase pressure, oil rifle temperature, exhaust port temperature etc). An entire instrumentation list can be found in the appendix.

Rosemount pressure transducers were installed with 3/8in (9.53mm) stainless steel tubing to measure critical engines parameters such as: turbine rear in pressure, turbine front in pressure, intake manifold pressure, compressor outlet, and crankcase pressure. The Rosemount pressure transducers were mounted to the control panel in a row along the south side of the engine (Figure 19). The remaining pressure measurements were recorded with pressure sensors as shown in Figure 8. Per Cummins request, type E thermocouples were used to monitor all temperature measurements.



Figure 19: Rosemount Pressure Transducers

All sensors are connected to the control panel which was being controlled by a National Instruments (NI) Compact FieldPoint cFP-2200 system. The system contains 8 modules that handle varying signals coming from the engine instrumentation. All signals were posted in an array which is extracted and displayed/recorded on the LabView engine interface software.

2.7.3 ENCODER INSTALLATION

The high resolution BEI rotary encoder was provided by Cummins to determine the crankshaft position for the cylinder pressure measurements. The encoder shaft is connected to the crankshaft with an adapter plate that was also provided by Cummins. Since the mounting locations were the same for the diesel and natural gas QSK19 engines, the encoder stand was taken from the installed QSK19G natural gas engine and placed in the diesel test cell. The encoder stand was fabricated by Frank Sutley [22]. Figure 20 shows the encoder, adapter plate and engine balancer for the QSK19 diesel engine.

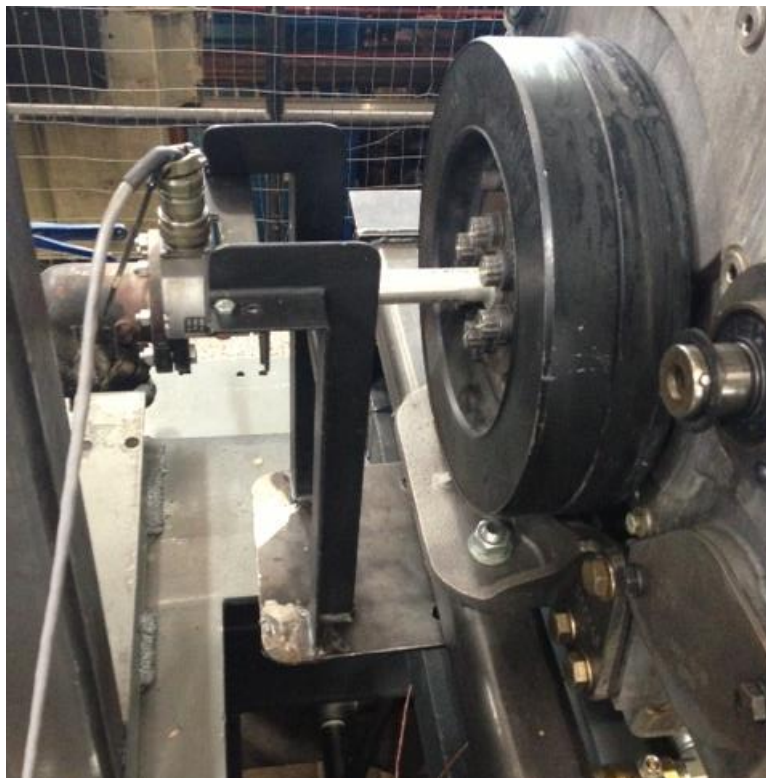


Figure 20: Encoder Mounting System

2.7.4 PRESSURE TRANSDUCER AND COMBUSTION CART

The Cummins QSK19 was shipped with a water cooled AVL QC34C piezoelectric pressure transducer. The pressure transducer signal cable was connected to a charge amplifier. The charge

amplifier was then connected to Colorado State University combustion analyzer to record the voltage. An ITW water to air heat exchanger was installed to keep the transducers at operating temperature. Figure 21 shows the combustion chart and the water to air heat exchanger. The software for the system was written by Kirk Evans.



Figure 21: Colorado State University Combustion Chart and Heat Exchanger

CHAPTER 3: QSK50 ENGINE INSTALLATION

3.1 ENGINE SPECIFICATION

The Cummins QSK50 is a 50L 16-cylinder diesel engine that utilizes two-stage Holset turbocharging coupled with an electronic wastegate for each bank. The engine has two-stage oil filter, steel pistons and operated using a modular common rail fuel system (MCRS). The Cummins QSK50 produces a peak power of 1865 kW (2500 hp) at 1900 rpm and a maximum torque of 9125 N-m (6730 ft-lbs) at 1800 rpm. The engine geometry and rating can be found on the following table.

Table 2: QSK50 Engine Geometry and Rating

Engine	Cummins QSK50
Configuration	V-16 Turbocharged
Displacement	50 liter
Bore	159 mm
Stroke	159 mm
Compression Ratio	14.7:1
Rated Power	1865 kW @1900 rpm
Maximum Torque	9125 N-m @ 1800 rpm

3.2 SOLIDWORKS TEST CELL MODEL

After the completed installation and testing for the Cummins QSK19, a Cummins QSK50 two-state diesel engine was installed in the same test cell. Similar to the QSK19, a three dimensional SolidWorks model was created to help with the engine installation. The model was critical in designing the engine mounts, air and exhaust plumbing, coolant plumbing and flywheel adapter. The engine dimensions (mounting locations, height, width, turbocharger connections) were

provided by Cummins via an installation drawing. Since the same drive-shaft was used for both the QSK19 and the QSK50, the center line of the flywheel was slightly offset from the dynamometer to ensure proper wear on the driveshaft bearings. The SolidWorks model is shown in Figure 22.

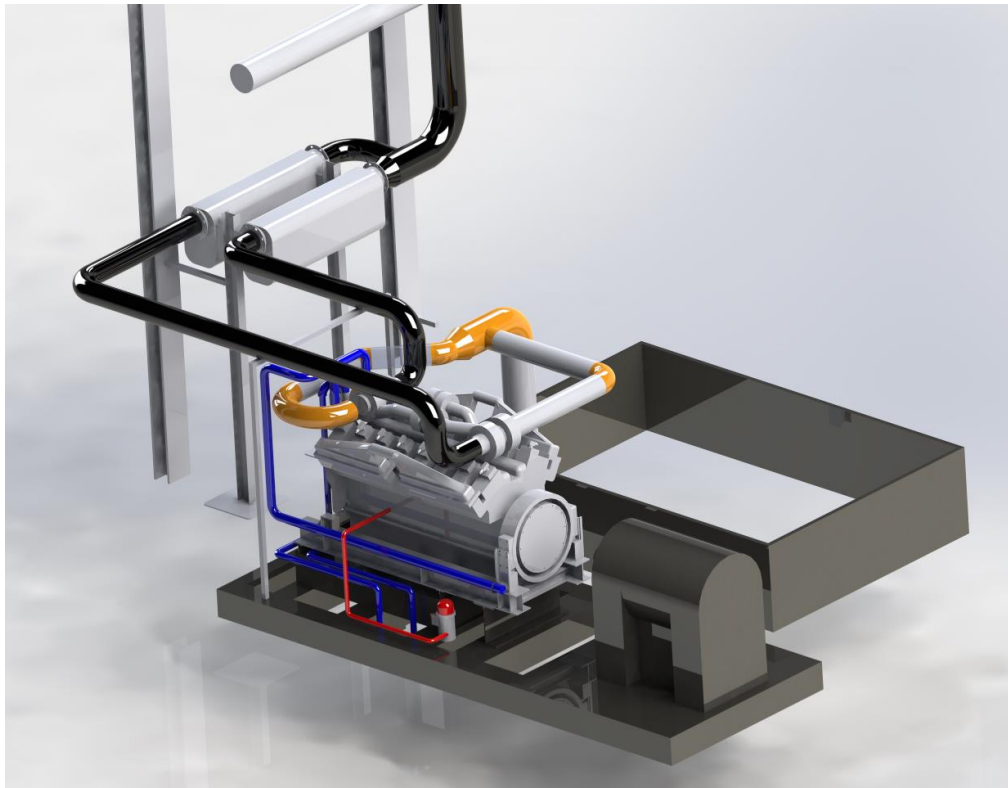


Figure 22: 3D QSK50 Solidworks Render Model

3.3 ENGINE MOUNT BRACKETS

The QSK50 three dimensional SolidWorks model was used to design the front and rear engine mounting brackets. The mounting brackets were MIG welded to an 8in (203.2mm) X 8in (203.2mm) X 144in (2895.6 mm) 35lb I-beam. The QSK50 mounting locations on the flywheel housing were much wider than the QSK19 mounting locations which caused the weight to be distributed offset from the center of the I-beam. To combat this issue and increase rigidity, 1/2in

(12.7mm) steel plates were welded underneath the mounting brackets and between the flanges of the I-beam.

The front engine mount bracket was constructed from a 30in (762mm) section of 2in (50.8 mm) X 4in (101.6mm) X 3/8in (9.525mm) thick rectangular tubing. The rectangular tubing was MIG welded to 1/2in (12.7mm) steel plate open boxes. The 1/2in (12.7mm) steel plate boxes were cut from a water jet using Bobcat software, whereas, the square tubing was cut with a horizontal band saw. To reduce the stress concentration on the corners of the box, 1/2in (12.7mm) steel triangular pieces were welded to the sides and bottom of the boxes. Figure 23 shows the model and the actual front engine bracket.

Unlike the QSK19 install, the rear engine mounting bracket was constructed differently than the front mounting bracket. The front engine mounting bracket was cut from 1/2in (12.7mm) steel plates with a water jet. Due to the allowable offset for the drive shaft, the height was determined by allowing enough clearance for a short radius elbow on the coolant and after coolant plumbing. The height of the brackets from the I-beam was 16.875in (428.625mm). This gave a 1/4in (6.35mm) height offset from the driveshaft and a 1/2in (12.7mm) clearance for the after cooler plumbing. As shown in Figure 24, a 1/2in (12.7mm) open box was welded to the bracket to distribute stress on the plate and bolts. To increase rigidity and to further reduce stress concentrations, gussets were welded to the side of the mounting plate. Since the weight of the engine and torque of the engine sit near the rear, additional plates were welded between the flanges of the I-beam. In addition, a 2in (50.8mm) X 6in (152.4mm) C-Channel was MIG welded between the I-beams to reduce skid vibration. Figure 24 shows the model and actual mounting brackets for the Cummins QSK50 engine.

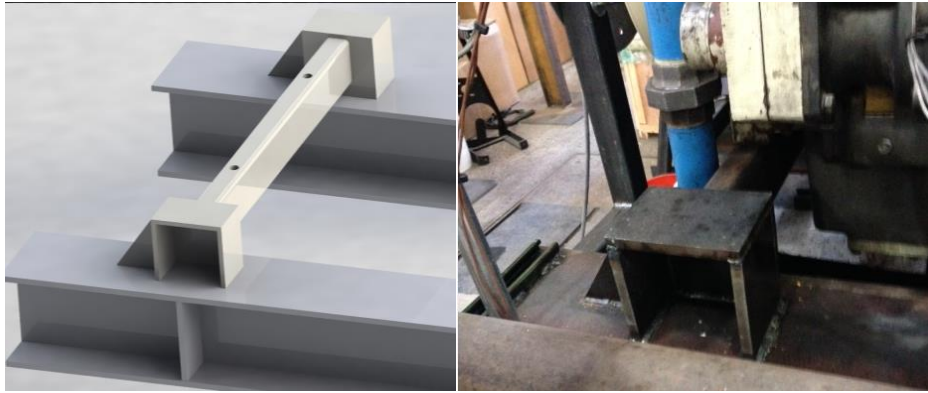


Figure 23: Model – Front Mounting Bracket (left), Actual- Rear Mounting Bracket (right)

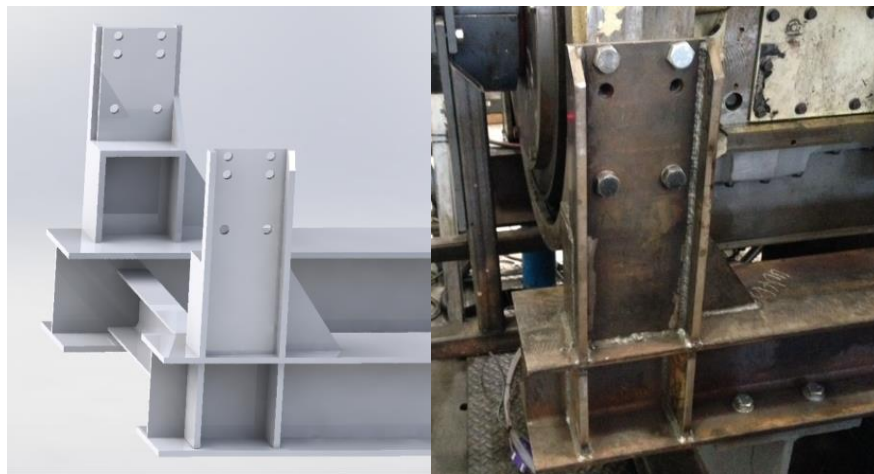


Figure 24: Model- Rear Mounting Bracket (left), Actual – Rear Mounting Bracket (right)

3.4 FLYWHEEL ADAPTER, DRIVESHAFT AND DYNAMOMETER CONNECTION

The flywheel adapter plate was designed to mate to the engine driveshaft with the QSK50 flywheel. The flywheel adapter plate was cut out of 1.5in (38.1mm) mild steel. A rough outline with an extra 1/2in (12.7mm) diameter was cut with a water jet. The 4in (101.6mm) hole in the center of the adapter plate was cut with the water jet so that the machinist could hold the flywheel adapter with a lathe. The remaining work on the flywheel adapter was sent to a machinist. He removed the remaining 1/2in (12.7mm) material off the diameter and 0.030in (0.762mm) of the back side of the adapter plate so that it would mate smoothly with the flywheel.

As previously mentioned, the 1/4in (6.35mm) engine to dynamometer height offset was determined to allow enough clearance for the coolant plumbing. Due to this, the alignment offset was less than 1.5° which is well within the 7° allowable offset for the driveshaft. The driveshaft cover was carried over from the QSK19 install.

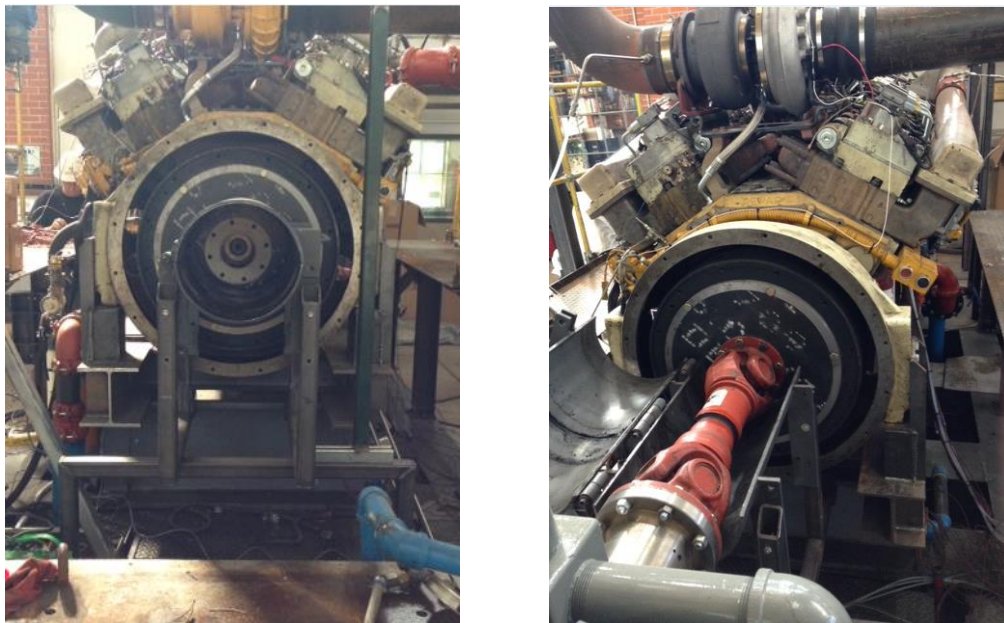


Figure 25: Flywheel Adapter (left), Driveshaft Cover and Dynamometer Connection (right)

3.5 PLUMBING SYSTEMS

3.5.1 DIESEL FUEL PLUMBING

The QSK50 engine required a maximum delivery of 2.5 GPM of diesel fuel. Due to this, the EECL purchased a used 2000 gallon (steel and concrete) UL2085 AST fuel tank. For the QSK50 engine, the fuel line was increased from 1in (25.4mm) to 1.5in (38.1mm) to maintain flowrate and pressure drop requirements. The remaining fuel system (pump, flowmeter, filters, heat exchanger, pressure and temperature measurements) were carry-over components from the QSK19 install. Refer to page 17 for more details.

3.5.2 INTAKE AIR PLUMBING

Cummins required that the QSK50 engine operate at sea-level conditions. To meet this requirement using the existing roots supercharger, the diameter of the pipe was increased from 8in (203.2mm) to 12in (304.8mm). This reduced the pressure losses across the pipe and allowed the lab to achieve sea-level pressure. The intake pipe was 12in (304.8mm) schedule 40 steel with Victaulic fittings (elbows, unions, tee). An orifice was installed below the engine to measure the volumetric flowrate via the American Gas Association (AGA) method. A bracket was fabricated to hold up the Rosemount pressure transducers. The temperature sensor was 12in (304.8mm) away from the flange connection – see Figure 26.



Figure 26: Orifice Installation for Intake Air Plumbing

The two-stage QSK50 has an intake system for each bank (left and right). Prior to the flow split for each bank, temperature and pressure measurements were recorded on the 12in steel pipe. The flow split was constructed of a Victaulic 12in (304.8mm) X 8in (203.2mm) X 8in (203.2mm) tee. The 12in (304.8mm) pipe was reduced to 8in (203.2mm) to match the diameter of the compressor inlet connection. Just before the connection to the right bank, a Cummins built pipe was installed to route the telemetry wires from the sensor to the telemetry transmitter. All

fittings (short radius elbow, long radius elbow, 45deg fitting) were constructed of Victaulic 8in (203.2mm) pipe. Figure 27 shows the intake air plumbing for both the right and left bank.



Figure 27: Left Bank Intake System (left), Right Bank Intake System (right)

3.5.3 EXHAUST AIR PLUMBING

Both the left and right bank turbine outlet flange connections are 8in (203.2mm). Connected to the engine were two 90 degree 8in elbows that aligned the exhaust plumbing 18in above the intake system. Straight exhaust pipe was welded to the exhaust elbows. A flexible steel section was installed to help engine vibration, thermal expansion and tolerance stack-up. After the straight sections, additional 8in elbows were installed prior to entering the SCR catalysts. Similar to the QSK19 install, the SCR catalysts were not injecting urea. For this particular case, the catalysts coupled with a butterfly valve were used to increase exhaust back pressure. Both SCR catalysts were mounted to a 6in (152.4mm) X 4in (101.6mm) 12lb I-beam. After leaving the SCR catalysts, the exhaust recombined to 12in (304.8mm). The pneumatic butterfly fly was installed once the exhaust was recombined. After leaving the butterfly valve, an additional

flexible section and a long radius 12in (304.8mm) elbow were installed to route the QSK50 exhaust pipe to the facilities main exhaust line – see below:



Figure 28: Plumbing from Engine (left), Plumbing post SCR Catalysts (right)

3.5.4 AFTER COOLER PLUMBING

The QSK50 uses an integrated low temperature aftercooler instead of a charge air cooler. The aftercooler plumbing was slightly modified from the QSK19 CAC plumbing arrangement. The aftercooler plumbing was a combination of threaded black steel pipe and TIG welded elbows and reducers. The supply line diameter is 2in (50.8mm) to match the pre-existing test cell pipe. Since the test cell aftercooler pump was oversized for the QSK19 and QSK50, a threaded ball valve was installed to help control the flow rate entering the aftercooler. After a few 90 degree elbows, a flex-section was installed to help with engine vibration and tolerance stack-up. The remaining supply line consists of a 2in (50.8mm) elbow followed by a 3X2in reducer that is TIG welded to a 3in (76.2mm) short radius elbow that mounted directly to the aftercooler supply pump inlet – see Figure 29.

The aftercooler outlet mounting connection was not provided by Cummins; therefore, it was cut out with a water jet using 3/8in (9.525mm) steel plate. To avoid a variety of engine components, the aftercooler plumbing was installed at a 45deg angle away from the engine.

Similar to the aftercooler supply plumbing, the aftercooler return plumbing was a combination of TIG welded and threaded pipe. Conveniently, the flex-section separated the TIG welded pipe from the threaded pipe. The entire return line diameter is 2in (50.8mm) to match the pre-existing test cell pipe and the aftercooler outlet diameter. For reference, refer to Figure 30.

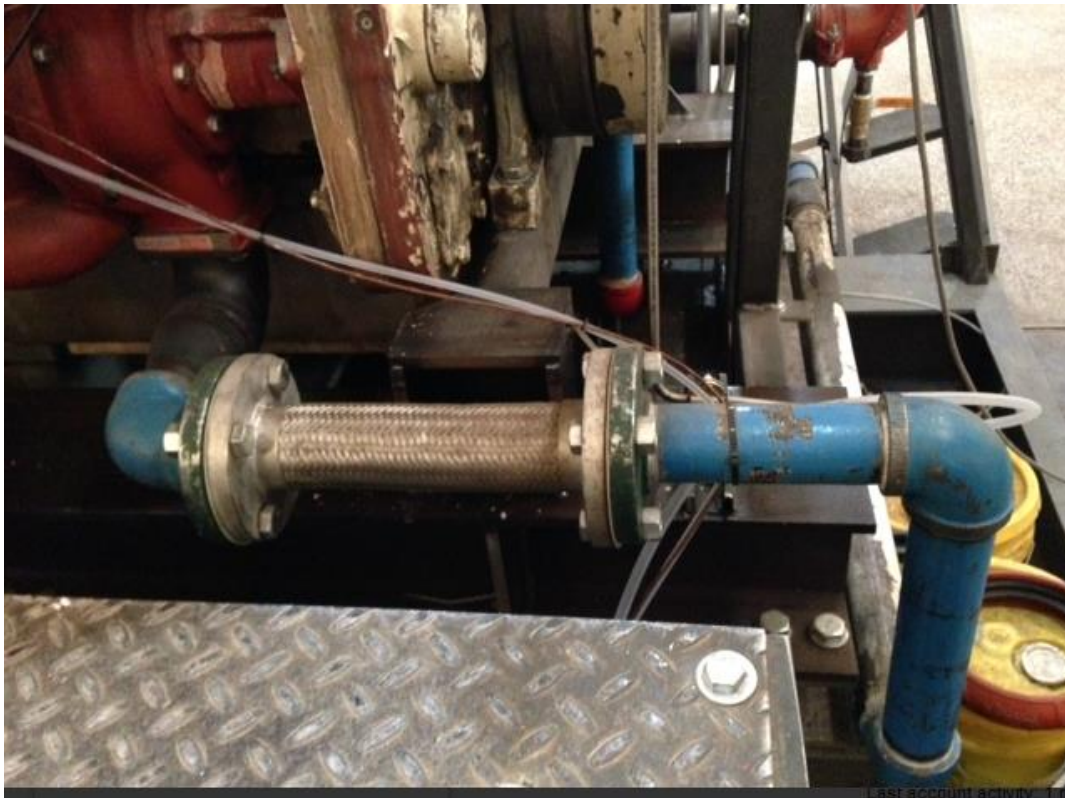


Figure 29: QSK50 Aftercooler Supply Plumbing



Figure 30: Aftercooler Return Plumbing

3.5.5 COOLANT PLUMBING

The coolant plumbing lines were modified from the QSK19 engine to fit the QSK50 engine. The coolant supply line was re-routed from the flange connection with the blue valve to the water pump inlet on the engine (Figure 31). From the blue valve, a 4in (101.6 mm) EPDM rubber flexible tube was installed. From the EPDM rubber tube, a flange connects two 4in (101.6mm) 90degree Victaulic orange fittings. After the Victaulic elbows, a 4in (101.6mm) butt-welded short radius elbow connects to the water pump inlet. 1in (25.4mm) threaded black steel pipe was used to drain the engine with coolant – see Figure 31.

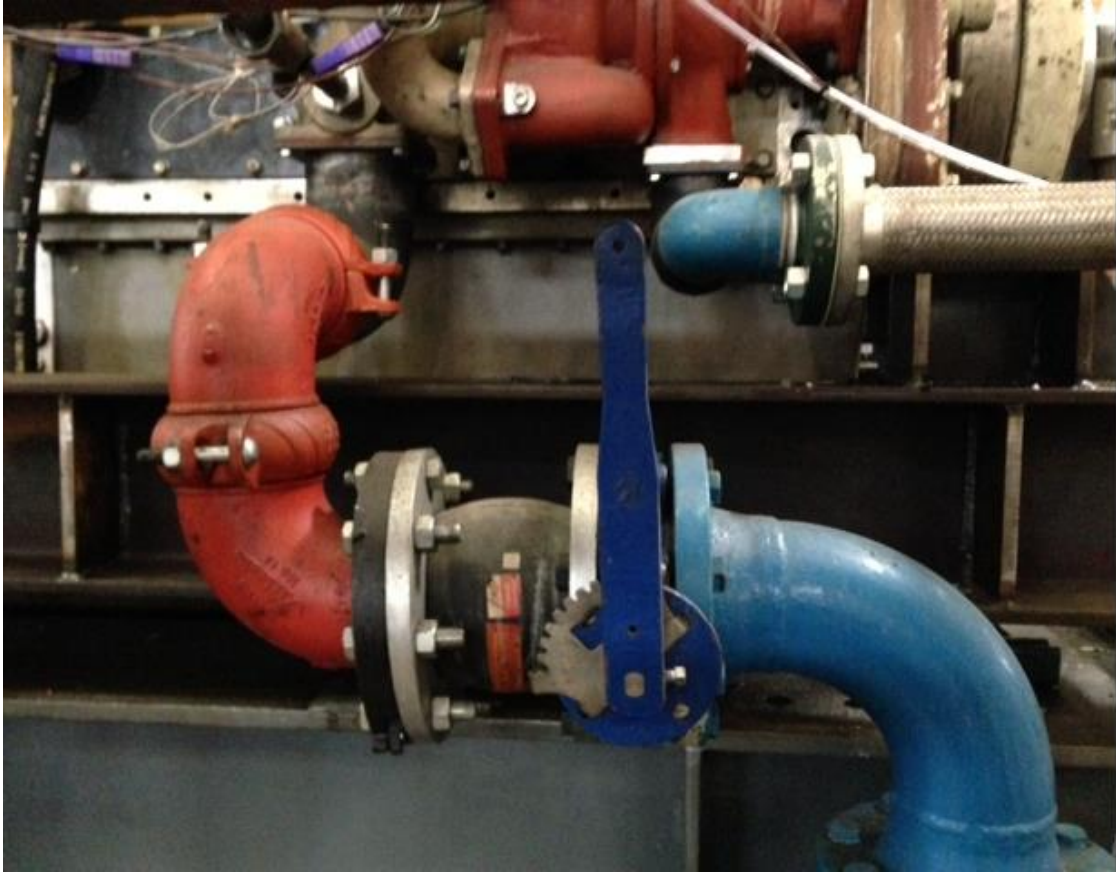


Figure 31: Coolant Supply Plumbing

The engine returns coolant at the highest point on the QSK50 engine. The coolant return line utilized a combination of TIG welded elbows, tees, Victaulic fittings and hoses. The jacket water return pipe was 3in (76.2 mm) in diameter. The coolant return plumbing was designed such that it had enough clearance to go above the inlet air plumbing and below the exhaust air plumbing. A Victaulic drain elbow and threaded ball valve was installed to drain the coolant of the return line. The coolant return plumbing is shown below:



Figure 32: Coolant Return Plumbing (left), Victaulic Drain Elbow (right)

3.5.6 OIL DRAIN PLUMBING

Since the QSK19 never required an oil change, the QSK50 never incorporated any plumbing for an oil drain. An oil drain port can be incorporated underneath the engine if necessary.

3.6 AIR STARTER

The air starter from the QSK19 could not be used for the QSK50 because it would interfere with the pre-lube pump; therefore, the air starter from the 69L natural gas caterpillar was used. As shown in Figure 33, the electronic solenoid is actuated by incoming air from the 1/2in (12.7mm) Swagelok line. After passing through the actuator, the air is returned to actuate a pneumatic valve that allows the main air to flow through the air starter. Similar to the QSK19, a threaded ball valve was installed next to the engine that ensures the engine isn't accidentally started.

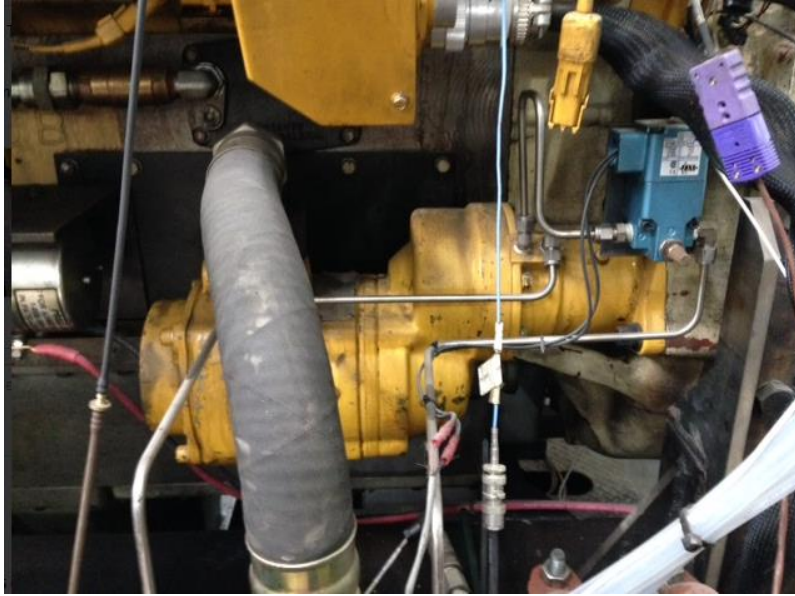


Figure 33: QSK50 Air Starter

3.7 INSTRUMENTATION

3.7.1 BATTERY INSTALLATION

The QSK50 testing required two 12 volt batteries wired in series to supply power to the ECM and to the control panel. The batteries were installed next to the engine and sit next to the control panel.

3.7.2 ENGINE INSTRUMENTATION AND CONTROL PANEL

Cummins provided CSU with an instrumentation list for the QSK50 testing. A total of forty-six temperature measurements and forty-three pressure measurements were installed on the QSK50 engine. Due to the number of temperature and pressure measurements, a portable NI PXIe-1078 Express Chassis was purchased to accommodate the extra measurements – see Figure 34. Of these, eleven temperature and pressure measurements were required to monitor test cell parameters (test cell ambient temperature, LP compressor inlet pressure – right bank, LP compressor inlet pressure-left bank, water pump inlet pressure etc). The remaining temperature and pressure measurements were required to monitor engine parameters (intake manifold

pressure – right bank, intake manifold pressure – left bank). An entire instrumentation list can be found in the appendix.

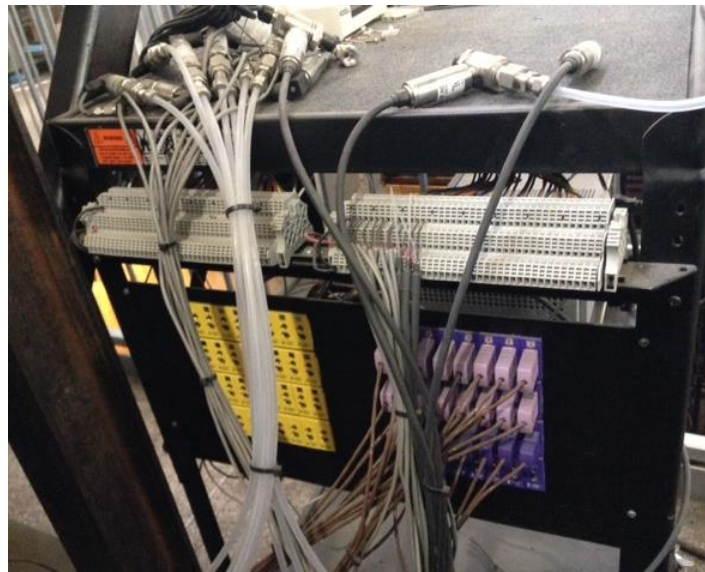


Figure 34: Portable NI PXIe-1078 Chassis Chart

The left and right bank turbocharger pressure parameters were monitored by Rosemount pressure transducers described on page 29. The other pressure measurements were being motored by the pressure sensors shown in

Figure 8. All thermocouples for the testing were type E. The remaining sensors were being controlled by a NI Compact FieldPoint cFP-2200 system described on page 29.

3.7.3 ENCODER INSTALLATION

The BEI rotary encoder used for the QSK50 testing was the same encoder used for the QSK19 testing. Similar to the QSK19 install, the encoder shaft was connected to the crankshaft with an adapter plate that mounted to the harmonic balancer. The encoder stand was built from 2in (50.8mm) square tubing. Angle iron was welded to the square tubing in order to bolt the stand to the test cell skid. The encoder is directly mounted to a 14in (355.6mm) diameter plate as shown in Figure 35.



Figure 35: QSK50 Encoder Installation

3.7.4 PRESSURE TRANSDUCER AND COMBUSTION CART

The Cummins QSK50 was shipped with water cooled AVL QC34C piezoelectric pressure transducer for cylinder 1R, 5R, 4L and 8L. Each transducer was connected to a charge amplifier that connects to the combustion analyzer. CSU combustion analyzer allows up to 6 pressure transducers. The same combustion analyzer was used for both the QSK19 and QSK50 testing. For more information, refer to section 2.7.4.

CHAPTER 4: GT-POWER MODELING RESULTS

4.1 QSK19 RESULTS

Eight steady state operating conditions were selected by Cummins to perform GT-Power modeling. At each operating point, GT-Power was matched against measured data at 5000ft (1526m) using the criteria set by Cummins. After each point was calibrated, the operating points were extrapolated to 8000ft (2438m). The turbine inlet temperature, rotor speed, and expansion ratio were recorded and sent back to Cummins for further review. The operating conditions can be found on the following table. The table can be separated into two categories: points 1-4 and points 5-8. Points 1-4 had higher rotor speeds than points 5-8. The rotor speed in the following table is normalized by the mechanical limit for the turbocharger.

Table 3: Operating Conditions for QSK19 GT-Power Modeling

Operating Point	Speed (rpm)	Power (hp)	Torque (ft-lbs)	Normalized Rotor Speed
1	1600	701.2	2304	0.94
2	1800	689	2013	0.96
3	2000	628.3	1650	0.96
4	2200	550.8	1316	0.97
5	1600	484.5	1592	0.70
6	1800	445.4	1301	0.76
7	2000	392.6	1031	0.77
8	2200	332.4	769.9	0.80

4.1.1 QSK19 IN-CYLINDER COMBUSTION RESULTS

Accurate representation of in-cylinder combustion is necessary to precisely model an engine's performance. As shown in the following figures, GT-Power matches experimental data

extremely well for in-cylinder pressure measurements. For operating points 1-4, peak cylinder pressure varied within 50 psi, whereas, peak cylinder pressure varied within 30 psi for operating points 5-8. In addition, GIMEP varied within 2 percent for all but one operating point (point 4) which varied within 5 percent. The following figures are normalized by the maximum cylinder pressure provided by Cummins.

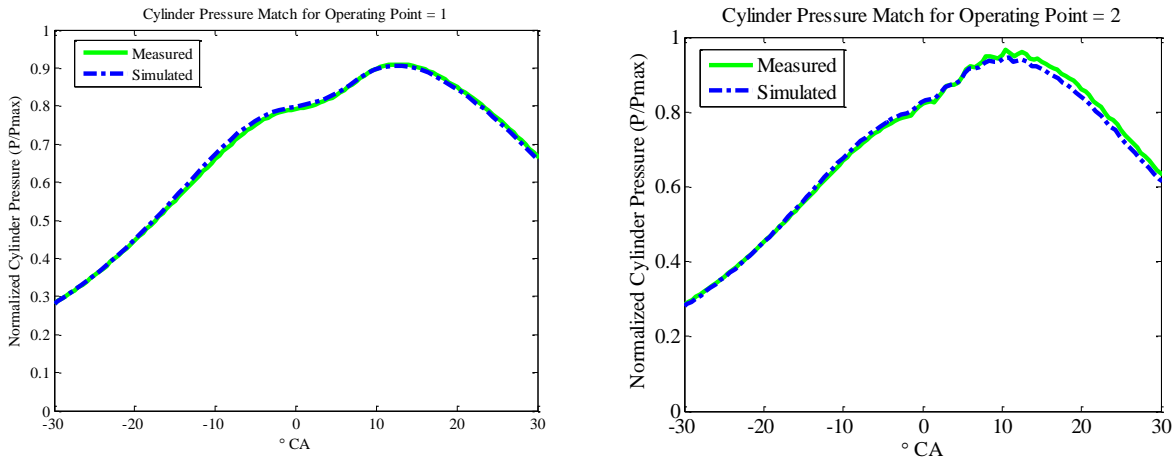


Figure 36: QSK19 Normalized Cylinder Pressure vs. CA for Operating Conditions 1 & 2

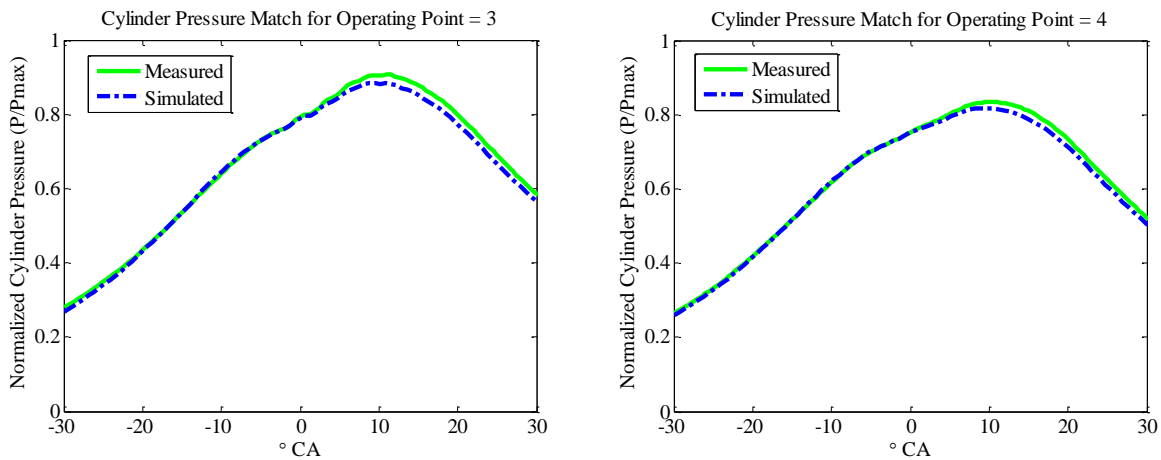


Figure 37: QSK19 Normalized Cylinder Pressure vs. CA for Operating Conditions 3 & 4

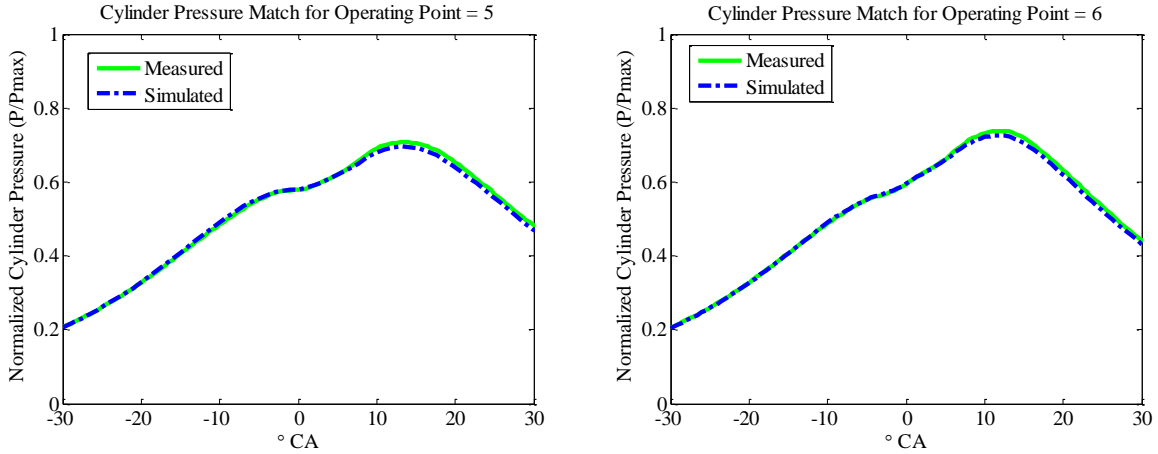


Figure 38: QSK19 Normalized Cylinder Pressure vs. CA for Operating Conditions 5 & 6

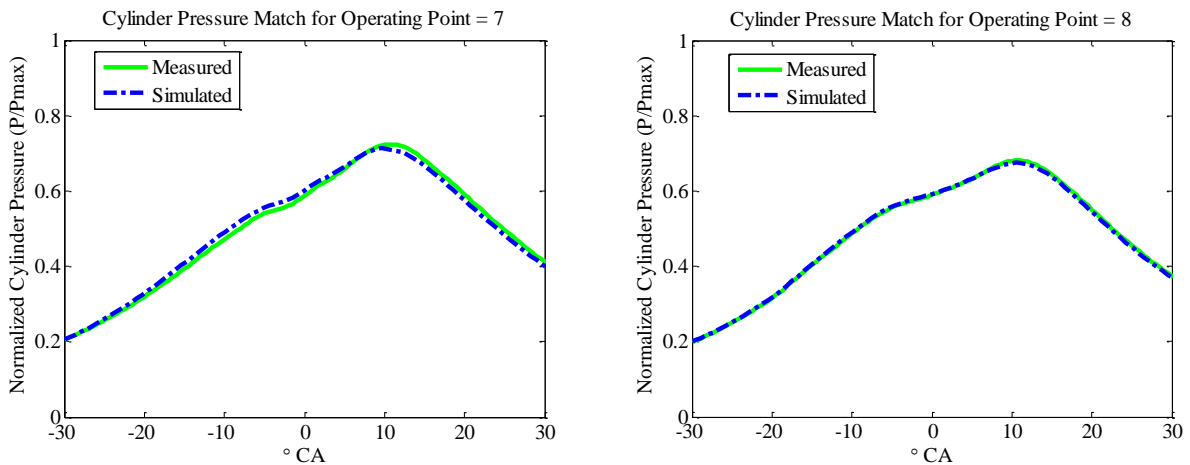


Figure 39: QSK19 Normalized Cylinder Pressure vs. CA for Operating Conditions 7 & 8

4.1.2 QSK19 CALIBRATION RESULTS FOR THE FIRST OPERATING POINT

Once the in-cylinder combustion model was complete, few adjustments were needed to match measured power, torque, rotor speed, intake manifold temperature, etc. Fueling was adjusted, within two percent of the experimental data, to match the engine power. The rotor speed was slightly adjusted by varying the friction mechanical efficiency term between 0.94 and 1. The heat exchanger effectiveness was adjusted to match intake manifold temperature.

The experimental vs. simulation result for the first operating point is reviewed below.

The remaining points can be found in the appendix. As shown in the following table, GT-Power

is able to predict within three percent of measured data for any of the following parameters.

Although the majority of the operation points varied with 5% of measured data, two operating point (4 and 8) varied within 7% from any measured data. Other researchers has shown that GT-Power can predict within 5-10% variation from measured data [3,23,24].

Table 4: Experimental vs. GT-Power Results for the First Operating Condition

Operating Point = 1				
Normalized Parameter	Test Cell	GT-Power	GT-Power Percent Variation	Measurement Error
Speed (rpm)	1600.00	1600.00	0.00	±1RPM
Power (bhp)	701.20	700.35	0.12	±0.50
BSFC	0.85	0.85	0.44	Calculated
Airflow	0.87	0.85	2.73	±0.50
A/F	0.63	0.62	2.18	Calculated
Compressor Out Temp	0.97	0.96	1.17	±0.75
Turbine In Temp	0.89	0.89	-0.56	±0.75
Turbocharger Speed	0.94	0.95	-1.44	±0.50
Cylinder Pressure	0.91	0.91	0.35	±0.106
Normalized Parameter	Test Cell	GT-Power	GT-Power Percent Variation	Measurement Accuracy
AMB_P	0.21	0.21	0.00	±0.50
Comp_in_P	0.20	0.20	0.44	±0.50
Comp_out_P	0.86	0.86	0.01	±0.50
Int_Mnf_P	0.85	0.84	0.83	±0.50
Tur_in_P	0.83	0.82	1.72	±0.50
Tur_out_P	0.23	0.23	0.01	±0.50
Expansion Ratio	0.90	0.89	1.72	Calculated
Normalized Parameter	Test Cell	GT-Power	GT-Power Percent Variation	Measurement Accuracy
AMB_T	0.31	0.31	0.00	±0.75
Comp_in_T	0.31	0.31	0.00	±0.75
Comp_out_T	0.53	0.52	1.17	±0.75
Int_Mnf_T	0.34	0.34	0.36	±0.75
Exh_port_T	0.82	0.86	-4.87	±0.75
Tur_in_T	0.88	0.89	-0.56	±0.75
Tur_out_T	0.69	0.70	-0.83	±0.75
Normalized Parameter	Test Cell	GT-Power	GT-Power Percent Variation	Measurement Accuracy
GIMEP	0.94	0.95	-0.95	Calculated
Volumetric Efficiency	0.93	0.92	1.00	Calculated

The normalized pressures and temperatures for the first operating point are shown graphically in the following two figures.

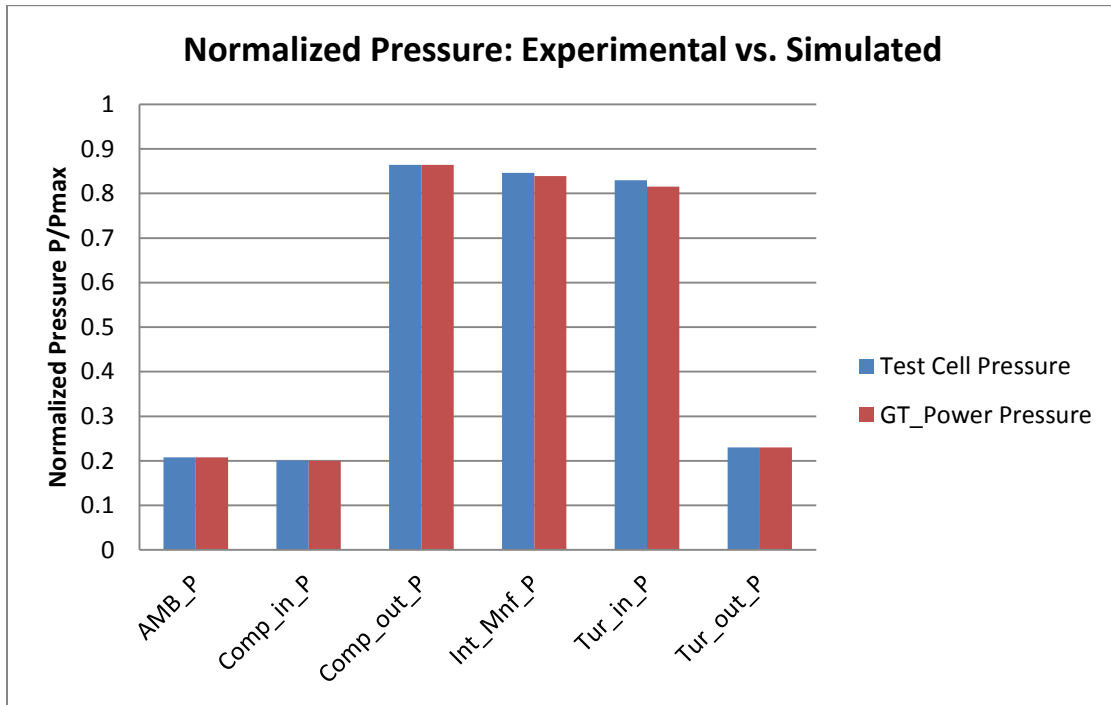


Figure 40: Normalized Pressure: Experimental vs. Simulated Results for Operating Point:1

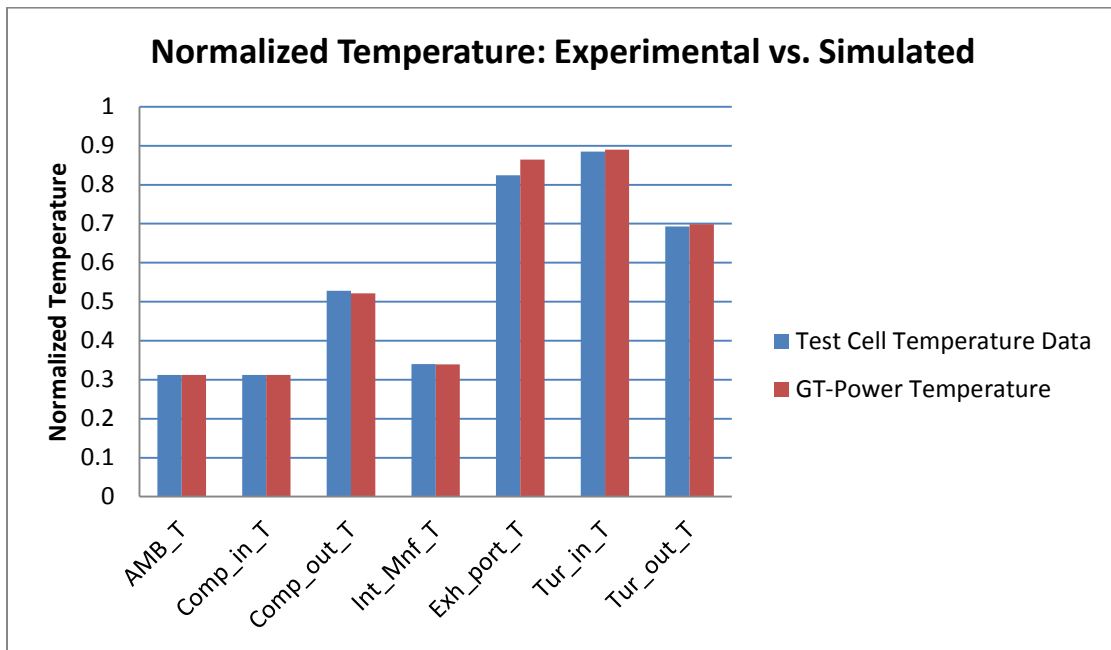


Figure 41: Experimental vs. Simulated Temperature Results for Operating Point:1

4.1.3 QSK19 CALIBRATION RESULTS FOR THE TURBOCHARGER

The rest of the results for the QSK19 modeling will focus on GT-Power prediction for rotor speed, expansion ratio and turbine inlet temperature. The simulated results vs. measured data are summarized on the following three figures. Seven of the eight operating points varied within 1.5% of measured data for the rotor speed. The last point (point 8) varied within 2% of measured data – see below:

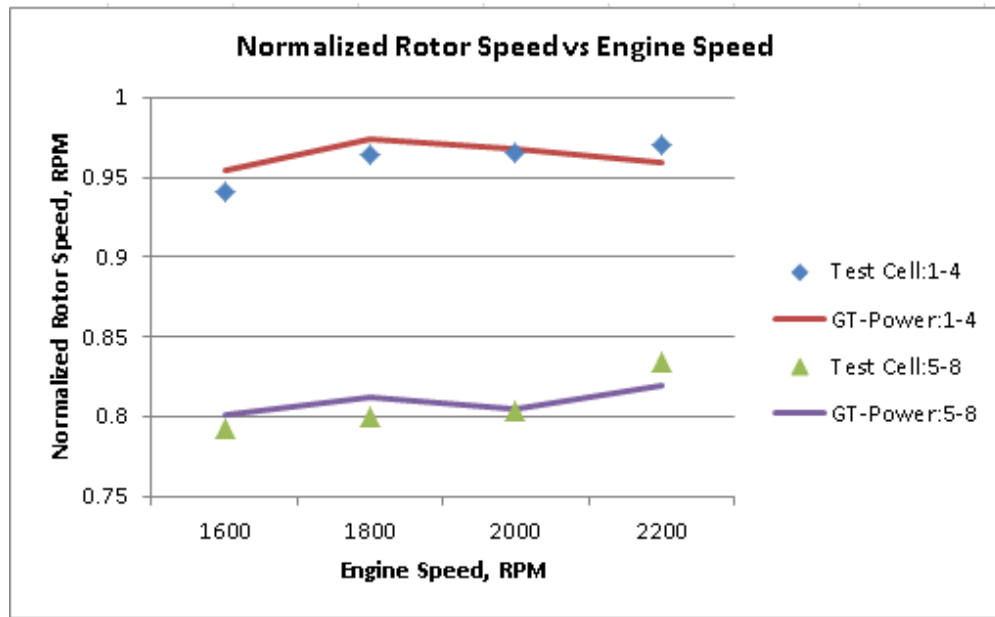


Figure 42: QSK19: Normalized Rotor Speed vs. Engine Speed

As engine speed increased, rotor speed, expansion ratio and charge flow increased for the measured data. Both the increase in expansion ratio and charge flow is a result from the wastegate position. As the wastegate closes, the turbine inlet pressure increase which slightly increases rotor speed. The increase in rotor speed causes an increase in charge flow. The turbine outlet pressure remained relatively constant for all operating points, therefore, the expansion ratio increases. GT-Power predictions varied within 3% of measured data for speeds below 1800 RPM, whereas, GT-Power predictions varied within 6.5% of measured data for speeds above

1800 RPM. The 6.5% variation can be contributed to the simulated time averaged value that neglects pressure pulsations from the exhaust manifold [15].

The time averaged value from GT-Power is selected due to two reasons. The power of the compressor and turbine cannot be calculated using the instantaneous values over the complete cycle. The other reason is because the static pressure measurement closely resembles the time averaged pressure from GT-Power [15]. The following figure is an example of the variation in expansion ratio vs. CA for the QSK19 engine.

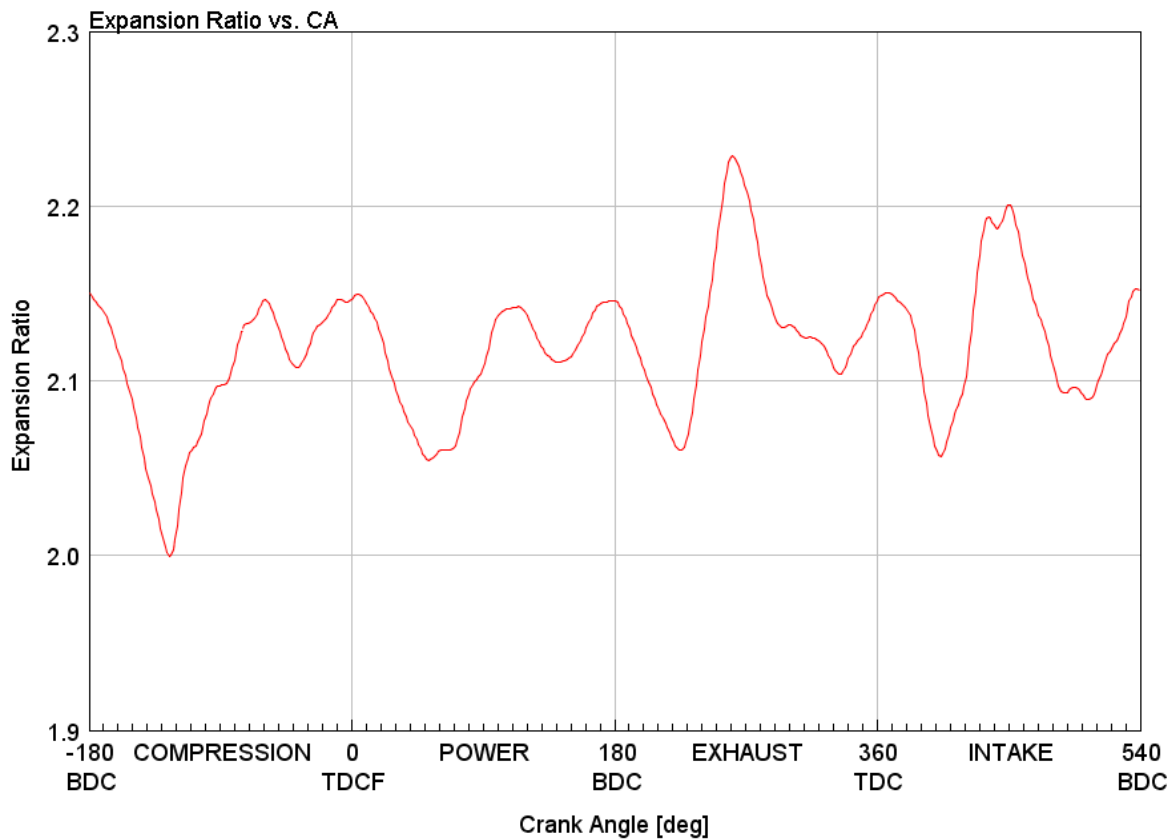


Figure 43: Expansion Ratio vs. CA Considering Pressure Pulsations

GT-Power was able to predict within 1.5% of measured data for turbine inlet temperature (TIT) at all operating conditions. Turbine inlet temperature decreases with engine speed as a result of reducing the engine power to match the rotor speed.

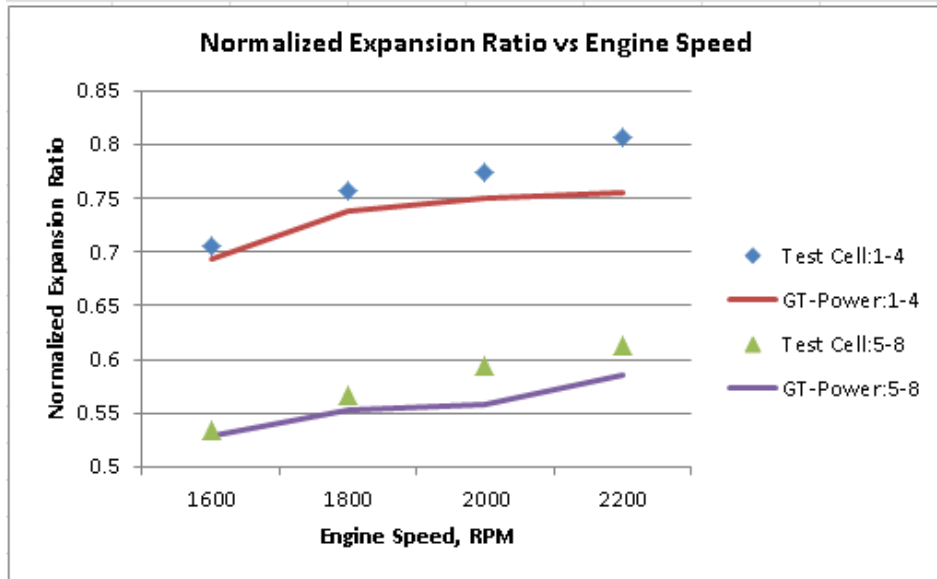


Figure 44: Normalized Expansion Ratio vs. Engine Speed

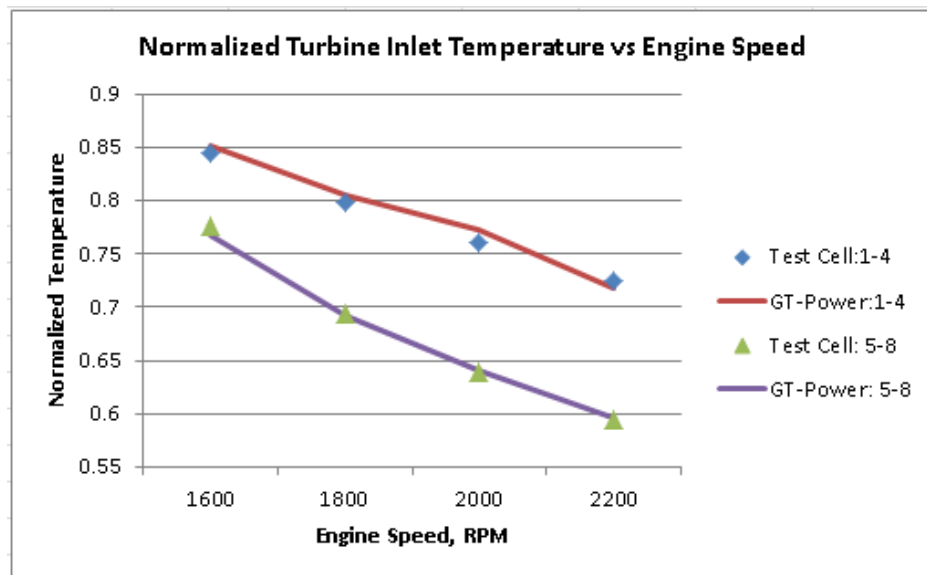


Figure 45: QSK19: Normalized Turbine Inlet Temperature vs. Engine Speed

4.1.4 QSK19 EXTRAPOLATION CASE STUDY RESULTS

Since the rotor speed varied within 2% percent of measured data for all points, a case study was performed to determine which rotor speed should be targeted (measured or simulated) when the model was extrapolated to 8000ft. GT-Power has the ability to solve for a target dependent variable by varying one or more independent variables. After the model was calibrated under

sections 4.1.1-4.1.3, GT-Power direct optimizer was used to target rotor speed by varying the fueling. After the rotor speed was matched within ± 1 RPM of measured data, the expansion ratio and the turbine inlet temperature was recorded and compared against the method described in sections 4.1.1 -4.1.3. Since this thesis is focused on turbocharger performance, other parameters were ignored for the direct optimizer method. The case study was validated against experimental results at 5000ft.

As shown in Table 5, columns B and C represent the method described in sections 4.1.1 - 4.1.3. This method matched power, BSFC, airflow, air to fuel ratio, cylinder pressure, GIMEP, expansion ratio, rotor speed, compressor outlet temperature and turbine inlet temperature against measured data. Columns E and F represent the results using the direct optimizer method that matched only the rotor speed. After the rotor speed was matched, the expansion ratio and the turbine inlet temperature were recorded and tabulated. The method described in sections 4.1.1 - 4.1.3 varied the rotor speed within 2%, whereas, the direct optimizer matched the rotor speed within ± 1 RPM. The method in sections 4.1.1 -4.1.3 varied the expansion ratio within 1% to 6.5% from measured data, whereas, the direct optimizer method varied the expansion from 2% to 6% from measured data. The turbine inlet temperature for both the direct optimizer and the 4.1.1- 4.1.3 method were very similar. Since the results were similar for all categories, both methods were extrapolated to 8000ft and then the expansion ratio and turbine inlet temperatures were recorded. The extrapolation results were provided to Cummins for further evaluation. Since the extrapolation results varied within 2% of each other, the method described in sections 4.1.1-4.1.3 is outlined in the following pages. The direct optimizer method for the measured rotor speed can be found in the appendix.

Table 5: QSK19- Case Study to Determine Target Rotor Speed at 8000ft

A	B	C	D	E	F	G
Normalized Rotor Speed Match: Experimental vs. Simulation						
Calibration Method			Direct Optimizer Method to Target Rotor Speed			
Operating Point	Test Cell at 5000ft	GT-Power at 5000ft	GT-Power Percent Variation	Test Cell at 5000ft	GT-Power at 5000ft	GT-Power Percent Variation
1	0.94	0.95	1.44	0.94	0.94	0.00
2	0.96	0.97	1.01	0.96	0.96	0.00
3	0.97	0.97	0.21	0.97	0.97	0.00
4	0.97	0.96	1.13	0.97	0.97	0.00
5	0.79	0.80	1.16	0.79	0.79	0.00
6	0.80	0.81	1.51	0.80	0.80	0.00
7	0.80	0.80	0.11	0.80	0.80	0.00
8	0.83	0.82	1.86	0.83	0.83	0.01
Normalized Expansion Ratio Match: Experimental vs. Simulation						
Calibration Method			Direct Optimizer Method to Target Rotor Speed			
Operating Point	Test Cell at 5000ft	GT-Power at 5000ft	GT-Power Percent Variation	Test Cell at 5000ft	GT-Power at 5000ft	GT-Power Percent Variation
1	0.71	0.69	1.72	0.71	0.68	4.33
2	0.76	0.74	2.49	0.76	0.72	4.27
3	0.77	0.75	3.19	0.77	0.75	3.67
4	0.81	0.75	6.48	0.81	0.77	4.52
5	0.53	0.53	1.15	0.53	0.52	2.69
6	0.57	0.55	2.66	0.57	0.54	4.65
7	0.59	0.56	6.20	0.59	0.56	6.09
8	0.61	0.59	4.56	0.61	0.60	2.09
Normalized Turbine Inlet Temperature Match: Experimental vs. Simulation						
Calibration Method			Direct Optimizer Method to Target Rotor Speed			
Operating Point	Test Cell at 5000ft	GT-Power at 5000ft	GT-Power Percent Variation	Test Cell at 5000ft	GT-Power at 5000ft	GT-Power Percent Variation
1	0.84	0.85	0.80	0.84	0.84	0.04
2	0.80	0.81	1.06	0.80	0.80	0.33
3	0.76	0.77	1.61	0.76	0.77	1.37
4	0.72	0.72	0.88	0.72	0.72	0.00
5	0.78	0.77	0.96	0.78	0.78	0.84
6	0.69	0.69	0.29	0.69	0.69	0.76
7	0.64	0.64	0.27	0.64	0.64	0.27
8	0.59	0.60	0.39	0.59	0.61	2.49

4.1.5 QSK19 EXTRAPOLATION RESULTS FOR THE TURBOCHARGER

A few parameters were adjusted to extrapolate the model from 5000ft to 8000ft. The ambient temperature and pressure were adjusted according to SAE J1349 (see appendix). The oil temperature and the coolant temperature (used to predict the surface temperatures of the piston, wall and head) were adjusted according to a criteria provided by Cummins. The rest of the initial

conditions (intake restriction, exhaust restriction, burn rate and fuel flow) were assumed constant and didn't change from 5000ft to 8000ft.

The results are summarized on the following three tables. As shown in

Table 6, the rotor speed at 8000ft was optimized based on the rotor speed from the simulation results at 5000ft. GT-Power can predict within ± 1 RPM of the result from GT-Power at 5000ft. This was intentionally done to see the effect of expansion ratio and turbine inlet temperature at a fixed rotor speed.

Table 6: GT-Power Predictions for Rotor Speed from 5000ft to 8000ft

Normalized Rotor Speed Match: Experimental vs. Simulation				
Calibration Method				
Operating Point	Test Cell at 5000ft	GT-Power at 5000ft	GT-Power at 8000ft	GT-Power Percent Variation
1	0.94	0.95	0.95	0.00
2	0.96	0.97	0.97	0.00
3	0.97	0.97	0.97	0.00
4	0.97	0.96	0.96	0.00
5	0.79	0.80	0.80	0.00
6	0.80	0.81	0.81	0.00
7	0.80	0.80	0.80	0.00
8	0.83	0.82	0.82	0.00

At higher rotor speeds, the expansion ratio increased an average of 2.17% over the simulated results at 5000ft. At lower rotor speeds, the expansion ratio increased an average of 1.25% over the simulation results at 5000ft. This is expected since the turbine outlet pressure drops significantly from 5000ft to 8000ft.

Table 7: GT-Power Predictions for Expansion Ratio from 5000ft to 8000ft

Normalized Expansion Ratio Match: Experimental vs. Simulation				
Calibration Method				
Operating Point	Test Cell at 5000ft	GT-Power at 5000ft	GT-Power at 8000ft	GT-Power Percent Increase in ER
1	0.71	0.69	0.71	1.80
2	0.76	0.74	0.75	2.20
3	0.77	0.75	0.77	2.62
4	0.81	0.75	0.77	2.07
5	0.53	0.53	0.52	1.03
6	0.57	0.55	0.56	1.40
7	0.59	0.56	0.57	1.72
8	0.61	0.59	0.59	0.86

To maintain a similar exhaust energy and rotor speed, fueling has to be decreased as inlet air density decreases. As shown in Figure 46, fueling was decreased an average of 9.04% to reach the required rotor speed and similar equivalence ratio. Figure 47 shows the difference in equivalence ratio from 5000ft to 8000ft. The difference in equivalence ratio falls within the predicted error from GT-Power.

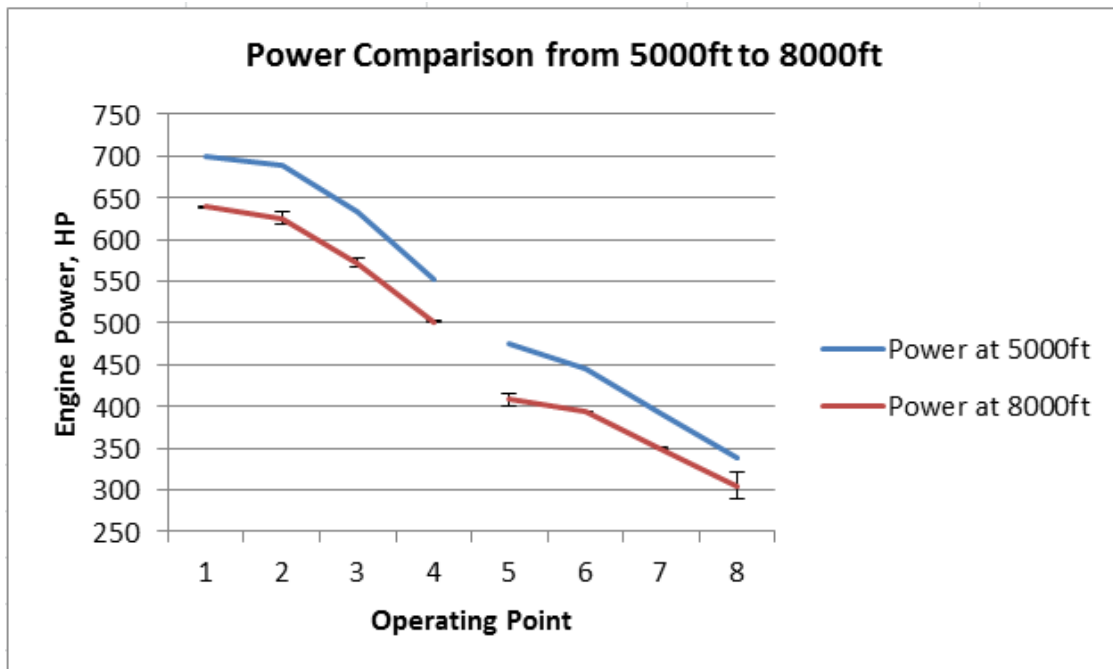


Figure 46: Power Predictions from 5000ft to 8000ft for the QSK19 Operating Points

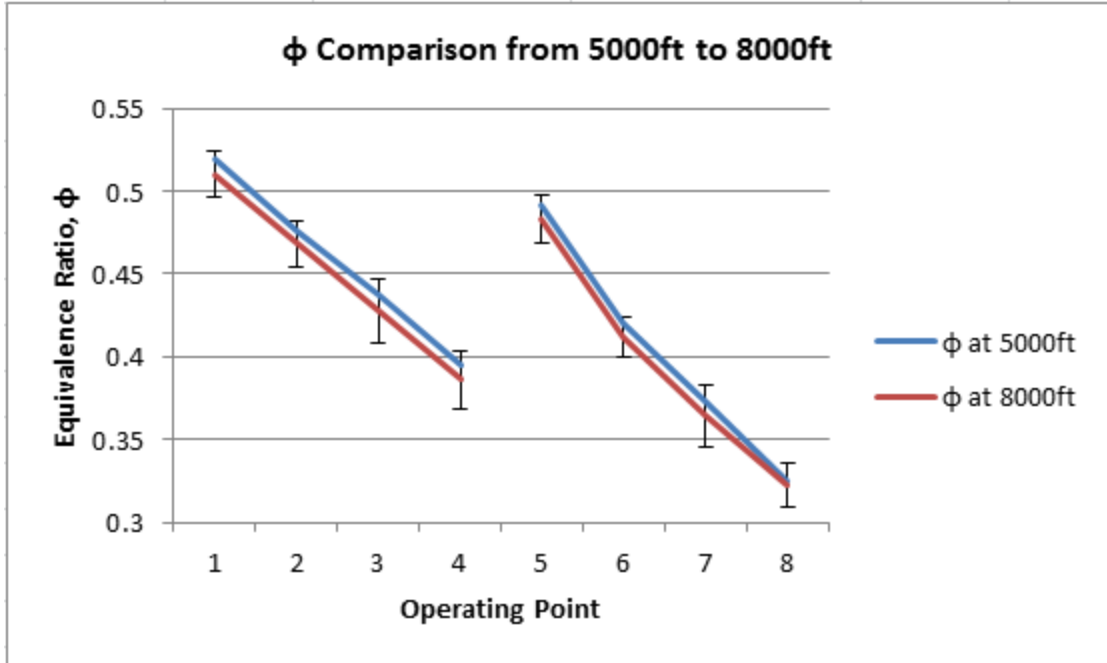


Figure 47: QSK19-GT-Power Equivalence Ratio Comparison from 5000ft to 8000ft

As a result of reduced fueling to maintain similar exhaust energy, the turbine inlet temperature decreased. As shown in Table 8, the turbine inlet temperature at 8000ft decreased an average of 2.69% for the first four operating points. The last four operating points decreased an average of 1.3% from the turbine inlet temperature at 8000ft-see below.

Table 8: GT-Power Predictions for Turbine Inlet Temperature from 5000ft to 8000ft

Normalized Turbine Inlet Temperature Match: Experimental vs. Simulation				
Calibration Method				
Operating Point	Test Cell at 5000ft	GT-Power at 5000ft	GT-Power at 8000ft	GT-Power Percent Decrease in TIT
1	0.84	0.85	0.83	2.22
2	0.80	0.81	0.79	2.50
3	0.76	0.77	0.75	3.22
4	0.72	0.72	0.70	2.86
5	0.78	0.77	0.77	0.04
6	0.69	0.69	0.68	2.08
7	0.64	0.64	0.63	2.16
8	0.59	0.60	0.59	0.85

4.2 QSK50 GT-POWER MODELING RESULTS

Six steady state operating conditions were selected by Cummins to perform GT-Power modeling for the QSK50 engine. Similar to the QSK19 results, each operating point was calibrated against measured data at 5000ft (1526m). After each point was calibrated, the operating points were extrapolated to 8000ft (2438m). Since the QSK50 has a two-stage turbocharger configuration, Cummins has requested that this study focus only on the low pressure (LP) turbocharger. The LP turbine inlet temperature, LP rotor speed, and LP expansion ratio were recorded and sent back to Cummins for further review. The operating conditions can be found on the following table. The table can be separated into two categories: points 1-2 and points 3-6. Points 1-2 had higher rotor speeds than points 3-6. The rotor speed in the following table is normalized by the mechanical limit for the turbocharger.

Table 9: Operating Conditions for QSK50 GT-Power Modeling

Operating Point	Speed (rpm)	Power (hp)	Torque (ft-lbs)	Normalized Rotor Speed
1	1800	2090	6102	0.61
2	2000	1953	5131	0.61
3	1400	1509	5664	0.49
4	1600	1575	5173	0.52
5	1800	1470	4291	0.52
6	1800	1324	3479	0.52

4.2.1 QSK50 IN-CYLINDER COMBUSTION RESULTS

The QSK50 GT-Power in-cylinder combustion matches experimental data extremely well for in-cylinder pressure measurements. As shown in the following figures, the simulated in-cylinder pressures are nearly identical to the measured in-cylinder pressure measurements. Five out of the

six points varied within 1.5% for GIMEP. The last point varied within 1.75% from measured data. For all the operating points, the peak cylinder pressure varied within 30 psi from measured data. Three of the six operating points varied within 10 psi from measured data. The pressures at BDC, IVC and SOI varied within a tenth of a bar from measured data. The following figures show the measured and simulated pressure vs. CA. The in-cylinder pressure is normalized by the maximum cylinder pressure provided by Cummins.

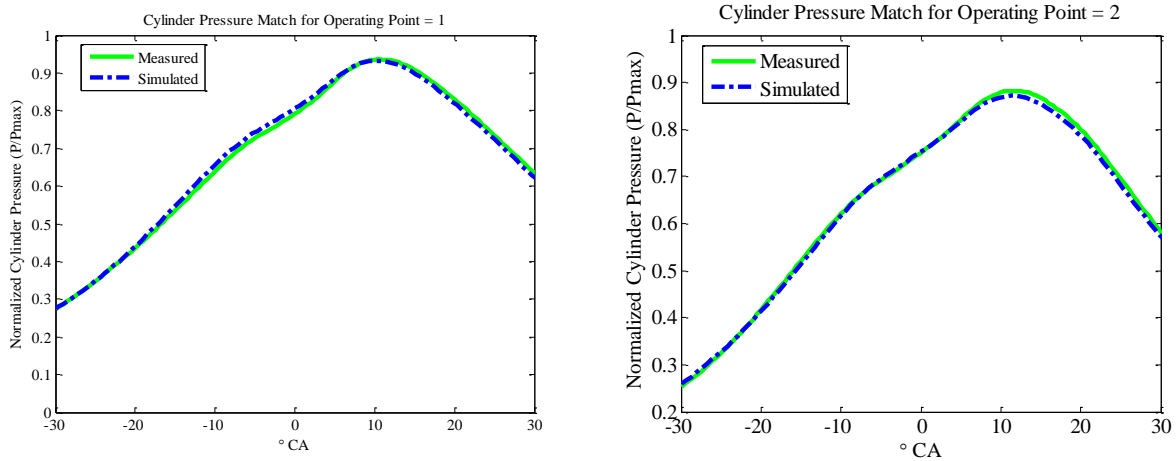


Figure 48: QSK50 Normalized Cylinder Pressure vs. CA for Operating Conditions 1&2

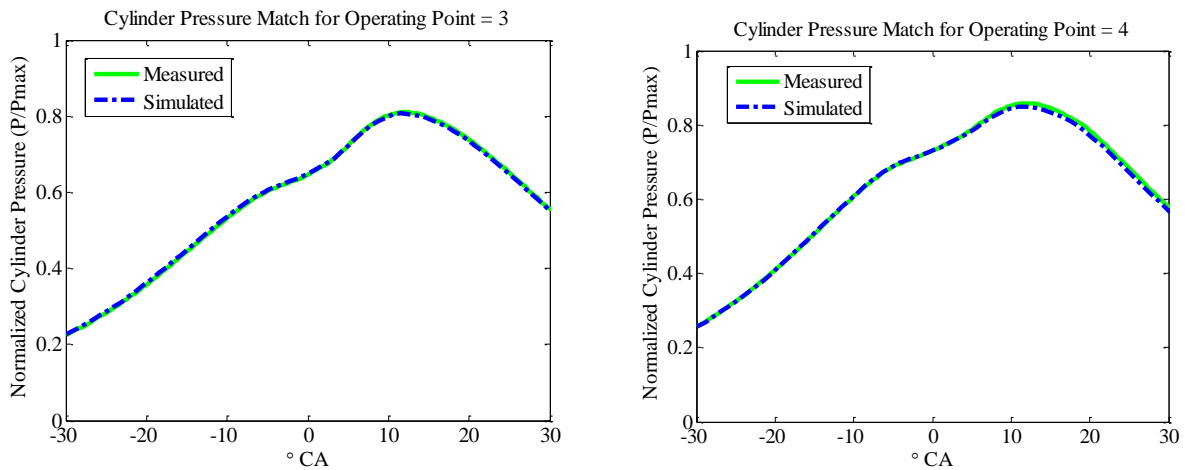


Figure 49: QSK50 Normalized Cylinder Pressure vs. CA for Operating Conditions 3&4

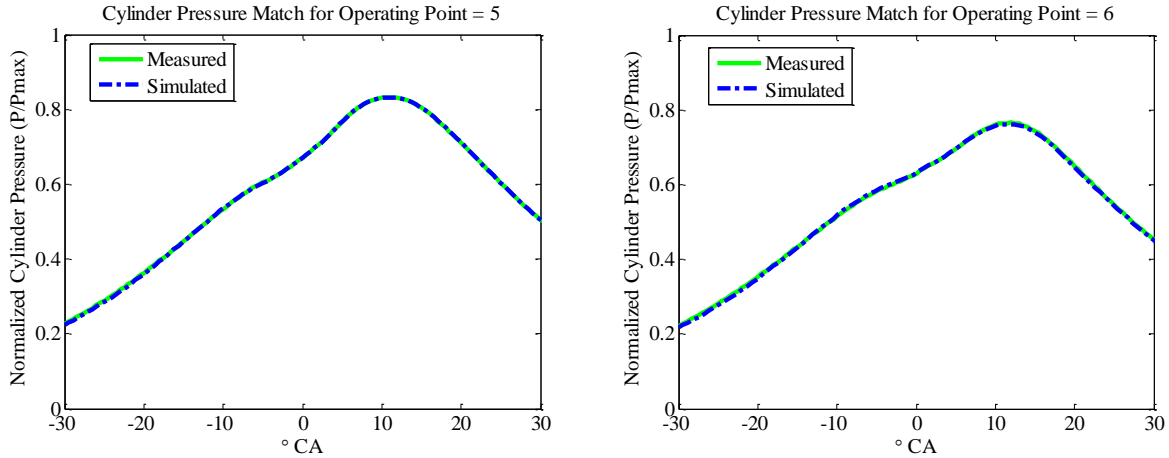


Figure 50: QSK50 Normalized Cylinder Pressure vs. CA for Operating Point 5 & 6

4.2.2 QSK50 CALIBRATION RESULTS FOR THE FIRST OPERATING POINT

The full engine model for the QSK50 was provided by Cummins. From the model, a proportional-integral-derivative (PID) controller was added to match airflow measurements by actuating the wastegate diameter ('ContTurboWG1Stage' object). After the burn rate and airflow was established, few adjustments were needed to match the engine and turbocharger performance. Similar to the QSK19 testing, fueling was slightly adjusted to match engine power. The aftercooler effectiveness was adjusted to match the measured intake manifold temperature. A friction multiplier was slightly adjusted to match the pressure drop across the aftercooler. The direct optimizer was used to match the intake manifold pressure by varying the friction multiplier. After the pressure drop was established, the friction multiplier remained constant for the rest of the modeling work. Unlike the QSK19 testing, the friction multiplier efficiency term in the turbocharger object was not adjusted. A table was provided by Cummins.

The experimental vs. simulation results for the first operating point is reviewed below. The remaining points can be found in the appendix. As shown in the following table, GT-Power is able to predict within 7.5% of measured data for any of the following parameters for the first operating point. Although the majority of the operation points varied within 5% of measured

data, a few operating points varied within 7.5%. The 7.5% variation can be contributed to matching operating points at part load conditions. Other researchers have shown that GT-Power can predict within 8.5% to 10% variation of measured data at part load conditions [25,26]. All points were normalized by the limit set by Cummins.

Table 10: QSK50- Measured vs. Simulated Results for the First Operating Point

Operating Point = 1				
Parameter	Test Cell	GT-Power	GT-Power Percent Variation	Measurement Error
Speed (rpm)	1800.00	1800.00	0.00	±1RPM
Power (bhp)	2090.00	2080.00	0.48	±0.50
BSFC	0.84	0.87	-2.95	Calculated
Airflow	2.53	2.52	0.11	±0.50
A/F Ratio	0.62	0.60	3.82	Calculated
LP Turbo Speed	0.61	0.60	0.33	±0.50
Cylinder Pressure	0.98	0.98	-0.82	±0.20
GIMEP	0.94	0.96	-1.66	Calculated
Volumetric Efficiency	89.00	87.30	1.91	Calculated
BMEP	0.75	0.76	-0.96	Calculated
AMB_P	0.21	0.21	-0.01	±0.50
LP_Comp_in_P	0.20	0.20	-0.02	±0.50
HP_Comp_in_P	0.62	0.58	6.50	±0.50
HP_Comp_out_P	0.93	0.87	7.24	±0.50
Int_Mnf_P	0.87	0.89	-2.02	±0.50
HP Turb_in_P	0.79	0.83	-4.76	±0.50
LP Tur_in_P	0.55	0.52	5.72	±0.50
LP Tur_out_P	0.25	0.25	0.00	±0.50
AMB_Temp	0.31	0.31	-0.09	±0.75
LP Comp In Temp	0.31	0.31	-0.09	±0.75
HP Comp In Temp	0.44	0.45	-1.06	±0.75
HP Comp Out Temp	0.51	0.53	-3.53	±0.75
Int_Mnf_Temp	0.33	0.33	-0.43	±0.75
HP Turb In Temp	0.90	0.90	0.79	±0.75
LP Turb In Temp	0.84	0.83	1.83	±0.75
LP Turb Ot Temp	0.71	0.71	1.00	±0.75
Expansion Ratio	2.19	2.06	5.72	Calculated

Graphically, the temperature and pressure comparisons are shown below:

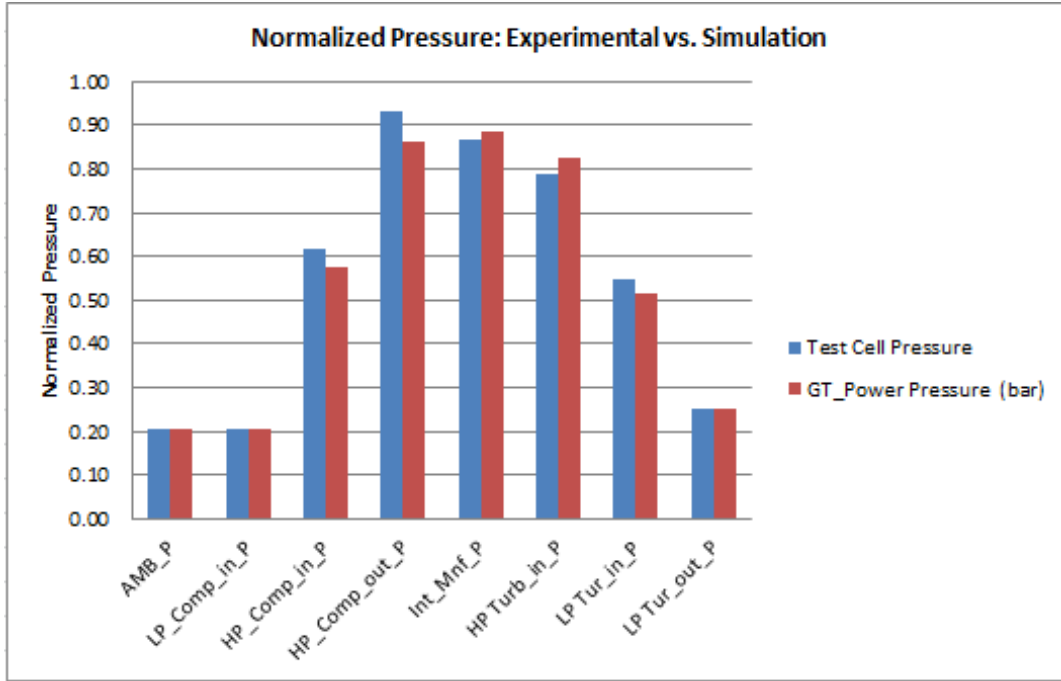


Figure 51: Normalized Pressure: Experimental vs. Simulated Results for Operating Point:1

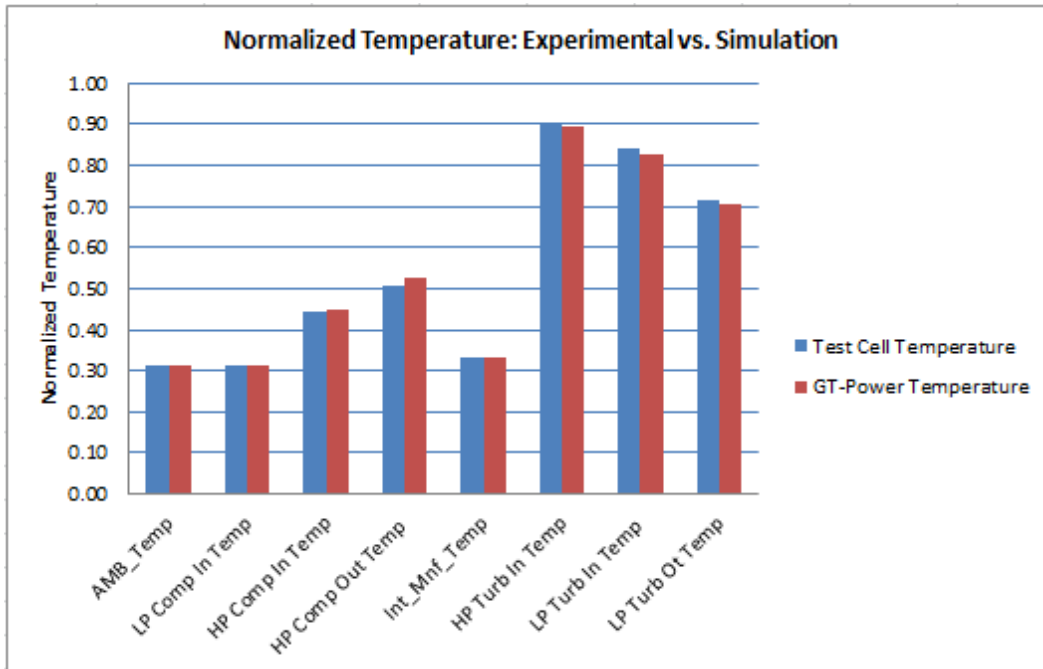


Figure 52: Experimental vs. Simulation Temperature Results for Operating Point:1

4.2.3 QSK50 CALIBRATION RESULTS FOR THE LP TURBOCHARGER

Similar to the QSK19 testing, the remaining results will focus on GT-Power predictions for the LP turbocharger performance. The simulated calibration results vs. measured data are summarized on the following three figures. GT-Power is able to predict within 1% of the measured LP rotor speed for the first three points. The last three points varied 2% of measured data for the LP rotor speed – see below:

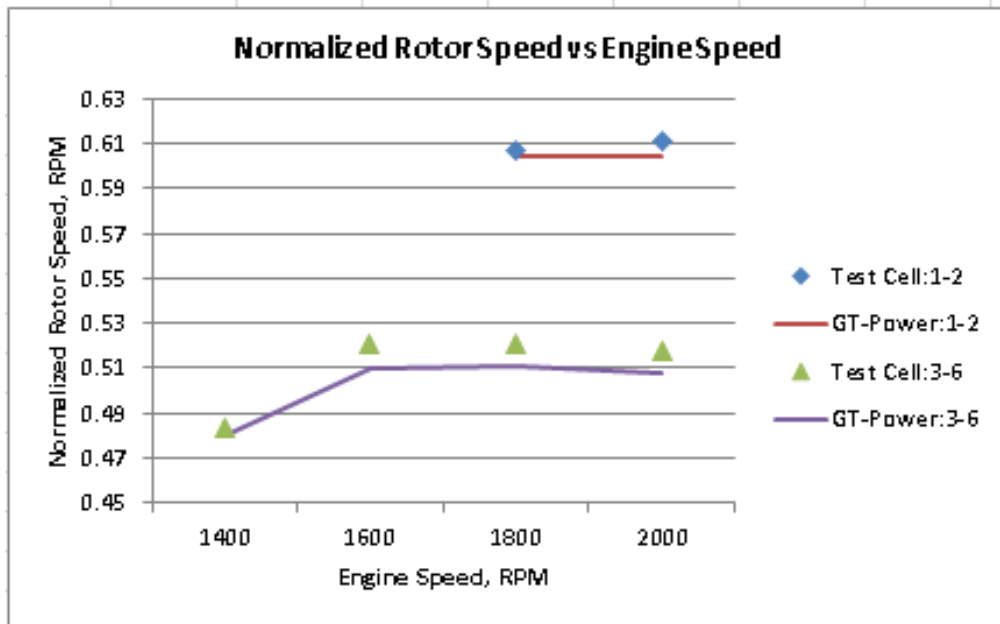


Figure 53: QSK50 - Normalized Rotor Speed vs. Engine Speed Comparison

The simulated LP expansion ratio for all six operating points varied between 5.72% and 7.5% of measured data. Compared with the QSK19 results, the slightly larger variation can be contributed to matching conditions that operate at much lower part load conditions. In addition, the time averaged LP turbine inlet pressure neglects pressure pulsations from the exhaust manifold [15].

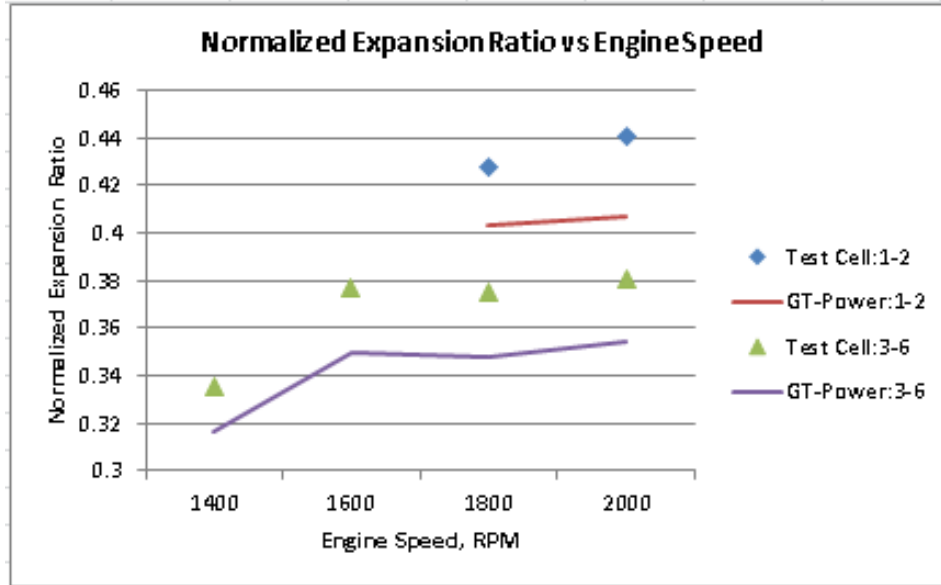


Figure 54: QSK50 – LP Simulated vs. Experimental Expansion Ratio Comparison

The experimental vs. simulated LP turbine inlet temperature varied within 65 degrees Fahrenheit for all operating points. The decrease in TIT is due to a decrease in fueling. The simulated GT-Power TIT varied between 2.65% to 8.5% from measured data – see below.

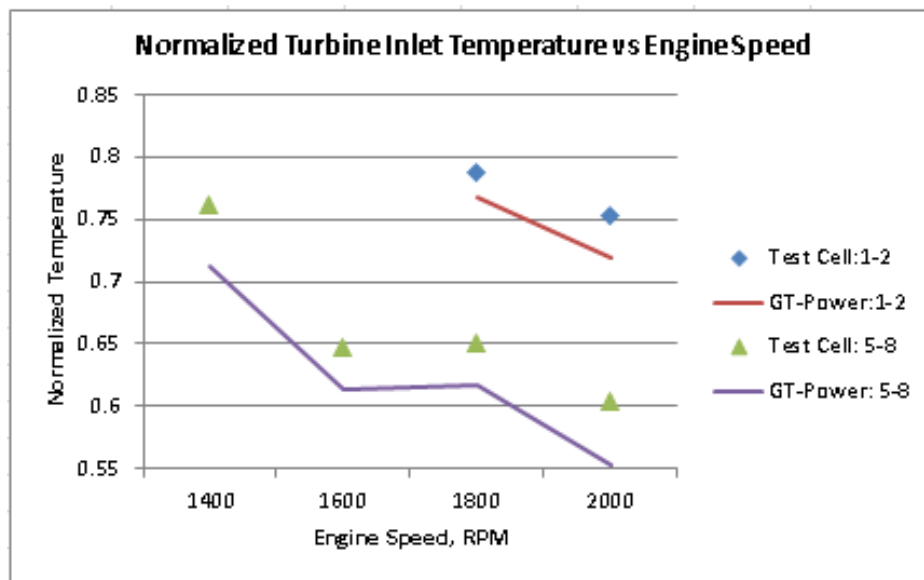


Figure 55: QSK50 – LP Simulated vs. Experimental TIT Comparison

4.2.4 QSK50 EXTRAPOLATION CASE STUDY RESULTS

The same case study outlined in section 4.1.4 was performed for the QSK50 engine to determine which rotor speed should be targeted (measured or simulated) when the model was extrapolated to 8000ft. The expansion ratio and the turbine inlet temperature was recorded and compared against the method described in sections 4.2.1-4.2.3. The case study was validated against experimental results at the test cell facility in Fort Collins Colorado.

As shown in Table 11, columns B and C represent the calibration method outlined in sections 4.2.1-4.2.3 that requires GT-Power to match power, BSFC, airflow, air to fuel ratio, cylinder pressure, GIMEP, expansion ratio, LP rotor speed, LP compressor outlet temperature and LP turbine inlet temperature against measured data. Columns E and F represent the results using GT-Power direct optimizer that varied fueling to match rotor speed. After the rotor speed was matched, the expansion ratio and the turbine inlet temperature were recorded and tabulated.

As shown in the following table, the calibration method varied the expansion ratio within 5.72% to 7.69% from measured data, whereas, the direct optimizer method varied the expansion ratio from 5% to 6.25% from measured data. The turbine inlet temperature varied within 8.5% for the calibration method, whereas, the direct optimizer method varied the turbine inlet temperature within 5%. Since the direct optimizer method matched the experimental results better than the calibration method, the following pages will focus on the extrapolation results from the direct optimizer method. The extrapolation results for the calibration method can be found in the appendix. The extrapolation results for both methods were provided to Cummins for further evaluation.

Table 11: QSK50- Case Study to Determine Target Rotor Speed at 8000ft

A	B	C	D	E	F	G
Normalized LP Rotor Speed Match: Experimental vs. Simulation						
GT-Power Calibration			Direct Optimizer Method to Target Rotor Speed			
Operating Point	Test Cell at 5000ft	GT-Power at 5000ft	GT-Power Percent Variation	Test Cell at 5000ft	GT-Power at 5000ft	GT-Power Percent Variation
1	0.61	0.60	0.33	0.61	0.61	0.11
2	0.61	0.60	1.02	0.61	0.61	0.09
3	0.48	0.48	0.75	0.48	0.48	0.08
4	0.52	0.51	2.01	0.52	0.52	0.07
5	0.52	0.51	1.79	0.52	0.52	0.03
6	0.52	0.51	1.94	0.52	0.52	0.10
Normalized LP Expansion Ratio Match: Experimental vs. Simulation						
GT-Power Calibration			Direct Optimizer Method to Target Rotor Speed			
Operating Point	Test Cell at 5000ft	GT-Power at 5000ft	GT-Power Percent Variation	Test Cell at 5000ft	GT-Power at 5000ft	GT-Power Percent Variation
1	0.43	0.40	5.72	0.43	0.40	5.72
2	0.44	0.41	7.59	0.44	0.41	6.27
3	0.34	0.32	5.70	0.34	0.32	5.06
4	0.38	0.35	7.15	0.38	0.35	6.05
5	0.37	0.35	7.22	0.37	0.35	6.12
6	0.38	0.35	6.77	0.38	0.36	5.58
Normalized LP Turbine Inlet Temperature Match: Experimental vs. Simulation						
GT-Power Calibration			Direct Optimizer Method to Target Rotor Speed			
Operating Point	Test Cell at 5000ft	GT-Power at 5000ft	GT-Power Percent Variation	Test Cell at 5000ft	GT-Power at 5000ft	GT-Power Percent Variation
1	0.79	0.77	2.66	0.79	0.77	2.30
2	0.75	0.72	4.62	0.75	0.73	2.41
3	0.76	0.71	6.59	0.76	0.72	4.95
4	0.65	0.61	5.36	0.65	0.64	0.44
5	0.65	0.62	5.22	0.65	0.65	0.54
6	0.60	0.55	8.53	0.60	0.58	3.71

4.2.5 QSK50 EXTRAPOLATION RESULTS FOR THE LP TURBOCHARGER

In order to extrapolate the model from 5000ft to 8000ft, a few parameters were adjusted. The parameters that were adjusted can be found in section 4.1.5. The remaining initial conditions remained constant. The results are summarized on the following three tables. As shown in Table 12, GT-Power is able to predict within 0.4% of the rotor speed from the GT-Power prediction at 5000ft. Again, this was intentionally done to see the effect of expansion ratio and turbine inlet temperature at a fixed rotor speed.

Table 12: QSK50 – GT-Power Rotor Speed Extrapolation from 5000ft to 8000ft

Normalized LP Rotor Speed Match: Experimental vs. Simulation				
Direct Optimizer Method to Target Rotor Speed				
Operating Point	Test Cell at 5000ft	GT-Power at 5000ft	GT-Power at 8000ft	GT-Power Percent Variation
1	0.61	0.61	0.61	0.45
2	0.61	0.61	0.61	0.00
3	0.48	0.48	0.49	0.28
4	0.52	0.52	0.52	0.00
5	0.52	0.52	0.52	0.00
6	0.52	0.52	0.52	0.00

The predicted expansion ratio increased significantly compared to the QSK19 results. The expansion ratio increased an average of 2.73% from 5000ft to 8000ft compared with 1.81% from the QSK19 results. GT-Power predicted that the first operating point increased 3.57% from 5000ft to 8000ft. An increase in expansion ratio is expected since the turbine outlet pressure drops from 5000ft to 8000ft- see below.

Table 13: QSK50 – GT-Power Expansion Ratio Extrapolation from 5000ft to 8000ft

Normalized LP Expansion Ratio Match: Experimental vs. Simulation				
Direct Optimizer Method to Target Rotor Speed				
Operating Point	Test Cell at 5000ft	GT-Power at 5000ft	GT-Power at 8000ft	GT-Power Percent Increase in ER
1	0.43	0.40	0.42	3.57
2	0.44	0.41	0.42	2.95
3	0.34	0.32	0.32	1.98
4	0.38	0.35	0.36	1.40
5	0.37	0.35	0.36	3.35
6	0.38	0.36	0.37	3.14

As previously mentioned, fueling has to decrease with increase altitude to maintain the same rotor speed and equivalence ratio. As shown in Figure 56, GT-Power predicted an average fueling decrease of 7.72% to maintain rotor speed and similar equivalence ratio. Figure 57 shows

the difference in equivalence ratio from 5000ft to 8000ft. The difference in equivalence ratio falls within the predicted error from GT-Power.

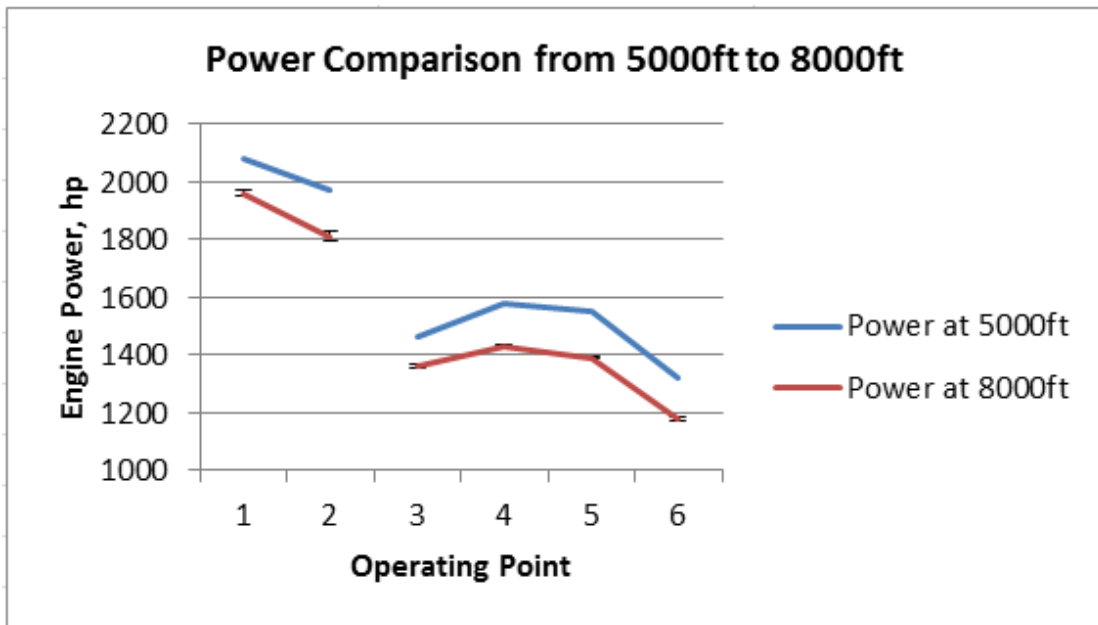


Figure 56: Power Predictions from 5000ft to 8000ft for the QSK50 Operating Points

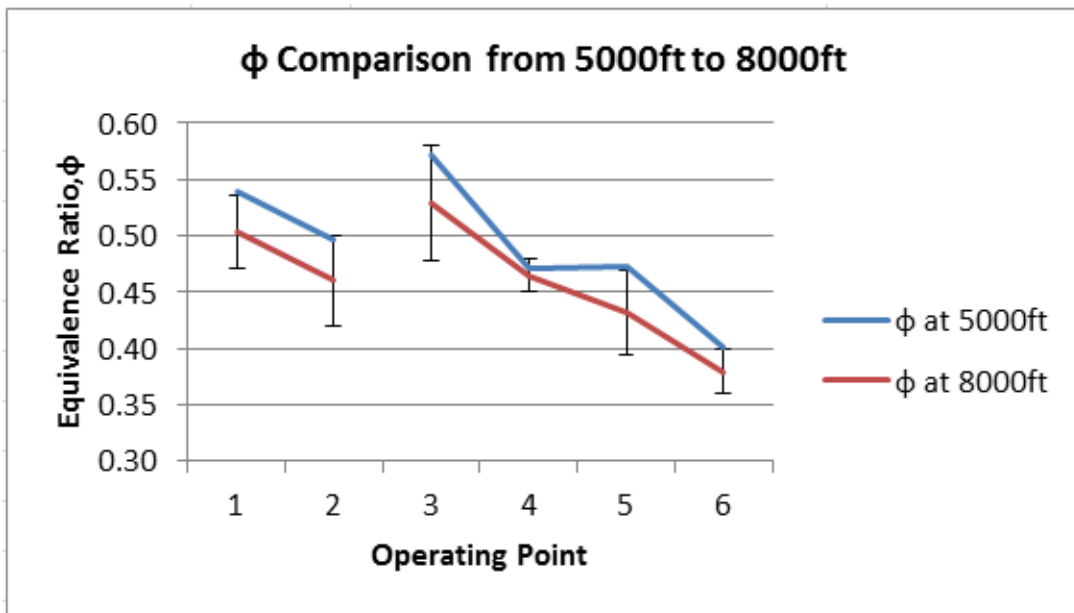


Figure 57: QSK50-GT-Power Equivalence Ratio Comparison from 5000ft to 8000ft

Since fueling is decreased, the turbine inlet temperature decreased an average of 9.12% from 5000ft to 8000ft. These results were significantly higher than the QSK19 results which predicted an average turbine inlet temperature decrease of 2%.

Table 14: QSK50 – GT-Power Turbine Inlet Temperature Extrapolation from 5000ft to 8000ft

Normalized LP Turbine Inlet Temperature Match: Experimental vs. Simulation				
Direct Optimizer Method to Target Rotor Speed				
Operating Point	Test Cell at 5000ft	GT-Power at 5000ft	GT-Power at 8000ft	GT-Power Percent Decrease in TIT
1	0.79	0.77	0.71	7.56
2	0.75	0.73	0.67	8.85
3	0.76	0.72	0.65	10.33
4	0.65	0.64	0.60	6.44
5	0.65	0.65	0.57	11.33
6	0.60	0.58	0.52	10.24

CHAPTER 5: SINGLE CYLINDER HCCI ENGINE

5.1 HCCI MOTIVATION FOR MODELING IN-CYLINDER HEAT TRANSFER

Because fuel economy and emissions continue to be a concern for spark ignition (SI) and compression ignition (CI) engines, research has continued into advanced combustion strategies such as homogeneous charge compression ignition (HCCI) to combat these issues. HCCI has the potential to deliver low NO_x formation, low PM and high efficiency. For example, HCCI can yield a 15-20 per cent increase in fuel economy while emitting lower levels of NO_x emissions [27]. The HCCI engine achieves lower emissions and higher efficiency through combining a homogeneous air-fuel intake mixture coupled with compression ignition.

In the ideal case, the entire in-cylinder homogeneous air-fuel mixture simultaneously ignites everywhere at once, which would result in unsuitably high pressure rise rates during the ignition event. In reality, the air/fuel mixture is not fully homogeneous and the in-cylinder heat transfer slows the combustion process down which directly affects the maximum pressure, pressure rise rate, autoignition timing, burn rate and efficiency of the HCCI process.

Temperature and equivalence ratio stratification are two other important parameters that directly affect combustion. Additionally, in-cylinder heat transfer affects exhaust emissions due to the impact that temperature has on emissions. Therefore, in-cylinder heat transfer is among the most important phenomena necessary to accurately simulate and effectively control HCCI. Since the in-cylinder heat transfer is mostly affected by forced convection of burned gases [28], the modeling approach considered herein neglects radiation and compares two convection heat transfer correlations against experimental data.

5.2 HCCI HEAT TRANSFER MODEL

The HCCI model in GT-Power relies on a predictive, single zone combustion model. The combustion rate is predicted based on the chemical kinetic mechanism provided by the user. The combustion model assumes a perfectly homogenous mixture and the user can specify the crank angle when GT-Power starts to run the reactions. For this study, the chemical kinetics were modeled using a reduced Primary Reference Fuel (PRF) mechanism from Ra and Reitz, which includes 41 species and 130 reactions [8]. To reduce computational time, GT-Power imposes a simple burn curve based on the initial conditions. This allows the airflow and intake manifold pressure to achieve a reasonable steady state convergence before the chemical kinetics are activated [15].

GT-Power uses global heat transfer models that characterize a spatially-averaged convection heat flux and a heat transfer coefficient based on a cylinder-averaged charge temperature. Woschni [20] and Hohenberg [21] are two of the most common correlations used in GT-Power. The default method uses the classical Woschni correlation without swirl. This heat transfer correlation assumes the form:

$$Nu = 0.035Re^a \quad (16)$$

where Nu is the Nusselt number that represents the heat transfer coefficient by multiplying the length scale and dividing by the thermal conductivity, Re the Reynolds number and a an empirical parameter ranging from 0.7 to 0.8 [15].

Woschni also assumed that:

$$k \propto T^{0.75} \text{ and } \mu_{gas} \propto T^{0.62} \text{ and } P = \rho RT \quad (17)$$

where k is the thermal conductivity, μ_{gas} the viscosity, P the pressure, ρ the density and R the specific gas constant. The heat transfer coefficient that is derived from the above assumptions is as follows:

$$h = 3.26B^{a-1}P^a w_{gas} T^{0.75-1.62a} \quad (18)$$

where B is the cylinder bore, P the cylinder pressure, T is the cylinder temperature and w_{gas} is the average gas velocity. Woschni reasoned that the average gas velocity in the cylinder is proportional to the mean piston speed during the intake, compression and exhaust strokes [20]. With this assumption, the Woschni correlation implicitly relates a change in the gas velocity to a change in the density from combustion. The average cylinder gas velocity (m/s) can therefore be modeled as:

$$w_{gas} = [C_1 w_P + C_2 \frac{V_d T_r}{\rho_r V_r} (p - p_m)] \quad (19)$$

where, w_P is the average piston speed, V_d the displaced volume, p is the instantaneous cylinder pressure, T_r the gas temperature at a reference state, ρ_r the gas density at a reference state, V_r the volume at a reference state, p_m the motored cylinder pressure at the same crank angle as p , and C_1 and C_2 are empirical constants. The reference state is typically chosen as the start of compression (SOC) or intake valve closure (IVC).

For the gas exchange period, the following empirical constants are used: $C_1 = 6.18$ and $C_2 = 0$. For the compression period, the following empirical constants are used: $C_1 = 2.18$ and $C_2 = 0$. And, for the combustion and expansion period, the following empirical constants are used: $C_1 = 2.18$ and $C_2 = 3.24E-3$ [m/sK].

Hohenberg modified the Woschni equation to provide better predictions of time-averaged heat flux measurements [21]. The Hohenberg correlation differs from the Woschni correlation in

three ways. Firstly, instead of using the bore as the characteristic length, Hohenberg changed the characteristic length to be based on the instantaneous cylinder volume. Secondly, Hohenberg suggested that previous publications (i.e. Woschni) had yet to encapsulate the additional turbulence caused by the velocity gradient from the result of the combustion reaction. Hohenberg further commented that the efficiency of the combustion process is related to the amount of turbulence caused from swirl during the intake stroke. Since these factors are extremely complex and hard to determine, Hohenberg assumed that the time-related variables, temperature and pressure, relate to a time-related velocity. The piston speed is also included in the Hohenberg correlation since the rise in the velocity is proportional to engine speed. Hohenberg assumes the flow velocity^{0.8} yields a more accurate value than Woschni since the velocity rises with engine speed and varies with crankshaft angle. Specifically, the gas velocity used in the Hohenberg correlation is as follows:

$$w_{gas}^{0.8} = P^{0.2} T^{0.1} * (V_p + C_2)^{0.8} \quad (20)$$

where w_{gas} is the time varying gas velocity, P the cylinder pressure, T the cylinder temperature from the Ideal Gas Law, V_p the mean piston speed and C_2 a constant for combustion turbulence.

The last modification Hohenberg made to the Woschni correlation was to change the exponent on the temperature term. By applying the gas velocity equation with the original Woschni correlation and approximating the pre-combustion pressure temperature as $P^{0.6} T^{-0.5}$ from experiments, the Hohenberg correlation yields a heat transfer coefficient [W/m² K] of the form:

$$h = C_1 * V_c^{-0.6} * P^{0.8} * T^{-0.4} * (V_p + C_2)^{0.8} \quad (21)$$

where, V_c is the cylinder volume and C_1 and C_2 are constants for swirl based on experimental data. The mean values for C_1 and C_2 are 130 and 1.4 respectively. GT-Power also uses these same constants in their heat transfer models [15].

5.3 HCCI ENGINE SETUP

To test the HCCI heat transfer approaches available using GT-Power, an engine simulation was performed on a single cylinder HCCI engine that was described previously by Baumgardner and coworkers [29]. In the experimental setup, one cylinder of a John Deere PowerTech 2.4L 4024 turbo-diesel engine was modified to operate in HCCI mode while the other three cylinders operated in diesel mode. The existing in-cylinder fuel injector was disconnected in favor of using port fuel injection (via a gasoline-type injector ~20 inches upstream of the intake valve) to produce a homogeneous mixture of air and fuel. The in-cylinder pressure was measured using a Kistler 6056A pressure transducer. Additional modifications consisted of alterations to the intake and exhaust manifolds to allow isolation of the HCCI cylinder and the installation of an air preheater necessary to achieve the higher intake temperatures typically associated with HCCI operation. The piston head of the HCCI cylinder was also modified such that the compression ratio can be adjusted to allow HCCI tests at various compression ratios. The engine geometry can be found in Table 15 and the operating conditions can be found in Table 16.

Table 15: HCCI Engine Geometry

Engine Type	2 valve, single cylinder
Bore/Stroke	86/105 mm
HCCI Cylinder Displacement	0.60 liter
Connecting Rod Length	170 mm
Compression Ratio	16:1
IVO/IVC	350.5/547.5
EVO/EVO	140/356.5

Table 16: HCCI Engine Operating Conditions

Engine Speed [RPM]	1500
Intake Temperature [deg C]	70
Boost Pressure [bar]	0.15
Global Equivalence Ratio	0.33
Flow Rate of Fuel [g/s]	0.175
Fuel Type (vol)	Gasoline (40% i-c8h18/ 60% n-c7h16)

5.4 RESULTS AND DISCUSSION

The objects of the simple GT-Power model (Figure 58) were based on the locations of experimental measurements of pressure and temperature. Since neither the compressor nor the turbine maps for the turbocharger were available, the authors modeled the inlet environment as the compressor outlet temperature and pressure. The outlet environment was modeled just after the exhaust manifold. An orifice was integrated into the model to output instantaneous air flow measurements. Filters were added to the intake and exhaust valves to smooth the intake and exhaust pressures for consistent burn rate results.

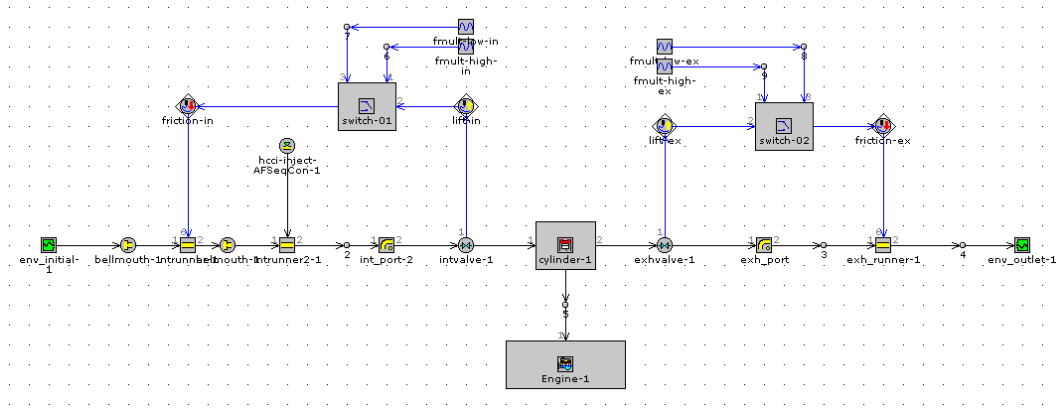


Figure 58: Single cylinder HCCI GT-Power model

The results from GT-Power™ were compared against a 0-D CHEMKIN® model that used the same chemical kinetic mechanism from Ra and Reitz. CHEMKIN® is a software tool that solves combustion problems through complex chemical kinetics. CHEMKIN® uses a different differential equation solver that results in better chemical species resolution than GT-Power™. Although CHEMKIN® can model the in-cylinder chemical kinetics, GT-Power™ has the advantage of modeling the performance of the entire engine. For instance, GT-Power™ can solve for volumetric efficiency of the engine, whereas CHEMKIN® cannot. Once a model has been calibrated, GT-Power™ can easily run sweeps of valve timing, equivalence ratio, intake pressure, intake temperature and RPM.

As shown in Figure 59, both the GT-Power™ and CHEMKIN® simulations produced reasonable agreement with the experimental data for the start of combustion. The Hohenberg correlation agreed extremely well with the 0-D CHEMKIN® model for the cylinder pressure. The Hohenberg, Woschni and CHEMKIN® models all had similar pressure rise rate. Since the 0-D models were coupled with a reduced chemical mechanism, the maximum cylinder pressure differed from experimental data within 15% error. The error was calculated using:

$$Error (\%) = 1 - \frac{Measured\ Max\ Cylinder\ Pressure}{Predicted\ Max\ Cylinder\ Pressure} \quad (22)$$

The error is the result from the 0-D model assuming a perfectly homogenous air-fuel mixture. In this case, the air-fuel ignites instantaneously all at once. The benefit of using a reduced mechanism and a 0-D model is the computational time that it takes to run a simulation. For this study, each GT-Power™ simulation took approximately 1.5 minutes to converge on a typical PC. The use of a more detailed chemical kinetic mechanism and/or a multi-zone combustion model would result in increases in computational time to hours and even days.

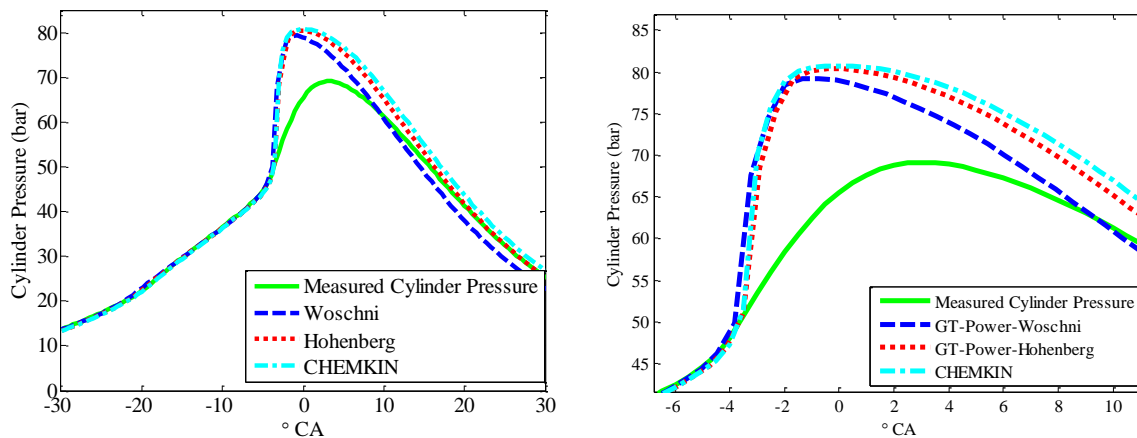


Figure 59: Measured and Predicted in-Cylinder Pressure from 0-D CHEMKIN Simulation and GT-Power Simulations using the Woschni and Hohenberg Heat Transfer Correlations.

To achieve better results, CHEMKIN® allows the user to use detailed kinetics and/or a multi-zone model for predicting HCCI combustion and emissions. For example, Aceves et al. used a multi-zone model to predict HCCI combustion and emissions [30]. Likewise, Smith et al. used a zero-dimensional model with detailed chemical kinetics for a HCCI engine using Methane [31]. Other detailed chemical kinetics for PRF can be found by C.K Westbrook et al. [32]. GT-Power™ uses a default single zone model but the user can provide their own detailed chemical kinetic and heat transfer model and link it to GT-Power’s main solver. For example, Yanbin Mo

from the University of Michigan used FORTRAIN DLL® in GT-Power™ to achieve better cylinder pressure and apparent heat release rate profiles [33].

Similarly in Figure 60, the GT-Power™ model and CHEMKin® model predict the start of combustion extremely well. The majority of the high temperature heat release occurs over a period of 8 °CA for each of the 0-D models, whereas the experimental high temperature heat release occurs over a period of 18 °CA. This shortened heat release of the 0-D model is caused by the homogenous air-fuel mixture igniting all at once. To combat the sharp heat release rate, authors such as Sjöberg and Dec have used enhanced thermal stratification to smooth the overall HCCI heat-release rate. Sjöberg and Dec found that reducing intake air or coolant temperature would also smooth the apparent heat release rate. However, they found this technique to be problematic since it was found to retard the combustion timing [34].

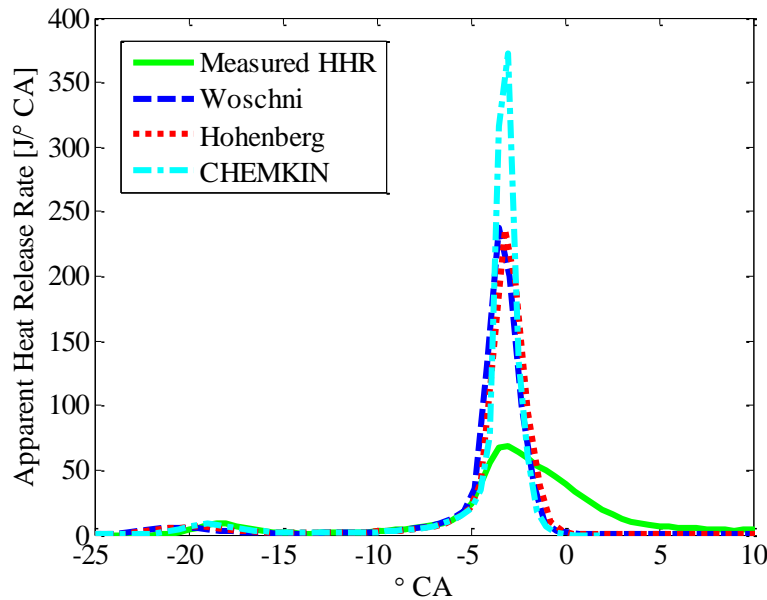


Figure 60: Measured and predicted apparent rate of heat release (J/deg) from 0-D CHEMKin simulation and GT-Power simulations using the Woschni and Hohenberg heat transfer correlations.

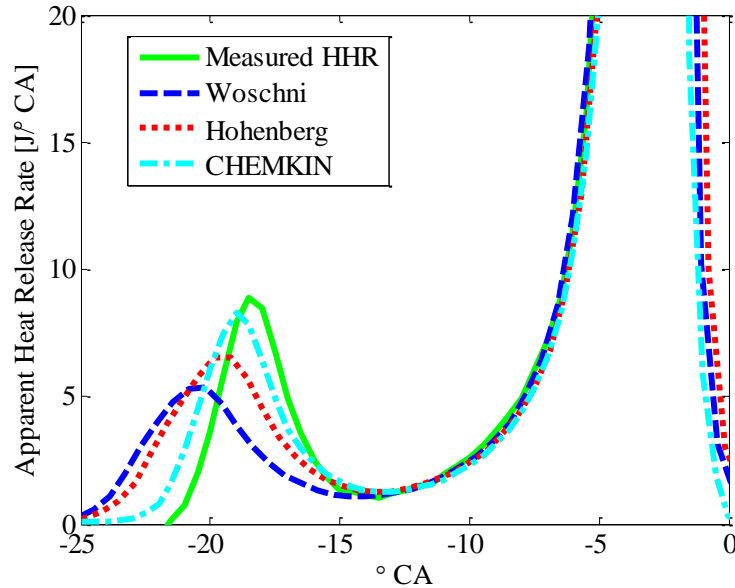


Figure 61: Measured and Predicted Low Temperature Heat Release (J/deg) from 0-D CHEMKIN Simulation and GT-Power Simulations using the Woschni and Hohenberg Heat Transfer Correlations.

Figure 61 demonstrates that GT-Power™ and CHEMKIN® both agree reasonably well with the experimental low temperature heat release rate, which is important in determining when the peak heat release will occur. Although the Hohenberg and Woschni correlation agree reasonably well with each other for in-cylinder pressure measurements, Figure 62 shows that there is a discrepancy in the heat flux and heat transfer coefficient. This variation agrees with literature and can be contributed to the three factors that are different between Woschni and Hohenberg (gas velocity term, difference in temperature exponent, and characteristic length) [35]. Researchers have shown that the flame propagation term in the Woschni correlation is not applicable to HCCI engines which results in considerably higher heat transfer coefficient and heat flux than Hohenberg [35].

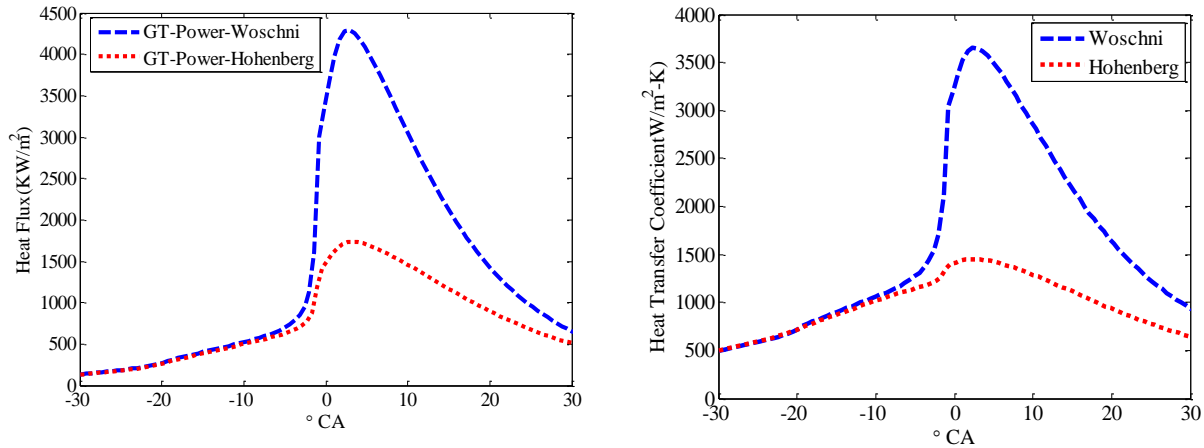


Figure 62: HCCI: Heat Flux vs. CA (left), Heat Transfer Coefficient vs. CA (right)

As shown in Figure 63: Apparent Heat Release Rate and Heat Transfer Rate for Woschni and Hohenberg, the pressure rise rate has a low sensitivity to the in-cylinder heat transfer rate because the apparent heat release rate is much more dominant than the heat transfer rate. Since HCCI combustion happens nearly everywhere at once, the in-cylinder heat transfer doesn't take effect until after the peak apparent heat release occurs. This explains why the pressure rise rate cannot be accurately modeled by empirically treating the in-cylinder transfer for a single zone heat transfer model. As previously mentioned, a multi-zone model coupled with detailed chemistry should be used.

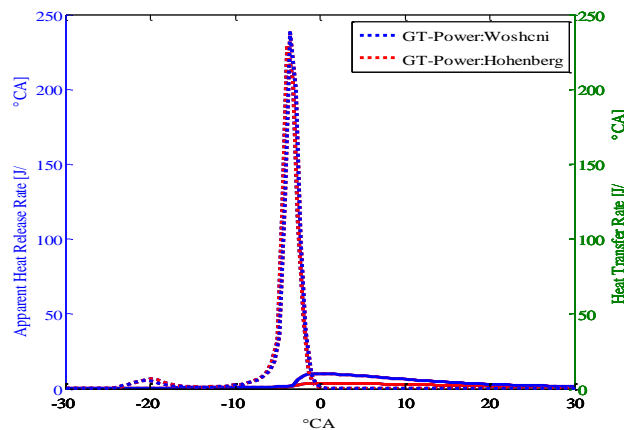


Figure 63: Apparent Heat Release Rate and Heat Transfer Rate for Woschni and Hohenberg

The following table further demonstrates that the Woshcni correlation has a higher heat transfer rate than expected. The Woschni correlation is much higher since the second term in the gas velocity term is not applicable for HCCI. This term accounts for the unsteady gas that is compressed by the advanced flame. In an internal combustion engine, the heat transfer rate (HTR) to apparent heat release rate (AHRR) should be approximately 33% [17]. Approximately a third should go to work output and the other third should go through the exhaust. See below:

Table 17: Woschni and Hohenberg Comparison for HTR to AHRR

Area Under Curve (720 deg)			
Correlation	AHRR (J)	Heat Transfer Rate (J)	HTR/AHRR (%)
Woshcni	541.064	257.28	47.5%
Hohenberg	546.548	152.76	27.9%

CHAPTER 6: CONCLUSION AND FUTURE WORK

The purpose of this thesis was to detail the installation process and perform GT-Power modeling for three engines: a Cummins QSK19 diesel engine, a Cummins QSK50 diesel engine and a John Deere single cylinder HCCI engine. The goal for the two Cummins engines was to quantify the effects of expansion ratio and turbine inlet temperature for a fixed rotor speed from 5000ft to 8000ft. The purpose of the HCCI modeling work was to evaluate the performance of the Woschni and the Hohenberg heat transfer correlation by comparing GT-Power engine model predictions with measured in-cylinder pressure data.

Eight steady state operating conditions were selected by Cummins to perform GT-Power modeling for the QSK19 CI engine. GT-Power was able to predict within 5% of measured data for most operating conditions. Two operating point (4 and 8) varied within 7% from any measured data. When the model was extrapolated to 8000ft, the simulation results show an average expansion ratio increase of 1.81% and an average turbine inlet temperature decrease of 2% from 5000ft to 8000ft. This was accomplished by reducing the fueling by an average of 9.04% to match the same rotor speed and air to fuel ratio at 5000ft.

Six steady state operating points were selected by Cummins to perform GT-Power modeling for the QSK50 CI engine. GT-Power was able to predict within 7.5% of measured data for all operating points. When the model was extrapolated to 8000ft, GT-Power predicted an average expansion ratio increase of 3.2% and an average turbine inlet temperature decrease of 11.3% from 5000ft to 8000ft. The turbine inlet temperature decreased due to the reduction in fueling. For the QSK50 model, fueling was reduced by an average of 7.72% from 5000ft to 8000ft. The expansion ratio increased for both the QSK19 and the QSK50 model because the

turbine outlet pressure decreased. Cummins will be processing this data and performing the CFD and FEA analysis to determine and evaluate the potential HCF risk.

Alternative engines strategies such as HCCI have shown to deliver high thermal efficiencies and low NO_x and PM emissions. Low NO_x is achieved through low temperature combustion and low PM emissions are achieved through a well-mixed fuel/air intake [1]. The in-cylinder heat transfer directly affects the start of combustion, peak cylinder pressure, burn rate and efficiency. In this study, the authors have shown that with a zero-dimensional model and a reduced primary reference fuel mechanism, empirically treating the in-cylinder heat transfer can predict the start of combustion within 1% error and the maximum in-cylinder pressure within 15% error. In addition, the authors have shown that the pressure rise rate has a low sensitivity to the in-cylinder heat transfer rate. This is a result of the nature of the instantaneous HCCI combustion. To reduce the error of the simulation for start of combustion and maximum in-cylinder pressure, detailed kinetics combined with multi-zone combustion models would be required. In doing so, the pressure rise rate, the end of combustion and the burn rate can be accurately predicted.

REFERENCES

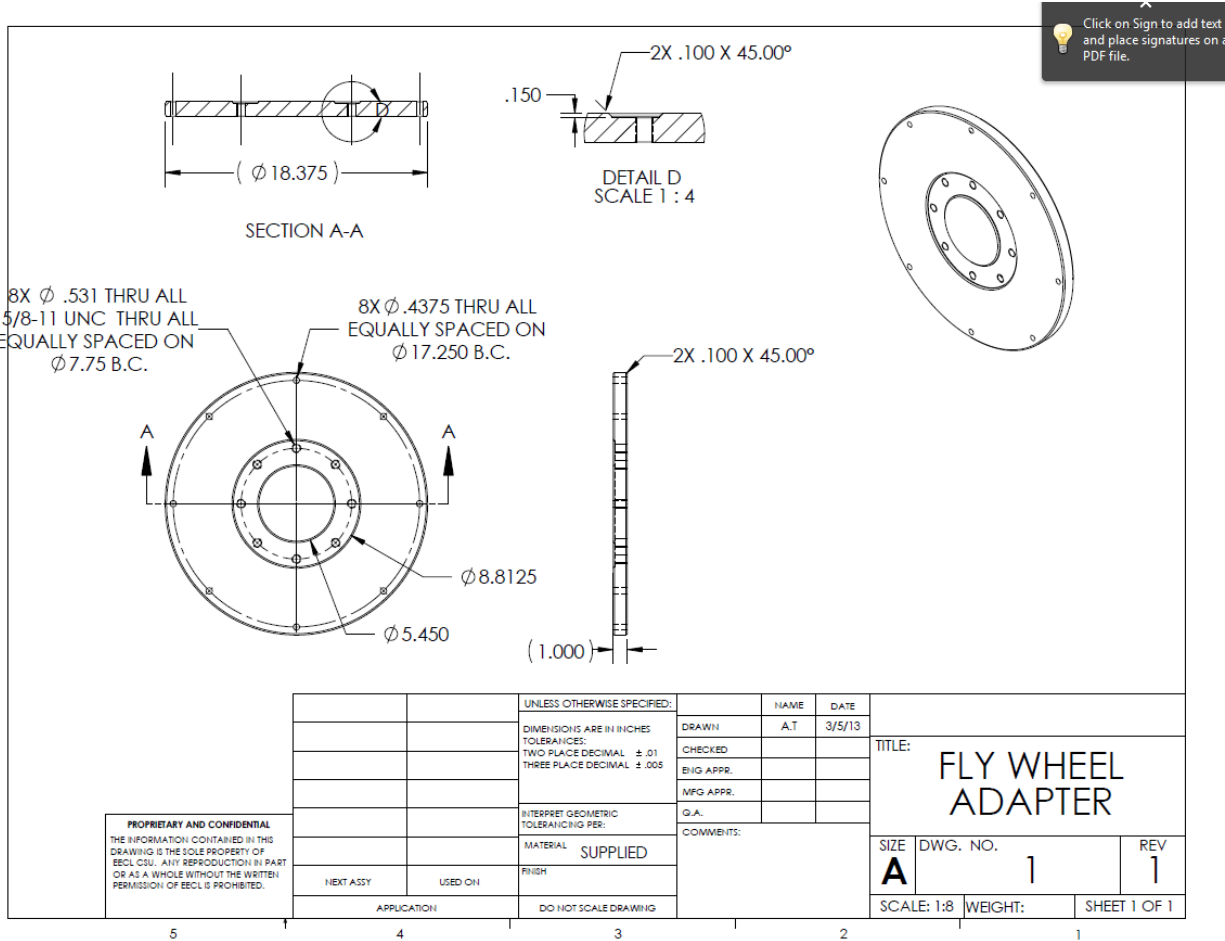
- [1] Encyclopedia Britannica. Colorado Plateau. Britannica Online. Web. 06 March 2014.
- [2] Marston RA. Rocky Mountains. Britannica Online. Web. 06 March 2014.
- [3] Zhang H, Zhuge W, Zhang Y, Hu L. Study of the control of the plateau self-adapted turbocharging system for diesel engine. SAE Paper 2008-01-1636, 2008.
- [4] Linbao Y, Lin Y, Zhihong G. Research on highland performance of turbocharged diesel engine for vehicle. Modern Vehicle Power. 2006.
- [5] Shen L, Shen Y, Yan W, Junding X. Combustion process of diesel engines at regions with different altitude. SAE Paper 950857, 1995.
- [6] Bauccio M. ASM metals reference book. 3rd ed. Ohio: ASM International; 1993. 603 p.
- [7] Kulkarni A, Tisserant D, Hosny D, Liang E, Krishnaraja N. Turbine wheel high cycle fatigue reliability prediction. Institution of Mechanical Engineers. 2010. 171-181.
- [8] Ra Y, Reitz RD. A reduced chemical kinetic model for IC engine combustion simulations with primary reference fuels. Combustion Flame. 2008. December; 155(4): 713-738.
- [9] Singer DA. Comparison of a supercharger vs. a turbocharger in a small displacement gasoline engine application. SAE Paper 850244, 1985.
- [10] Amy P. Increasing BMEP for downsizing of internal combustion engines through an advanced turbocharging concept [thesis]. Fort Collins (CO): Colorado State University; 2012. 97 p.
- [11] Allen K, Rinschler P. Turbocharging the Chrysler 2.2 Liter Engine. SAE Paper 840252, 1984.
- [12] Rakopoulos C, Giakoumis E. Study of the Transient Operation of Low Heat Rejection Turbocharged Diesel Engine Including Wall Temperature Oscillations. SAE Paper 2007-01-1091, 2007.
- [13] Kulkarni A, LaRue G. Vibratory response characterization of a radial turbine wheel for automotive turbocharger application. Proceedings of ASME Turbo Expo 2008: Power for Land, Sea and Air; 2008 June 9-13. Berlin. 2008. p GT2008-51335.
- [14] Huzel D, Huang D. Modern engineering for design of liquid-propellant rocket engines. Washington, DC: American Institute of Aeronautics and Astronautics Inc: 1992. 427 p.
- [15] GT-Power User's Manual and Tutorial: Gamma Technologies. V7.3
- [16] Heywood JB. Internal combustion engine fundamentals. Mcgraw-Hill Inc; 1988. 917 p.

- [17] Ferguson CR, Kirkpatrick A. Internal combustion engines. New York: John Wiley and Sons Inc; 2001. 969 p.
- [18] Poonawala YM. Effect of EGR, injection pressure and swirl ratio on engine-out emissions for a HSDI diesel engine at low load and medium speed condition. Detroit (MI): Wayne State University; 2006. 162 p.
- [19] Morel T, Keribar R. A model for predicting spatially and time resolved convective heat transfer in bowl-in-piston combustion chambers," SAE Paper 850204, 1985.
- [20] Wochini G. Universally applicable equation for the instantaneous heat transfer coefficient in the internal combustion engine. SAE Paper 670931, 1967.
- [21] Hohenberg G. Advanced approaches for heat transfer calculations. SAE Paper 790825, 1979.
- [22] Sutley FH. Installation and testing of a Cummins QSK19 lean burn natural gas engine. Fort Collins (CO): Colorado State University; 2013. 167 p.
- [23] Trajkovic S, Tunsetal P, Johansson B. Simulation of a pneumatic hybrid powertrain with VVT in GT-Power and comparison with experimental data. SAE Paper 2009-01-1323, 2009.
- [24] Liu M, Wang P, Yuan F. Simulation and experiment research of working process of exhaust turbocharged and intercooled diesel engine. Advanced Materials Research. 2013; 744:13-17.
- [25] Zhao J, Min X. Fuel economy optimization of an Atkinson cycle engine using genetic algorithm. Applied Energy. 2013; 105(C); 335-348.
- [26] Nerkar A. Optimization and validation for injector nozzle hole diameter of a single cylinder diesel engine using GT-Power simulation tool. SAE Paper 2012-01-2306, 2012.
- [27] Zhao F, Asmus TW, Assanis DN, Dec JE, Eng JE, Najt PM. Homogeneous charge compression ignition engines: key research and development issues. Warrendale: Society of Automotive Engineers Inc; 2003. 655 p.
- [28] Soyhan HS, Yasar H, Walmsley H, Head B, Kalghatgi GT, Sorousbay C. Evaluation of heat transfer correlations for HCCI engine modeling. Applied Thermal Engineering. 2009. February; 29(2-3): 541-549.
- [29] Baumgardner M, Marchese AJ, Sarathy SM. Autoignition characterization of primary reference fuels and n-heptane/n-butanol mixtures in a constant volume combustion device and homogeneous charge compression ignition engine. Unpublished paper presented at the 8th U.S National Combustion Meeting. Combustion Institute. University of Utah.
- [30] Aceves S, Flowers D, Westbrook C, Smith J. A multi-zone model for prediction of HCCI combustion and emissions. SAE Paper 2000-01-0327, 2000.

- [31] Smith JR, Aceves SM, Westbrook C, Pitz W. Modeling of homogeneous charge compression ignition (HCCI) of methane. Proceedings of the ASME Internal Combustion Engine Fall Technical Conference. 2009. New York, New York. ASME; 2009. 85-90.
- [32] Westbrook CK, Pitz WJ, Mehl M, Curran HJ. Detailed chemical kinetic reaction mechanisms for primary reference fuels for diesel cetane number and spark-ignition octane number. Proceedings of the Combustion Institute. 2011. 33(1): 185-192.
- [33] Yanbin M. HCCI heat release rate and combustion efficiency: a coupled Kiva multi-zone modeling study [dissertation]. Ann Arbor (MI); University of Michigan; 2008. 209 p.
- [34] Sjoberg M, Dec J, Babajimopoulos A, Assanis DN. Comparing enhanced natural thermal stratification against retarded combustion phasing for smoothing of HCCI heat-release rate. SAE Paper 2004-01-2994, 2004.
- [35] Chang J, Guralp O, Filipi Z, Assanis DN. New heat transfer correlation for an HCCI engine derived from measurements of instantaneous surface heat flux. SAE Paper 2004-01-2996, 2004.

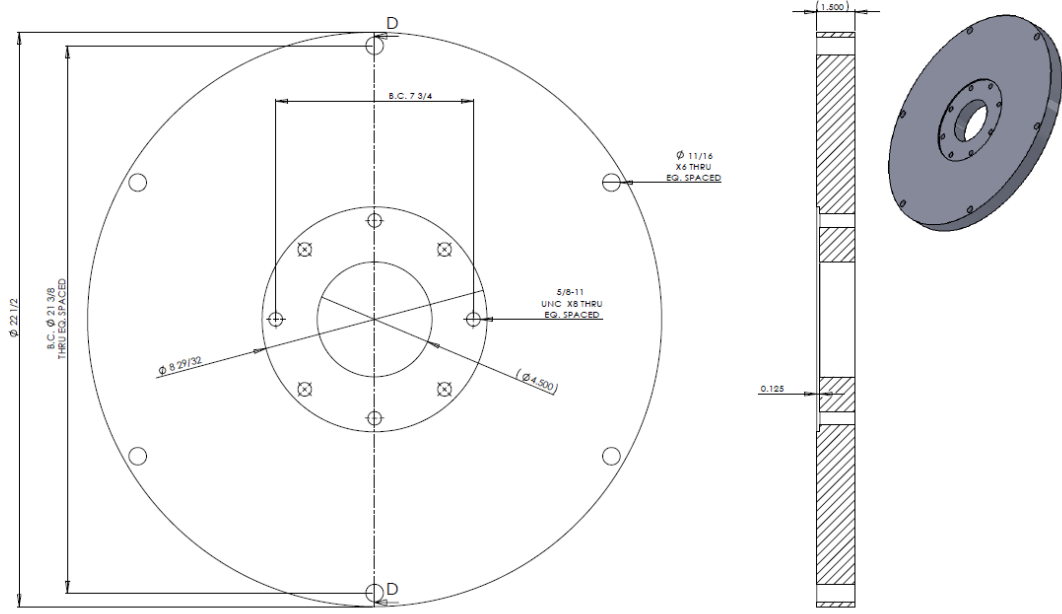
APPENDIX A – QSK19 AND QSK50 INSTALLATION INFORMATION

QSK19 Flywheel Drawing:



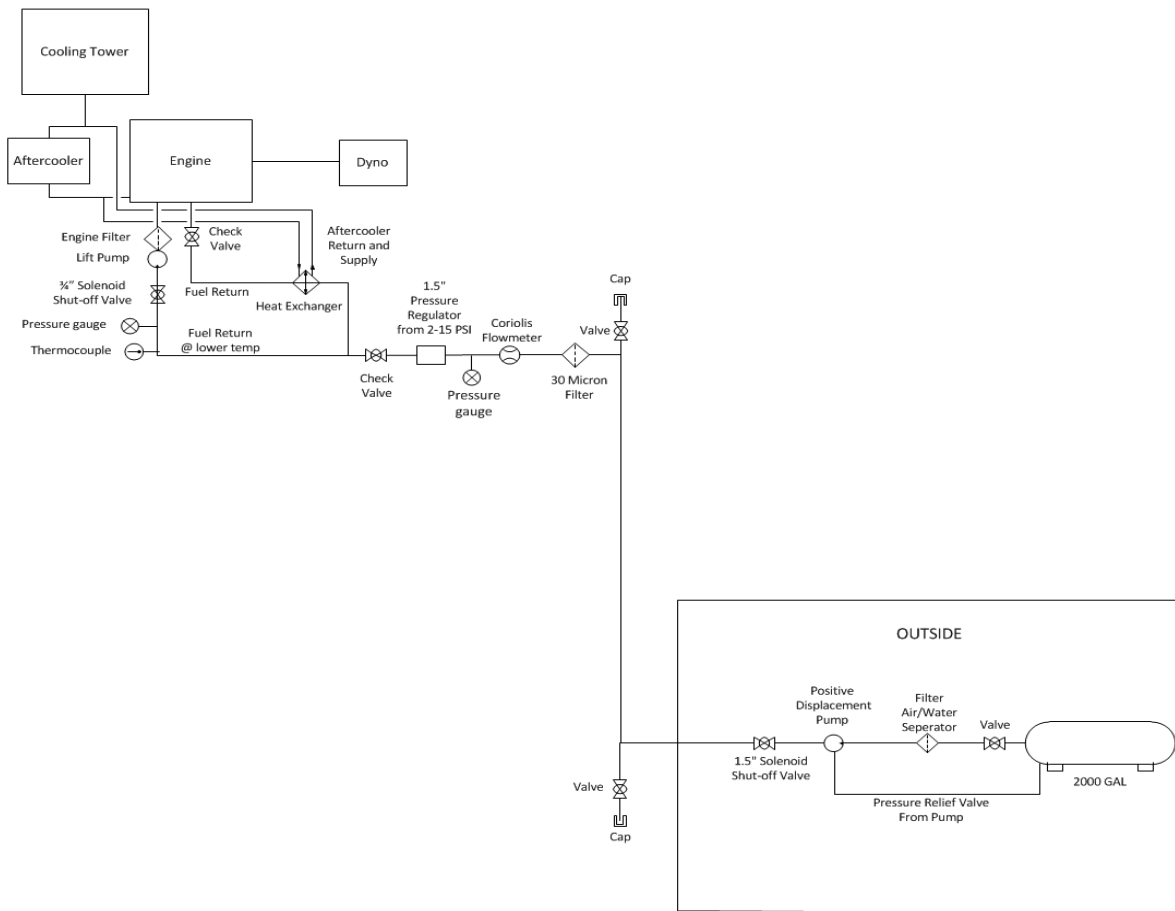
Click on Sign to add text and place signatures on a PDF file.

QSK50 Flywheel Drawing:



TITLE BLOCK FLYWHEEL ADAPTER		PART NO. FlyWheel_G0K50		SHEET NO. 12	
DRAWN BY 12/10/2010		CHECKED BY 12/10/2010		DATE	
MATERIAL 12/10/2010		QUANTITY 12/10/2010		UNIT PRICE 12/10/2010	
TOTAL PRICE 12/10/2010		TOTAL WEIGHT 12/10/2010		TOTAL VOLUME 12/10/2010	

Fuel Diagram for QSK19 and QSK50:



QSK19 Instrumentation List:

<u>Measuring Location</u>	<u>INSTRUMENTATION</u>			<u>PAM</u>	<u>ASSET</u>
<u>Test Cell/Engine</u>	<u>PARAMETER</u>		<u>UNITS</u>	<u>CODE</u>	<u>LABEL</u>
Test Cell	Torque	M	lb-ft	ANA_TORQ	ENG_TORQ
Test Cell	Analog Speed	M	rpm	ANA_SPD	ANA_spd
Test Cell	AVL Smoke	M	FSN	AVL_415_SMK	AVL_smk
Test Cell	Transient Smoke	M	Ceasco	OPAC	opac
Test Cell	Fuel Weight	M	lbm	FUEL_WT	fuel_bucket
Test Cell	Elapsed Time	M	min	ET	FR_time
Test Cell	Torque Variation	C	lb-ft	TORQ_VAR	FR_torq_var
Test Cell	Speed Variation	C	rpm	ENG_SPD_VAR	FR_speed_var
Test Cell	Test Time	M	hr	TEST_TM	test_hrs
Flowmeters and Frequencies					
Test Cell	Air Meter Pressure	M	in H ₂ O	AIR_MTR0_P	air_mtr0P
Test Cell	Air Meter Output delta Pres	C	in H ₂ O	AIR_MTR0_DP	air_mtr0DP
Test Cell	Air Meter Temperature	M	°F	AIR_MTR0_T	air_mtr0T
Test Cell	Air Meter Mass Flow	C	lbm/min	AIR_MTR0_MF	air_mtr0_mf
Test Cell	Air Meter Volume Flow	C	ft ³ /min	AIR_MTR0_VF	air_vf
Test Cell	Continuous total fuel flow	M		TOT_FUEL_VF	fuel_flow
Test Cell	Coolant Meter for Engine	M	gal/min	CLNT_MTR0_VF	jw_flow
Test Cell	Tower Water Flow	O	gal/min	CLNT_MTR1_VF	Twr_w_Flow
Engine	Turbocharger Speed	M	rpm	TRB_SPD	trb_spd
Engine	Shaft Encoder	M			
Engine	Cylinder Pressures	M	psi	H_PEAK_CYL_P@11 H_PEAK_CYL_P@12	h_pk_cyl_p1 h_pk_cyl_p6
Engine	Current Probe	M	Amps	none	
Usage codes: C= used in calculation, M=used to monitor but mandatory, O=used to monitor but optional					

QSK19 Pressure Instrumentation:

		CSU	CMI				
Measuring Location	INSTRUMENTATION	How	UNITS	PAM CODE	ASSET LABEL	MEASUREMENT LOCATION	FITTING SIZE
Test Cell/Engine	PARAMETER						COMMENTS
Test Cell	Barometer	M	in Hg	BAROMETER, SAE_REF_PA			Test Cell
Test Cell	Vapor Pressure	C	in Hg	VAP_PA			Test Cell
Intake System							
Test Cell	Air Inlet Restriction	M	in H ₂ O	CMP_IN_P	cmp_inP	compressor inlet pipe	5 PSI channel
Engine	Compressor Out	M	in Hg	CMP_OT_P	cmp_otP	Test cell connection from compressor to intake manifold housing	50 PSI channel
Engine	Intake Manifold	M	in Hg	INT_MNF_P	int_mnfP		50 PSI channel
	Air 2 Air Delta P	C	in Hg	AC_AIR_DP	air2air_dp		
Lubrication System							
Engine	Oil Rifle	M	psi	OILRFL_P	oilrfI_P	engine rifle	300 PSI channel
Engine	Oil Filter In	M	psi	OFL_IN_P	oFl_inP		300 PSI channel
Engine	Oil Filter Out	M	psi	OFL_OT_P	oFl_otP		300 PSI channel
Engine	Oil Filter Delta P	C	psi	OFL_DP	oFl_dp		
Exhaust System							
Test Cell	Exhaust Restriction	M	in Hg	TUR_OT_P, EXH_STK_P	exh_stkP	exhaust stack	5 PSI channel
Engine	Turbine Inlet - Front	M	in Hg	TUR_IN_P@F, TUR_IN_P	tur_finP	exhaust manifold flange - Front	1/8" NPT - on exhaust manifold prior to turbine; 50PSI channel
Engine	Turbine Inlet - Rear	M	in Hg	TUR_IN_P@R, TUR_IN_P	tur_rinP	exhaust manifold flange - Rear	1/8" NPT - on exhaust manifold prior to turbine; 50PSI channel
Test Cell	SCR in-pressure	M	in Hg	AT_IN_P	SCR_inP	Exhaust pipe upstream of SCR	5 PSI channel (only required if long route between turbine out and scr in)
Test Cell	SCR out-pressure	M	in Hg	AT_OT_P	SCR_otP	Exhaust pipe downstream of SCR	5 PSI channel
Test Cell	SCR Delta P	M	in Hg	AT_DP	SCR_dp	On both sides of SCR	5 PSI channel
Cooling System							
Test Cell	Water Pump Inlet	M	psi	W_PMP_IN_P, CLNT_IN_P, HT_HX_W_OT_P, RAD_OT_P, HT_W_PMP_IN_P	w_pmp_inP	water pump inlet connection	50 PSI channel
Engine	Water Pump Outlet	M	psi	W_PMP_OT_P, BLK_IN_P, HT_W_PMP_OT_P	blk_inP	Water pump discharge	50 PSI channel - will need to drill wpump hsg
Engine	Coolant Out Pressure -Engine (Thermostat out coolant pressure)	M	psi	CLNT_OT_P, BLK_OT_P, TS_OT_P, HT_HX_W_IN_P, RAD_IN_P, HT_TS_OT_P	ts_otP	Engine coolant outlet tube on thermostat hsg	50 PSI channel - add during pipe fab
Engine	Coolant delta pressure	C	psi	CLNT_DP	clnt_delta_P		
Fuel System							
Test Cell	Fuel 1st stage Filter Inlet Pressure	M	in Hg	FL_FIL_IN_P@11, FUEL_IN_P	LfI_fil_inP		50 PSI channel
Test Cell	Fuel 1st stage Filter Outlet Pressure	M	in Hg	FL_FIL_OT_P@11	LfI_fil_otP		50 PSI channel
Test Cell	Stage 1 Delta Pressure	C	in Hg	FL_FIL_DP@11	Stage1_dp		
Engine	Fuel 2nd stage Filter Inlet Pressure	M	in Hg	FL_FIL_IN_P@12, FL_FIL_IN_P	HfI_fil_inP	See the Fuel System Tab for location of measurement	300 PSI channel
Engine	Fuel 2nd stage Filter Outlet Pressure	M	in Hg	FL_FIL_OT_P@12	HfI_fil_otP		300 PSI channel
Engine	Stage 2 Delta Pressure	C	in Hg	FL_FIL_DP@12	Stage2_dp		
Engine	Fuel Return Pressure	M	in Hg	FUEL_RTN_P	fuel_rtnP		50 PSI channel
Engine	Fuel Pump Gear Housing Pressure	M	in Hg	FPMF_HSG_P@11	fpmf_gh		100 PSI channel
Engine	Dedicated Lube Filter Outlet Pressure	M	in Hg	FL_FIL_OT_P@13	dlf_p		100 PSI channel
Miscellaneous							
Engine	Crankcase Pressure	M	in_hg	CRNKCS_P	crnkcs_P		5 PSI channel
Engine	Blowby - 0.406" orifice plate	M	in_hg	BLOW_BY	blow_by		5 PSI channel - 0.406" orifice plate

Useage codes: C= used in calculation, M=used to monitor but mandatory, O=used to monitor but optional

QSK19 Temperature Instrumentation:

Measuring Location	INSTRUMENTATION	How	UNITS	P&M CODE	ASSET LABEL	MEASUREMENT LOCATION
Test Cell/Engine	PARAMETER					
Intake System						
Test Cell	DEWPOINT	C	F	DEWPOINT	dewpoint	
Test Cell	Compressor In	M	F	CMP_IN_T, SAE_REF_T	cmp_inT	air inlet pipe
Test Cell	Compressor Out	M	F	CMP_OT_T, AC_AIR_IN_T	cmp_otT	Compressor outlet (test cell pipe to air-to-
Engine	Intake Manifold	M	F	INT_MNF_T, AC_AIR_OT_T	int_mnfT	intake manifold housing
Lubrication System						
Engine	Oil Rifle	M	F	OILRFL_T	oilrflT	oil filter outlet housing - near rifle
Engine	Oil Pan Temperature	M	F	OILPAN_T	oilpanT	oil pan fitting
Exhaust System						
Engine	Exhaust Port - 1	M	F	EXH_PRT1_T	exhprt1	cylinder head exhaust port 1
Engine	Exhaust Port - 2	M	F	EXH_PRT2_T	exhprt2	cylinder head exhaust port 2
Engine	Exhaust Port - 3	M	F	EXH_PRT3_T	exhprt3	cylinder head exhaust port 3
Engine	Exhaust Port - 4	M	F	EXH_PRT4_T	exhprt4	cylinder head exhaust port 4
Engine	Exhaust Port - 5	M	F	EXH_PRT5_T	exhprt5	cylinder head exhaust port 5
Engine	Exhaust Port - 6	M	F	EXH_PRT6_T	exhprt6	cylinder head exhaust port 6
Engine	Turbine Inlet - Front	M	F	TUR_IN_T@F, TUR_IN_T	tur_inT_F	exhaust manifold flange - Front
Engine	Turbine Inlet - Rear	M	F	TUR_IN_T@R, TUR_IN_T	tur_inT_R	exhaust manifold flange - Rear
Test Cell	Turbine Outlet	M	F	TUR_OT_T, EXH_STK_T	exh_stkT	exhaust stack
Test Cell	BGC in-Temperature	M	F		BGC_inT	Upstream of BGC
Test Cell	BGC out-temperature	M	F		BGC_otT	Downstream of BGC
Test Cell	SCR in Temperature	M	F	AT_IN_T@R	SCR_inT	Upstream of SCR
Test Cell	SCR out Temperature	M	F	AT_OT_T@R	SCR_otT	Downstream of SCR
Cooling System						
Test Cell	Water Pump Inlet	M	F	HT_W_PMP_IN_T, W_PMP_IN_T, CLNT_IN_T, HT_HX_W_OT_T, RAD_OT_T	w_pmp_inT	water pump inlet temperature
Engine	Water Pump Outlet	M	F	W_PMP_OT_T, BLK_IN_T, HT_W_PMP_OT_T	w_pmp_otT	water outlet tube - engine circuit
Engine	Thermostat outlet temperature	M	F	CLNT_OT_T, HT_TS_OT_T, TS_OT_T, HT_HX_W_IN_T, CLNT_MTR0_T, BLK_OT_T, RAD_IN_T	ts_otT	
Fuel System						
Engine	Fuel Inlet Temperature	M	F	FUEL_IN_T	fuel_inT	Please refer the Fuel Systems Tab for locations of measurement
Engine	Fuel Pump Housing Temperature	M	F	FPMP_HSG_T	fpmp_hsgT	
Engine	Fuel Pump Inlet Temperature	M	F	FPMP_IN_T	fpmp_inT	
Engine	Fuel Pump Drain Temp	M	F	FPMP_RTN_T	fpmp_drnT	
Engine	Injector Drain Temp	M	F	FUEL_RTN_T@11	inj_drnT	
Engine	Fuel Return Temperature	M	F	FUEL_RTN_T	fuel_rtnT	
Engine	Fuel Drain Temperature	M	F	FUEL_RTN_T@12	fuel_drnT	
Cylinder Temperatures						
Engine	TC#1 Intake Seat	M	°C	User29@52	int_seat	Cylinder Head
Engine	TC#2 Int-Int-Brdg	M	°C	User29@53	int_int_brdg	Cylinder Head
Engine	TC#3 Int-Ex-Brdg	M	°C	User29@54	int_ex_brdg	Cylinder Head
Engine	TC#4 Ex-Seat	M	°C	User29@55	exh_seat	Cylinder Head
Engine	TC#5 Ex-Ex-Brdg	M	°C	User29@56	exh_ex_brdg	Cylinder Head
Engine	TC#6 Ex-Port	M	°C	User29@57	exh_port	Cylinder Head
Engine	TC#7 Ex-Exit	M	°C	User29@58	exh_exit	Cylinder Head
Engine	TC#8 Ex-Int-Brdg	M	°C	User29@59	exh_int_brdg	Cylinder Head
Miscellaneous						
Test Cell	Test Cell	M	F	TEST_CELL_T	cell_ambT	test cell

QSK50 Instrumentation List:

Priority	Function Reference #) Component Measurement	Location on Engine	Tap Size & Thread
	1.) Oil:		
	1.01P) Oil Filter Head Assembly Inlet Pressure: 1.01T) Oil Filter Head Assembly Inlet Temperature:	Right Bank - Bottom of Block, Back of Oil Filter Head Assembly	1/8" - 27 NPT 1/8" - 27 NPT
	1.02P) Oil Filter Head Assembly Outlet Pressure: 1.02T) Oil Filter Head Assembly Outlet Temperature:	Right Bank - Bottom of Block, Front of Oil Filter Head Assembly	1/8" - 27 NPT 1/8" - 27 NPT
ECM sensor - SAFETY	1.03P) Main Oil Rifle Pressure: 1.03T) Main Oil Rifle Temperature:	Middle of Block, Furthest from Oil Filter Assembly	1/8" - 27 NPT
	1.04T) Oil Pan Temperature - Right Front:	Right Bank - Front, Bottom of Oil Pan at Threaded Plug	1/8" - 27 NPT
	1.05T) Oil Pan Temperature - Left Front:	Left Bank - Front, Bottom of Oil Pan at Threaded Plug	1/8" - 27 NPT
	2.) Fuel:		
CSU measurement	2.01P) Fuel Inlet Pressure: 2.01T) Fuel Inlet Temperature:	Left Bank, Front - LP Fuel Pump, Right Side of Fuel Inlet Manifold Block	1/8" - 27 NPT
	2.02P) Fuel Filter Head Assembly Inlet Pressure: 2.02T) Fuel Filter Head Assembly Inlet Temperature:	Left Bank, Front - Bottom of Block, Right Side of Fuel Filter Head Assembly	1/8" - 27 NPT
	2.03P) Fuel Filter Head Assembly Outlet Pressure: 2.03T) Fuel Filter Head Assembly Outlet Temperature:	Left Bank - Bottom of Block, HP Pump Return From Fuel Filter Assembly Hose Fitting	1/8" - 27 NPT
	2.04P) Fuel Drain Pressure: 2.04T) Fuel Drain Temperature:	Left Bank - Underneath Air Intake, Left Side of Drain Manifold Block	1/8" - 27 NPT
	2.05T) Fuel Pump Housing Temperature:	Left Bank - Bottom of Block, Top of HP Fuel Pump Housing	None
	2.06T) Supply Line Temperature:	Left Bank Fuel Supply Line Inlet	None
	2.07P) Fuel Tank Return Pressure: 2.07T) Fuel Tank Return Temperature:	Left Bank - Just Below Aftercooler, Right Side of Tank Return Manifold Blo	1/8" - 27 NPT
	3.) Intake:		
CMI Sensor	3.01P) LP Compressor Outlet Pressure (4) - Front: 3.01T) LP Compressor Outlet Temperature - Front:	9" Upstream of (Before) High Pressure Compressor Inlet 7" Upstream of (Before) High Pressure Compressor Inlet	4 x 1/8" - 27 NPT 1/8" - 27 NPT
CMI Sensor	3.02P) LP Compressor Outlet Pressure (4) - Rear: 3.02T) LP Compressor Outlet Temperature - Rear:	9" Upstream of (Before) High Pressure Compressor Inlet 7" Upstream of (Before) High Pressure Compressor Inlet	4 x 1/8" - 27 NPT 1/8" - 27 NPT
CMI Sensor	3.03P) HP Compressor Outlet Pressure (4) - Left: 3.03T) HP Compressor Outlet Temperature - Left:	9" Downstream of (After) High Pressure Compressor Outlet 7" Above Crossover Split	4 x 1/8" - 27 NPT 1/8" - 27 NPT
CMI Sensor	3.04P) HP Compressor Outlet Pressure (4) - Right: 3.04T) HP Compressor Outlet Temperature - Right:	9" Downstream of (After) High Pressure Compressor Outlet 7" Above Crossover Split	4 x 1/8" - 27 NPT 1/8" - 27 NPT
ECM Sensor	3.05P) Manifold Pressure - Right Front:	Below Aftercooler, Approx 7" Below Aftercooler Cover Bolt-on	1/8" - 27 NPT
ECM Sensor	3.05T) Manifold Temperature - Right Front:	Below Aftercooler, Approx 7" Below Aftercooler Cover Bolt-on	1/8" - 27 NPT

Priority	Function Reference #) Component Measurement	Location on Engine	Tap Size & Thread
	3.06P) Manifold Pressure - Right Rear: 3.06T) Manifold Temperature - Right Rear:	Below Aftercooler, Approx 7" Below Aftercooler Cover Bolt-on Below Aftercooler, Approx 7" Below Aftercooler Cover Bolt-on	1/8" - 27 NPT 1/8" - 27 NPT
	3.07P) Manifold Pressure - Left Front: 3.07T) Manifold Temperature - Left Front:	Below Aftercooler, Approx 7" Below Aftercooler Cover Bolt-on Below Aftercooler, Approx 7" Below Aftercooler Cover Bolt-on	1/8" - 27 NPT 1/8" - 27 NPT
ECM Sensor	3.08P) Manifold Pressure - Left Rear:	Below Aftercooler, Approx 7" Below Aftercooler Cover Bolt-on	1/8" - 27 NPT
ECM Sensor	3.08T) Manifold Temperature - Left Rear:	Below Aftercooler, Approx 7" Below Aftercooler Cover Bolt-on	1/8" - 27 NPT
CSU sensor	Intake Pressure Test cell		
CSU sensor	Exhaust Pressure Test cell		
	4.) Exhaust:		
CMI Sensor	4.01P) LP Turbine Inlet Pressure (3) - Rear: 4.01T) LP Turbine Inlet Temperature - Rear:	Rear - 6" Upstream of (Before) LP Turbine Connection Flange Rear - 3" Upstream of (Before) LP Turbine Connection Flange	3 x 1/8" - 27 NPT 1/8" - 27 NPT
CMI Sensor	4.02P) LP Turbine Inlet Pressure (3) - Front: 4.02T) LP Turbine Inlet Temperature - Front:	Front - 6" Upstream of (Before) LP Turbine Connection Flange Front - 3" Upstream of (Before) LP Turbine Connection Flange	3 x 1/8" - 27 NPT 1/8" - 27 NPT
CMI Sensor	4.03P) HP Turbine Inlet Pressure (2) - Right: 4.03T) HP Turbine Inlet Temperature - Right:	Right Bank - 1.5" Below HP Turbine Connection Flange Right Bank - 1.5" Below HP Turbine Connection Flange	2 x 1/8" - 27 NPT 1/8" - 27 NPT
CMI Sensor	4.04P) HP Turbine Inlet Pressure (2) - Left: 4.04T) HP Turbine Inlet Temperature - Left:	Left Bank - 1.5" Below HP Turbine Connection Flange Left Bank - 1.5" Below HP Turbine Connection Flange	2 x 1/8" - 27 NPT 1/8" - 27 NPT
	4.05T) LP Turbine Wastegate Temperature - Front:	Front - Front LP Turbine Wastegate Valve	1/8" - 27 NPT
	4.06T) LP Turbine Wastegate Temperature - Rear:	Rear - Rear LP Turbine Wastegate Valve	1/8" - 27 NPT
	5.) Cylinder:		
CMI sensor	5.01P) 1R Pressure:	Right Bank - Cylinder Head 1	NA
CMI sensor	5.02P) 5R Pressure:	Right Bank - Cylinder Head 5	NA
CMI sensor	5.03P) 4L Pressure:	Left Bank - Cylinder Head 4	NA
CMI sensor	5.04P) 8L Pressure:	Left Bank - Cylinder Head 8	NA
	5.05T) 4R Head Temperature:	Right Bank - Cylinder Head 4	NA
	5.06T) 5L Head Temperature:	Left Bank - Cylinder Head 5	NA
	6.) Low Temperature Coolant Circuit:		
	6.01P) Aftercooler Tee Water Return Pressure - Left Front: 6.01T) Aftercooler Tee Water Return Temperature - Left Front:	Left Bank, Front Side of Top Aftercooler Tee	1/8" - 27 NPT
	6.02P) Aftercooler Tee Water Return Pressure - Left Rear: 6.02T) Aftercooler Tee Water Return Temperature - Left Rear:	Left Bank, Rear Side of Top Aftercooler Tee	1/8" - 27 NPT
	6.03P) Aftercooler Tee Water Supply Pressure - Left Front: 6.03T) Aftercooler Tee Water Supply Temperature - Left Front:	Left Bank, Front Side of Bottom Aftercooler Tee	1/8" - 27 NPT

Priority	Function Reference #) Component Measurement	Location on Engine	Tap Size & Thread
	6.04P) Aftercooler Tee Water Supply Pressure - Left Rear: 6.04T) Aftercooler Tee Water Supply Temperature - Left Rear:	Left Bank, Rear Side of Bottom Aftercooler Tee	1/8" - 27 NPT
	6.05P) Aftercooler Water Return to Pump Pressure: 6.05T) Aftercooler Water Return to Pump Temperature:	Front - Pipe Off Aftercooler Thermostat, Right-Facing	1/8" - 27 NPT
CMI sensor	6.06P) Aftercooler Water Supply from Pump Pressure: 6.06T) Aftercooler Water Supply from Pump Temperature:	Right Bank, Front - Pipe from Pump, 6" Before Thermostat Connection Flange	1/8" - 27 NPT
	6.07P) Aftercooler Tee Water Return Pressure - Right Front 6.07T) Aftercooler Tee Water Return Temperature - Right Front:	Right Bank, Front Side of Top Aftercooler Tee	1/8" - 27 NPT
	6.08P) Aftercooler Tee Water Return Pressure - Right Rear: 6.08T) Aftercooler Tee Water Return Temperature - Right Rear:	Right Bank, Rear Side of Top Aftercooler Tee	1/8" - 27 NPT
	6.09P) Aftercooler Tee Water Supply Pressure - Right Front: 6.09T) Aftercooler Tee Water Supply Temperature - Right Front:	Right Bank, Front Side of Bottom Aftercooler Tee	1/8" - 27 NPT
	6.10P) Aftercooler Tee Water Supply Pressure - Right Rear: 6.10T) Aftercooler Tee Water Supply Temperature - Right Rear:	Right Bank, Rear Side of Bottom Aftercooler Tee	1/8" - 27 NPT
CMI sensor	6.11P) Aftercooler Water Thermostat Return Pressure - Right: 6.11T) Aftercooler Water Thermostat Return Temperature - Right:	Right Bank, Front - 8" Before Thermostat	1/8" - 27 NPT
CMI sensor	6.12P) Aftercooler Water Thermostat Return Pressure - Left: 6.12T) Aftercooler Water Thermostat Return Temperature - Left:	Left Bank, Front - 8" Before Thermostat	1/8" - 27 NPT
	7.) High Temperature Coolant Circuit:		
CMI sensor	7.01P) Water Pump Block Inlet Pressure: 7.01T) Water Pump Block Inlet Temperature:	Right Bank, Front - Behind Water Pump 3" from Block Mount Flange	1/8" - 27 NPT
	7.02P) Water Supply Bypass Return Inlet Pressure: 7.02T) Water Supply Bypass Return Inlet Temperature:	Right Bank, Front - 5" from Thermostat Bolt-on Flange	1/8" - 27 NPT
	7.03P) Water Supply Inlet Pressure: 7.03T) Water Supply Inlet Temperature:	Right Bank, Front - Bottom of Y-Joint Pump Inlet	1/8" - 27 NPT
	7.04P) HP Turbocharger Coolant Inlet Pressure - Right: 7.04T) HP Turbocharger Coolant Inlet Temperature - Right:	Right Bank - Back of Water Manifold Return to Thermostat	1/8" - 27 NPT
	7.05P) HP Turbocharger Coolant Outlet Pressure - Right: 7.05T) HP Turbocharger Coolant Outlet Temperature - Right:	Right Bank - Right Side of Block Thermostat Housing	1/8" - 27 NPT
	7.06P) HP Turbocharger Coolant Inlet Pressure - Left: 7.06T) HP Turbocharger Coolant Inlet Temperature - Left:	Left Bank - Back of Water Manifold Return to Thermostat	1/8" - 27 NPT
	7.07P) HP Turbocharger Coolant Outlet Pressure - Left: 7.07T) HP Turbocharger Coolant Outlet Temperature - Left:	Left Bank - Left Side of Block Thermostat Housing	1/8" - 27 NPT
	7.08P) Water Supply Bypass Return Outlet Pressure: 7.08T) Water Supply Bypass Return Outlet Temperature:	Right Bank, Front - 5" Above Y-Joint Pump Inlet Bolt-on Flange	1/8" - 27 NPT

APPENDIX B – QSK19 GT-POWER EXTRA INFORMATION

Operating Point = 2			
Normalized Parameter	Test Cell	GT-Power	Percent Variation
Speed (rpm)	1800.00	1800.00	0.00
Power (bhp)	688.80	681.13	1.11
BSFC	0.86	0.87	1.23
Airflow	0.95	0.96	0.48
A/F	0.70	0.68	2.85
Compressor Out Temp	0.49	0.48	1.72
Turbine In Temp	0.59	0.60	1.06
Turbocharger Speed	0.96	0.97	1.01
Cylinder Pressure	0.95	0.95	0.30
AMB_P	0.21	0.21	0.01
Comp_in_P	0.20	0.20	0.37
Comp_out_P	0.87	0.87	0.29
Int_Mnf_P	0.86	0.84	2.53
Tur_in_P	0.90	0.88	2.42
Tur_out_P	0.23	0.23	0.07
Expansion Ratio	0.00	0.00	0.83
AMB_T	0.31	0.31	0.00
Comp_in_T	0.31	0.31	0.00
Comp_out_T	0.53	0.53	0.87
Int_Mnf_T	0.34	0.34	0.37
Exh_port_T	0.79	0.84	6.30
Tur_in_T	0.85	0.86	0.73
Tur_out_T	0.65	0.67	2.04
GIMEP	0.84	0.85	1.37
Volumetric Efficiency	0.93	0.92	1.00

Operating Point = 3			
Normalized Parameter	Test Cell	GT-Power	Percent Variation
Speed (rpm)	2000.00	2000.00	0.00
Power (bhp)	628.30	633.43	-0.82
BSFC	0.89	0.89	0.68
Airflow	1.00	0.95	4.33
A/F	0.77	0.74	4.46
Compressor Out Temp	0.97	0.96	1.24
Turbine In Temp	0.82	0.83	-1.10
Turbocharger Speed	0.97	0.97	-0.21
Cylinder Pressure	0.91	0.87	4.28
AMB_P	0.21	0.21	0.02
Comp_in_P	0.20	0.20	-0.27
Comp_out_P	0.84	0.83	0.41
Int_Mnf_P	0.82	0.80	1.73
Tur_in_P	0.92	0.89	3.20
Tur_out_P	0.23	0.23	0.01
Expansion Ratio	0.99	0.96	3.19
AMB_T	0.31	0.31	0.00
Comp_in_T	0.31	0.31	0.00
Comp_out_T	0.53	0.52	1.24
Int_Mnf_T	0.35	0.35	0.41
Exh_port_T	0.75	0.83	-10.12
Tur_in_T	0.82	0.83	-1.10
Tur_out_T	0.62	0.64	-3.02
GIMEP	255.00	259.33	-1.70
Volumetric Efficiency	0.91	0.91	0.40

Operating Point = 4			
Normalized Parameter	Test Cell	GT-Power	Percent Variation
Speed (rpm)	2200.00	2200.00	0.00
Power (bhp)	550.80	552.62	-0.33
BSFC	0.94	0.94	0.12
Airflow	1.04	0.97	6.20
A/F	0.85	0.82	4.46
Compressor Out Temp	0.96	0.94	1.48
Turbine In Temp	0.80	0.79	0.59
Turbocharger Speed	0.97	0.96	1.13
Cylinder Pressure	0.83	0.80	4.39
AMB_P	0.21	0.21	0.02
Comp_in_P	0.20	0.20	-0.38
Comp_out_P	0.81	0.80	1.00
Int_Mnf_P	0.80	0.77	4.57
Tur_in_P	0.95	0.89	6.49
Tur_out_P	0.23	0.23	0.01
Expansion Ratio	1.03	0.96	6.48
AMB_T	0.31	0.31	0.00
Comp_in_T	0.31	0.31	0.00
Comp_out_T	0.52	0.51	1.48
Int_Mnf_T	0.35	0.34	0.36
Exh_port_T	0.77	0.79	-2.02
Tur_in_T	0.80	0.79	0.59
Tur_out_T	0.60	0.61	-1.61
GIMEP	208.00	217.49	-4.56
Volumetric Efficiency	0.88	0.88	0.64

Operating Point = 5			
Normalized Parameter	Test Cell	GT-Power	Percent Variation
Speed (rpm)	1600.00	1600.00	0.00
Power (bhp)	484.50	475.86	1.78
BSFC	0.86	0.87	-1.97
Airflow	0.65	0.63	2.70
A/F	0.67	0.65	2.85
Compressor Out Temp	0.39	0.38	2.99
Turbine In Temp	0.57	0.58	-1.09
Turbocharger Speed	0.79	0.80	-1.16
Cylinder Pressure	0.71	0.69	2.83
AMB_P	0.21	0.21	0.00
Comp_in_P	0.20	0.20	0.52
Comp_out_P	0.63	0.63	0.24
Int_Mnf_P	0.63	0.61	2.26
Tur_in_P	0.61	0.60	1.41
Tur_out_P	0.22	0.22	0.26
Expansion Ratio	0.68	0.68	1.15
AMB_T	0.31	0.31	0.00
Comp_in_T	0.31	0.31	0.00
Comp_out_T	0.48	0.47	1.35
Int_Mnf_T	0.33	0.33	0.30
Exh_port_T	0.78	0.82	-4.73
Tur_in_T	0.83	0.84	-0.75
Tur_out_T	0.69	0.70	-0.50
GIMEP	0.67	0.67	0.49
Volumetric Efficiency	0.92	0.94	-1.19

Operating Point = 6			
Normalized Parameter	Test Cell	GT-Power	Percent Variation
Speed (rpm)	1800.00	1800.00	0.00
Power (bhp)	445.40	445.11	0.07
BSFC	0.87	0.88	-0.27
Airflow	0.71	0.69	2.76
A/F	0.79	0.77	2.97
Compressor Out Temp	0.86	0.86	0.85
Turbine In Temp	0.77	0.77	0.19
Turbocharger Speed	0.80	0.81	-1.51
Cylinder Pressure	0.74	0.71	3.36
AMB_P	0.21	0.21	-0.02
Comp_in_P	0.20	0.20	0.53
Comp_out_P	0.63	0.63	0.13
Int_Mnf_P	0.62	0.61	1.25
Tur_in_P	0.65	0.63	2.74
Tur_out_P	0.22	0.22	0.09
Expansion Ratio	0.72	0.71	2.66
AMB_T	0.31	0.31	0.00
Comp_in_T	0.31	0.31	0.00
Comp_out_T	0.47	0.47	0.85
Int_Mnf_T	0.33	0.33	0.29
Exh_port_T	0.73	0.76	-4.21
Tur_in_T	0.77	0.77	0.19
Tur_out_T	0.63	0.63	-0.80
GIMEP	0.57	0.58	-1.63
Volumetric Efficiency	0.92	0.92	-0.60

Operating Point = 7			
Normalized Parameter	Test Cell	GT-Power	Percent Variation
Speed (rpm)	2000.00	2000.00	0.00
Power (bhp)	392.60	392.26	0.09
BSFC	0.93	0.92	1.05
Airflow	0.76	0.72	6.13
A/F	0.91	0.86	5.06
Compressor Out Temp	0.86	0.37	57.03
Turbine In Temp	0.73	0.73	-0.17
Turbocharger Speed	0.80	0.80	-0.11
Cylinder Pressure	0.72	0.67	7.08
Normalized Parameter	Test Cell	GT-Power	Percent Variation
AMB_P	0.21	0.21	0.00
Comp_in_P	0.20	0.20	0.33
Comp_out_P	0.62	0.61	2.36
Int_Mnf_P	0.62	0.58	5.28
Tur_in_P	0.68	0.64	6.03
Tur_out_P	0.22	0.22	-0.18
Expansion Ratio	0.76	0.71	6.20
Normalized Parameter	Test Cell	GT-Power	Percent Variation
AMB_T	0.31	0.31	0.00
Comp_in_T	0.31	0.31	0.00
Comp_out_T	0.47	0.46	1.31
Int_Mnf_T	0.33	0.33	0.29
Exh_port_T	0.70	0.73	-4.06
Tur_in_T	0.73	0.73	-0.17
Tur_out_T	0.58	0.60	-3.18
Normalized Parameter	Test Cell	GT-Power	Percent Variation
GIMEP	0.48	0.49	-1.73
Volumetric Efficiency	0.93	0.92	1.00

Operating Point = 8			
Normalized Parameter	Test Cell	GT-Power	Percent Variation
Speed (rpm)	2200.00	2200.00	0.00
Power (bhp)	322.40	337.86	-4.80
BSFC	0.98	0.99	-1.44
Airflow	0.81	0.77	5.47
A/F	1.03	0.99	4.10
Compressor Out Temp	0.85	0.85	0.20
Turbine In Temp	0.70	0.70	-0.24
Turbocharger Speed	0.83	0.82	1.86
Cylinder Pressure	0.68	0.64	5.76
AMB_P	0.21	0.21	0.00
Comp_in_P	0.20	0.20	-0.04
Comp_out_P	0.61	0.61	-0.41
Int_Mnf_P	0.61	0.59	2.97
Tur_in_P	0.70	0.67	5.34
Tur_out_P	0.22	0.22	0.82
Expansion Ratio	0.78	0.75	4.56
AMB_T	0.31	0.31	0.00
Comp_in_T	0.31	0.31	0.00
Comp_out_T	0.46	0.46	0.20
Int_Mnf_T	0.33	0.33	0.31
Exh_port_T	0.68	0.70	-2.94
Tur_in_T	0.70	0.70	-0.24
Tur_out_T	0.55	0.56	-2.93
GIMEP	0.44	0.41	6.10
Volumetric Efficiency	0.92	0.94	-1.19

Direct Optimizer Method Extrapolation Results for QSK19:

Normalized Rotor Speed Match: Experimental vs. Simulation				
Match Criteria Set B		Target ONLY Test Cell Rotor Speed		
Operating Point	Test Cell at 5000ft	GT-Power at 5000ft	GT-Power at 8000ft	Rotor Speed Percent Variation
1	0.941474966	0.941473613	0.941474966	0.00014373
2	0.963802436	0.963802436	0.963801083	0
3	0.965832206	0.965833559	0.965833559	0.000140105
4	0.970568336	0.970549391	0.970568336	0.0019519
5	0.792692828	0.792687415	58579.4	0.000682827
6	0.800575101	0.800560217	59162.7	0.001859286
7	0.803518268	0.803510149	59379.7	0.001010441
8	0.834790257	0.834893099	61683.2	0.012319463
Normalized Expansion Ratio Match: Experimental vs. Simulation				
Match Criteria Set		Target ONLY Test Cell Rotor Speed		
Operating Point	Test Cell at 5000ft	GT-Power at 5000ft	GT-Power at 8000ft	Expansion Ratio Variation
1	0.705711354	0.675184831	0.687896578	4.32563866
2	0.756236847	0.723973321	0.739981141	4.266325662
3	0.774558443	0.746163937	0.766568469	3.665895875
4	0.806923018	0.770457359	0.785902514	4.519100126
5	0.534555125	0.520193971	0.526469473	2.686561861
6	0.567417121	0.541060169	0.549792502	4.645075142
7	0.594747647	0.558498514	0.566577937	6.094876196
8	0.613127902	0.600299537	0.608687429	2.092282023
Normalized Turbine Inlet Temperature Match: Experimental vs. Simulation				
Match Criteria Set		Target ONLY Test Cell Rotor Speed		
Operating Point	Test Cell at 5000ft	GT-Power at 5000ft	GT-Power at 8000ft	TIT Variation
1	0.844615385	0.844313231	0.824737538	0.035774135
2	0.797692308	0.800361385	0.779560308	0.334599807
3	0.761307692	0.771745538	0.747564654	1.37104173
4	0.724769231	0.724776662	0.703723569	0.00102526
5	0.775384615	0.781863	0.769458154	0.835505952
6	0.693538462	0.688260123	0.672212462	0.761073647
7	0.638846154	0.640593385	0.626467538	0.273497893
8	0.593846154	0.608632308	0.598534262	2.489896373

SAE Pressure and Temperature Table:

Standard Day SAE Table				
Altitude (ft)	Temp. (°R)	Temp. (°F)	Barometric Pressure (psia)	Barometric Pressure (in Hga)
0	546.50	86.80	14.69	29.91
500	545.00	85.30	14.43	29.38
1000	542.90	83.20	14.17	28.85
2000	539.40	79.70	13.66	27.81
3000	535.80	76.10	13.16	26.79
4000	532.20	72.50	12.69	25.84
5000	528.70	69.00	12.22	24.88
6000	525.10	65.40	11.77	23.96
7000	521.50	61.80	11.34	23.09
8000	518.00	58.30	10.91	22.21
9000	514.50	54.80	10.50	21.38
10000	510.80	51.10	10.10	20.56
11000	507.30	47.60	9.72	19.79
12000	503.70	44.00	9.34	19.02
13000	500.10	40.40	8.98	18.28
14000	496.60	36.90	8.63	17.57
15000	493.00	33.30	8.29	16.88
16000	489.40	29.70	7.96	16.21
17000	485.90	26.20	7.64	15.56
18000	482.30	22.60	7.34	14.94

APPENDIX C – QSK50 GT-POWER EXTRA INFORMATION

Operating Point = 2			
Parameter	Test Cell	GT-Power	Percent Variation
Speed (rpm)	2000	2000	0
Power (bhp)	1953	1970	-0.870455709
BSFC	0.891806329	0.9025	-1.199102421
Airflow	2.676751033	2.669230769	0.280947465
A/F Ratio	0.665974014	0.648888889	2.565434149
LP Turbo Speed	0.611096076	0.604871448	1.018600531
Cylinder Pressure	0.904	0.932	-3.097345133
GIMEP	0.840857143	0.842857143	-0.237852531
Volumetric Efficiency	89.4	85.8	4.026845638
BMEP	0.628927195	0.6375	-1.36308381
AMB_P	0.206225	0.20625	-0.012122682
LP_Comp_in_P	0.202443275	0.2025	-0.028020195
HP_Comp_in_P	0.6025	0.56	7.053941909
HP_Comp_out_P	0.8925	0.83	7.00280112
Int_Mnf_P	0.835	0.8525	-2.095808383
HP Turb_in_P	0.8125	0.865	-6.461538462
LP Tur_in_P	0.5625	0.525	6.666666667
LP Tur_out_P	0.25	0.2525	-1
AMB_Temp	0.315513704	0.315854677	-0.108069164
LP Comp In Temp	0.315513704	0.315854677	-0.108069164
HP Comp In Temp	0.444401507	0.449857075	-1.227621483
HP Comp Out Temp	0.500093768	0.526576006	-5.295454545
Int_Mnf_Temp	0.335062824	0.332221382	0.848032564
HP Turb In Temp	0.882551842	0.860047623	2.549903413
LP Turb In Temp	0.817198679	0.791512045	3.14325452
LP Turb Ot Temp	0.70280223	0.671830514	4.406889302
Expansion Ratio	2.25	2.079207921	7.590759076

Operating Point = 3			
Parameter	Test Cell	GT-Power	Percent Variation
Speed (rpm)	1400	1400	0
Power (bhp)	1509	1460	3.247183565
BSFC	0.850894632	0.8775	-3.126752336
Airflow	1.676361123	1.676923077	-0.033522249
A/F Ratio	0.565750119	0.564444444	0.230786507
LP Turbo Speed	0.484032476	0.48037889	0.754822477
Cylinder Pressure	0.83	0.856	-3.13253012
GIMEP	0.84	0.834285714	0.680272109
Volumetric Efficiency	90.6	89	1.766004415
BMEP	0.694207547	0.675	2.766830632
AMB_P	0.20613425	0.206	0.065127459
LP_Comp_in_P	0.2002405	0.20375	-1.752642447
HP_Comp_in_P	0.45	0.43	4.444444444
HP_Comp_out_P	0.78	0.735	5.769230769
Int_Mnf_P	0.7275	0.745	-2.405498282
HP Turb_in_P	0.5725	0.615	-7.423580786
LP Tur_in_P	0.3925	0.37	5.732484076
LP Tur_out_P	0.229075	0.229	0.032740369
AMB_Temp	0.29985736	0.300510891	-0.217947503
LP Comp In Temp	0.29985736	0.300510891	-0.217947503
HP Comp In Temp	0.38905022	0.391550688	-0.642711072
HP Comp Out Temp	0.466223781	0.474407133	-1.755241346
Int_Mnf_Temp	0.331880409	0.336313059	-1.335616438
HP Turb In Temp	0.885961572	0.865162218	2.347658756
LP Turb In Temp	0.823449851	0.78639745	4.499654934
LP Turb Ot Temp	0.712633619	0.706609762	0.845295056
Expansion Ratio	1.713412638	1.615720524	5.701610436

Operating Point = 4			
Parameter	Test Cell	GT-Power	Percent Variation
Speed (rpm)	1600	1600	0
Power (bhp)	1575	1580	-0.317460317
BSFC	0.868794223	0.86	1.012233187
Airflow	2.146923077	2.146153846	0.035829452
A/F Ratio	0.6859729	0.684444444	0.222815736
LP Turbo Speed	0.520838972	0.51014885	2.052481164
Cylinder Pressure	0.8804	0.9	-2.226260791
GIMEP	0.8	0.811428571	-1.428571429
Volumetric Efficiency	89.8	88.7	1.224944321
BMEP	0.633999189	0.6375	-0.55217914
AMB_P	0.206025	0.206	0.01213445
LP_Comp_in_P	0.20334085	0.20325	0.044678676
HP_Comp_in_P	0.4875	0.45	7.692307692
HP_Comp_out_P	0.8825	0.8125	7.932011331
Int_Mnf_P	0.8175	0.8275	-1.22324159
HP Turb_in_P	0.7075	0.6725	4.946996466
LP Tur_in_P	0.455	0.4225	7.142857143
LP Tur_out_P	0.23624425	0.23625	-0.002433922
AMB_Temp	0.304989004	0.305625487	-0.208690467
LP Comp In Temp	0.304989004	0.305625487	-0.208690467
HP Comp In Temp	0.401779879	0.402802798	-0.254596888
HP Comp Out Temp	0.486454847	0.495888434	-1.939252336
Int_Mnf_Temp	0.326197526	0.332221382	-1.846689895
HP Turb In Temp	0.82742787	0.800718317	3.228021978
LP Turb In Temp	0.739400001	0.713770196	3.466297748
LP Turb Ot Temp	0.637733211	0.625799156	1.871324185
Expansion Ratio	1.925972801	1.788359788	7.145117158

Operating Point = 5			
Parameter	Test Cell	GT-Power	Percent Variation
Speed (rpm)	1800	1800	0
Power (bhp)	1470	1550	-5.442176871
BSFC	0.868124586	0.8775	-1.079961832
Airflow	2.136788078	2.138461538	-0.078316639
A/F Ratio	0.706825573	0.682222222	3.480823494
LP Turbo Speed	0.520838972	0.51150203	1.792673422
Cylinder Pressure	0.8324	0.888	-6.679481019
GIMEP	0.742857143	0.728571429	1.923076923
Volumetric Efficiency	89	87.4	1.797752809
BMEP	0.525984512	0.555	-5.516414875
AMB_P	0.205938	0.20775	-0.879876468
LP_Comp_in_P	0.204806	0.20475	0.027342949
HP_Comp_in_P	0.4875	0.4525	7.179487179
HP_Comp_out_P	0.795	0.7275	8.490566038
Int_Mnf_P	0.725	0.7425	-2.413793103
HP Turb_in_P	0.685	0.725	-5.839416058
LP Tur_in_P	0.4525	0.42	7.182320442
LP Tur_out_P	0.23615	0.23625	-0.042345967
AMB_Temp	0.307887274	0.307671325	0.070139171
LP Comp In Temp	0.307887274	0.307671325	0.070139171
HP Comp In Temp	0.403086942	0.405871555	-0.690821937
HP Comp Out Temp	0.47065643	0.483613405	-2.752958223
Int_Mnf_Temp	0.326197526	0.332221382	-1.846689895
HP Turb In Temp	0.810379219	0.789466207	2.580645161
LP Turb In Temp	0.741957299	0.716838953	3.385416667
LP Turb Ot Temp	0.643870726	0.628867913	2.330097087
Expansion Ratio	1.916154986	1.777777778	7.221608349

Operating Point = 6			
Parameter	Test Cell	GT-Power	Percent Variation
Speed (rpm)	2000	2000	0
Power (bhp)	1324	1320	0.302114804
BSFC	0.829191518	0.93	-12.15744256
Airflow	2.272457162	2.269230769	0.141978163
A/F Ratio	0.786998151	0.802222222	-1.934448105
LP Turbo Speed	0.517456022	0.50744249	1.935146444
Cylinder Pressure	0.766	0.8	-4.438642298
GIMEP	0.581428571	0.597142857	-2.702702703
Volumetric Efficiency	88.5	87.2	1.468926554
BMEP	0.426369486	0.425	0.321197039
AMB_P	0.205825	0.20575	0.036438722
LP_Comp_in_P	0.2046175	0.20275	0.912678534
HP_Comp_in_P	0.4875	0.4275	12.30769231
HP_Comp_out_P	0.7675	0.705	8.143322476
Int_Mnf_P	0.7	0.7225	-3.214285714
HP Turb_in_P	0.7175	0.6425	10.45296167
LP Tur_in_P	0.46	0.4275	7.065217391
LP Tur_out_P	0.23675	0.236	0.316789863
AMB_Temp	0.30971148	0.309717163	-0.001834896
LP Comp In Temp	0.30971148	0.309717163	-0.001834896
HP Comp In Temp	0.402007195	0.402802798	-0.197907831
HP Comp Out Temp	0.4642916	0.485659243	-4.602203182
Int_Mnf_Temp	0.326197526	0.332221382	-1.846689895
HP Turb In Temp	0.780828223	0.747526525	4.264919942
LP Turb In Temp	0.706780249	0.668761756	5.379110718
LP Turb Ot Temp	0.611478289	0.582836555	4.68401487
Expansion Ratio	1.942977825	1.811440678	6.769873803

Calibration Method for Extrapolation Results for QSK50:

Normalized LP Rotor Speed Match: Experimental vs. Simulation				
Calibration Method				
Operating Point	Test Cell at 5000ft	GT-Power at 5000ft	GT-Power at 8000ft	GT-Power Percent Variation
1	0.606901218	0.604871448	0.608930988	0.334448161
2	0.611096076	0.604871448	0.607577808	0.575730735
3	0.484032476	0.48037889	0.48579161	0.363433044
4	0.520622463	0.51014885	0.51014885	2.011748194
5	0.520838972	0.51150203	0.51420839	1.273057937
6	0.517456022	0.50744249	0.50744249	1.935146444
Normalized LP Expansion Ratio Match: Experimental vs. Simulation				
Calibration Method				
Operating Point	Test Cell at 5000ft	GT-Power at 5000ft	GT-Power at 8000ft	GT-Power Percent Increase in ER
1	0.427592955	0.403131115	0.417538295	5.720823799
2	0.440313112	0.406890004	0.424877298	7.590759076
3	0.3353058	0.316187969	0.324612089	5.701610436
4	0.376902701	0.349972561	0.350096052	7.145117158
5	0.374981406	0.347901718	0.361560677	7.221608349
6	0.380230494	0.354489369	0.361317079	6.769873803
Normalized LP Turbine Inlet Temperature Match: Experimental vs. Simulation				
Calibration Method				
Operating Point	Test Cell at 5000ft	GT-Power at 5000ft	GT-Power at 8000ft	GT-Power Percent Decrease in TIT
1	0.787692308	0.766769231	0.711384615	2.65625
2	0.753076923	0.718307692	0.662923077	4.616956078
3	0.761538462	0.711384615	0.649076923	6.585858586
4	0.647769231	0.613076923	0.599230769	5.355658473
5	0.651230769	0.617230769	0.554923077	5.220883534
6	0.603615385	0.552153846	0.516153846	8.525551166